DIFFUSION IN THIN FILMS

by

DALE BERNARD JOHNSON

B.Sc.(Hons), The University of British Columbia, 1964

A THESIS SUBMITTED IN PARTIAL FULFILMENT OF

THE REQUIREMENTS FOR THE DEGREE OF

DOCTOR OF PHILOSOPHY

in the Department

of

METALLURGY

We accept this thesis as conforming to the
required standard

THE UNIVERSITY OF BRITISH COLUMBIA

March, 1968

In presenting this thesis in partial fulfilment of the requirements for an advanced degree at the University of British Columbia, I agree that the Library shall make it freely available for reference and study. I further agree that permission for extensive copying of this thesis for scholarly purposes may be granted by the Head of my Department or by his representatives. It is understood that copying or publication of this thesis for financial gain shall not be allowed without my written permission.

Dale Bernard Johnson

Department of Metallurgy

The University of British Columbia
Vancouver 8, Canada

Date April 10, 1968

ABSTRACT

The nature of diffusion along thin evaporated films has been studied by optical and transmission electron microscopy. The thicknesses of the films were measured by multiple-beam interferometry.

A preliminary survey of some 22 binary metal systems showed that only four - Ag-Se, Cu-Se, Cu-Te, and Ag-Te - diffused measurably at room temperature. In these four systems it was found possible to study only the diffusion of Cu or Ag into Se and Te; the reverse diffusion experiments failed, presumably because of extensive Kirkendall porosity which developed on the Se or Te side of the diffusion couples, impeding the motion of these atoms.

The room temperature growth rates in each system were observed to be higher when the structure of the Se or Te consisted of isolated islands with a highly disordered inter-island network. This effect was attributed to a short circuit diffusion process analogous to grain boundary diffusion which took place in the inter-island channels. The effect was more pronounced in Cu-Te and Ag-Te where electron microscopy observations of the phase boundary interfaces showed a marked tendency for grain

boundary diffusion to occur at all Se and Te thicknesses. For continuous films of Se and Te, the growth rates were found to be independent of the absolute thickness.

Because of the evaporation geometry used in depositing the couples, there was a critical thickness ratio of Ag or Cu to Se or Te that had to be exceeded in order for diffusion to proceed. Theoretical treatment of the problem, based on the stoichiometry of the phases formed during diffusion, gave predictions of the critical ratio that were generally in good agreement with the experimental values obtained. In each system the critical ratio was found to be independent of the absolute Se or Te thickness. It was also possible to predict the composition of the phase formed during diffusion using the critical ratio. In every system but Cu-Te, the composition determined in this way was in agreement with that given by electron diffraction analysis of the diffusion zone.

The activation energies for diffusion in Ag-Se, Cu-Te, and Ag-Te were fairly low suggesting that short circuit diffusion was the predominant mechanism in these systems. The activation energy in Cu-Se was quite large (23 kcal/mole), and it appears that the diffusion mechanism in this case is not consistent with that in the other systems. An interesting observation made during electron microscopy studies in Cu-Se was the formation of a second phase when high electron beam intensities were used. This phase (Cu_3Se_2), not observed in normal diffusion experiments up to 50°C, grew dendritically in the presence of the electron beam.

TABLE OF CONTENTS

Table of Contents (Cont'd)

Table of Contents (Cont'd)

LIST OF FIGURES

List of Figures (Cont'd)

List of Figures (Cont'd)

List of Figures (Cont'd)

LIST OF TABLES

ACKNOWLEDGEMENT

The author would like to express his gratitude to his research director, Dr. L.C. Brown, for his advice and encouragement during the course of this research project. He also wishes to thank other faculty members and fellow graduate students for many useful and stimulating discussions. The assistance of the technical staff is gratefully acknowledged. This research was financed in part by a National Research Council Studentship, a Cominco Fellowship, and a Defense Research Board Research Assistantship.

CHAPTER 1

INTRODUCTION

In recent years thin films have acquired a wide range of applications in the fields of optics and electronics[1,2]. The development of the technology of thin film electronics devices, in particular, has led to a great deal of interest in their structure and properties[3,4,5,6]. Therefore, many investigations have been centered around their fundamental properties and how they compare with those of bulk material[7]. Comparatively little work has been carried out, however, on thin film diffusion. Such studies are of considerable potential interest since evaporated thin films are of high purity, can be grown in both single-crystal and polycrystalline form, and can be observed by transmission electron microscopy.

1.1 Previous Work

The methods used to investigate diffusion in bulk couples are generally inapplicable to evaporated films because any method of sectioning is impossible and the quantity of material available is inadequate for chemical

analysis. Radioactive tracer techniques cannot be used since the absorption of the films is negligible even for low energy β-rays. Consequently no changes in emission can be detected as radioactive particles diffuse through the films.

In the past, most measurements of diffusion in thin films have involved the use of optical methods[8]. One technique employed to study diffusion in two superimposed thin films uses variations in reflectivity as the diffusion zone reaches the metal surface.

Weaver and Brown[9] have investigated diffusion in superimposed Au-Al films by this method. They found that changes in reflectivity at the metal surface were due to a sharply defined phase boundary and that the compound formed during diffusion was Au_2Al. The growth of the diffusion layer obeyed the parabolic law $x^2 = kt$ where k is the diffusion rate constant. The diffusion rate constant and activation energy for diffusion of Al into a Au film were independent of the Au film thickness in the range 70 Å to 3000 Å indicating that the diffusion mechanism for the very thin films was the same as for thicker ones.

Reflectivity measurements were also used by Schopper[10] and Weaver and Brown[9] to investigate thin film diffusion in the Au-Pb system where, in contrast to Au-Al, reflectivity changes result from the growth of a diffuse phase boundary. The growth rate, however, was still

parabolic with time. Measurements showed that variations in reflectivity were due to the formation of $AuPb_2$ during diffusion.

The possibility of investigating diffusion along a film parallel to the surface was first demonstrated by Monch[11]. The work apparently started with attempts to produce radiation detectors. A film of Te was evaporated so as to form a bridge between two thick Ag electrodes which had themselves been evaporated onto a collodion film. On ageing, the Ag diffused into the Te, forming a yellowish-brown band of Ag_2Te spreading outwards from the silver. Mohr[12,13] measured the coefficient of diffusion of the Ag by determining the widths of the diffusion zone as a function of time. A variation with the thickness of Te was attributed to a folding or crinkling of the thicker films which became detached from their underlying substrates. Measurements over a range of temperature gave $D = D_o \exp(-B/T)$ where $D_o = 5 \times 10^7$ cm^2/day and $B = 6010$ deg^{-1}.

Similar experiments were carried out using Se instead of Te by Kienel[14] and Zorll[15] but the films were deposited on substrates at liquid nitrogen temperatures because of the relative volatility of the Se. Measurements of diffusion rate were again made by determining the width of the diffusion zone as a function of time and the results, although approximate, were in general agreement with the earlier results for Ag-Te.

In 1963 Parkinson[16] studied lateral diffusion in

the Cu-Te system by electron microscopy. Observations were made on the moving diffusion zone interface and no evidence of grain boundary diffusion was seen. Volume diffusion was the proposed mechanism for diffusion in the film couples with $K = K_o \exp[-E/RT]$ where $K_o = 7.55 \times 10^{-2}$ cm^2/sec and $E = 10.0$ kcal/mole.

1.2 Object of the Present Investigation

The main purpose of this study was to carry out a thorough investigation of lateral diffusion - that is, diffusion along a film parallel to the surface - in several two-component systems. A survey of some 22 metal pairs at room temperature showed that only four - Cu-Te, Ag-Te, Cu-Se and Ag-Se - gave suitable diffusion zones. Even in these systems only diffusion in Se and Te could be studied. It had originally been hoped to study diffusion along thin films produced from the bulk. However, it proved impracticable to produce such films in Se and Te, the only metals in which lateral diffusion could be seen. This portion of the work was therefore abandoned. The effect of varying the thicknesses of both components on the diffusion rate constant was examined. Also the temperature dependence of the rate constant in each system was determined. In addition a detailed study of the diffusion front and the nature of its movement as well as the microstructure and composition of the diffusion zone was carried out using transmission electron microscopy.

1.3 Diffusion Theory

1.3.1 Atomic Models for Diffusion

A. Lattice Diffusion

Some proposed mechanisms for lattice diffusion are illustrated in Figure 1.1. A brief description of each model is given below:

(1) Interchange mechanism: It is now generally agreed that direct interchange of atoms does not occur in view of the large lattice distortions involved.

(2) Interstitial mechanism: Interstitial diffusion can take place when the two atom sizes are markedly different. For example, in ionic compounds, where there is often a great size difference between anion and cation, diffusion is usually due to the smaller cation.

(3) Vacancy mechanism: Diffusion is usually considered to take place by a vacancy mechanism. If an atom is missing in the lattice, atomic motion will result if any of the adjacent atoms jump into the vacant site, interchanging positions with the vacancy. The vacancy will thereby advance one atomic distance and enable other atoms to move in the next jump.

B. The Kirkendall Effect

Point defects such as interstitials and vacancies permit net translational motion of atoms relative to a fixed lattice under the driving force of a

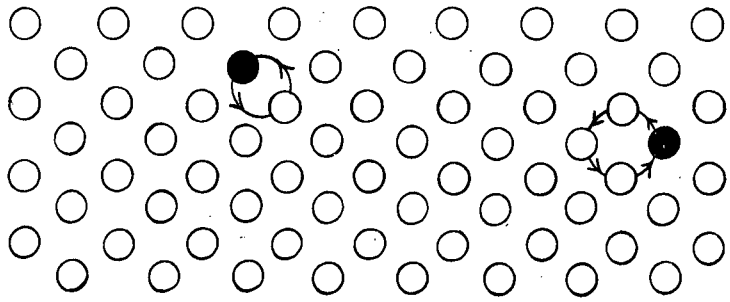

a) Interchange pair and ring of four

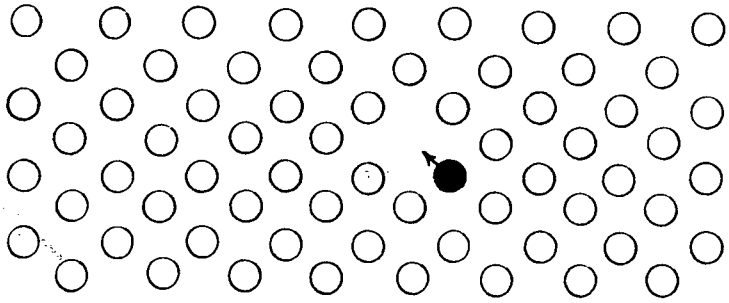

b) Vacancy

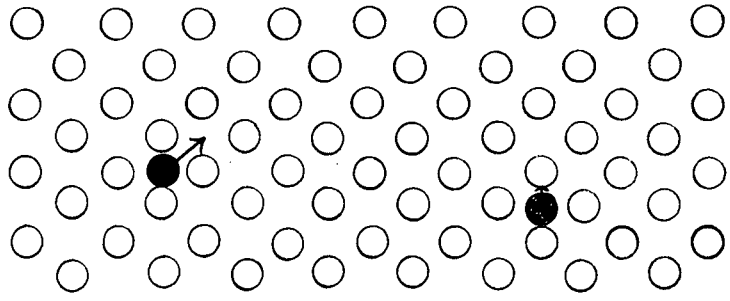

c) Interstitial

Figure 1.1 Models for Diffusion

chemical or thermal gradient. In other words, relative to the crystal lattice, the atomic species in a binary alloy diffuse at unequal rates. This phenomenon is called the Kirkendall effect[17,18] and is evidenced by a macroscopic shift in the center of gravity of an initial concentration gradient with respect to inert markers fixed in the lattice. The Kirkendall shifts observed in some oxide layers and intermetallic compounds can be very large. In these cases only one species diffuses and the shift can therefore be nearly the full width of the diffusion zone. The Kirkendall experiment demonstrates that a net flow of atoms can take place during diffusion. It has often been observed that voids, or pores, form in that region of the diffusion zone from which there is a flow of mass. This is called Kirkendall porosity - its origin being a vacancy flux which moves in a direction opposite to the net mass flow during diffusion.

C. Short Circuit Diffusion

The diffusion rate of atoms along grain boundaries, surfaces, and dislocations is considerably greater than the rate of bulk diffusion. Figure 1.2 shows the apparent self-diffusion coefficients in silver as determined by a radioactive silver tracer experiment for single-crystal and polycrystal samples[19]. It can be seen that the same value of the diffusion coefficient is obtained for both types of samples at high temperature. Below 700°C, how-

ever, the diffusion coefficient values obtained using a polycrystal lie consistently above the values obtained with a single crystal. This graph illustrates that the activation energy for grain boundary diffusion is about 60% of the value for bulk diffusion and also that grain boundary diffusion becomes increasingly important at low temperatures. The apparent lattice diffusion coefficient can also be affected by dislocations especially if their density is high. The effect of dislocations on diffusivity also becomes more important at lower temperatures.

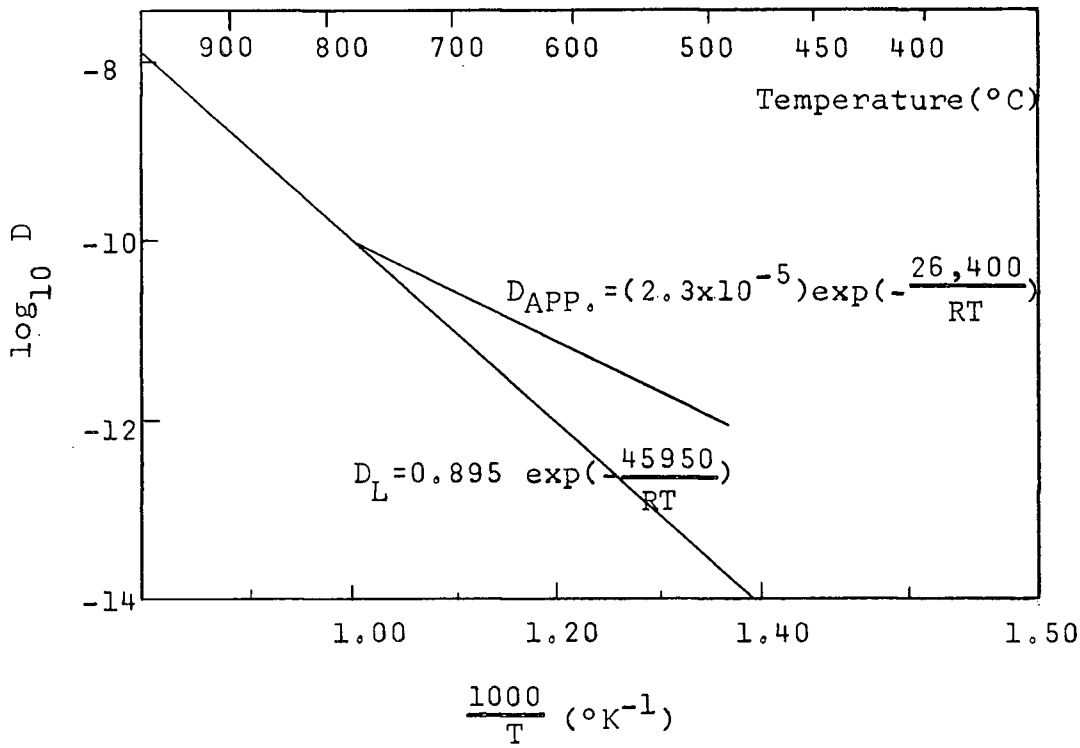

Figure 1.2 Self-diffusion in Single-Crystal and Polycrystalline Silver. (After Turnbull[20])

Many workers report that the diffusion coefficient along a surface is greater than both the grain boundary and lattice diffusion coefficients. The driving force for

surface diffusion may be surface tension or surface free energy. Two of the main methods for determining the surface diffusion coefficient are surface scratch smoothing and grain boundary grooving[21]. Surface contamination can lead to tremendous scatter in the results obtained. For example, a comparison of the activation energies for surface, grain boundary and lattice diffusion for self diffusion of Ag is given in the table below[22]:

Mechanism	E(kcal/mole)
Surface	10.3
Grain boundary	26.4
Volume	45.9

In contrast to these results the grain boundary grooving analysis of Mullin's[23,24] for D_s on copper gives an activation energy of 49 kcal/mole which is nearly the same as the activation energy for bulk self diffusion (46.8 kcal/mole). This high value found by surface smoothing is not too surprising since a copper atom moving on the surface is well on its way to being an evaporated atom. Thus the activation energy for its motion is related more closely to the heat of vaporization (80 kcal/mole for Cu) than to the bulk activation energy. It would appear, however, that more work on very clean surfaces must be done to remove some of the inconsistencies from surface diffusion results.

D. Diffusion in Intermetallic Compounds[25]

Intermetallic compounds which are present in most binary systems often have only small deviations from stoichiometry associated with them. Such deviations are usually due to a defect structure in which some of the atoms of one species are missing from their normal lattice positions. For example, ZrO_2 can exist from its stoichiometric composition to $ZrO_{2-.001}$. This is probably a Schottky defect structure with oxygen vacancies. Another example of a defect intermetallic compound is $Cu_{1.8}Se$ which is a copper deficient form of Cu_2Se. As might be expected, diffusion in such compounds is often greatly dependent on the exact deviation from stoichiometry since this determines the vacancy and interstitial concentrations. The "open" structures which occur in defect intermetallic compounds can result in very high atomic mobilities. It is known, for example, that Ag ions in the high temperature modification of Ag_2S (α-Ag_2S) possess extremely high mobilities[26]. The reason for this is that the cations do not occupy fixed lattice positions in this structure and can migrate from site to site just like in a liquid.

1.3.2 Mathematics of Diffusion

Fick's first and second laws of diffusion in one-dimensional form are:

$$J = -D \frac{\partial c}{\partial x} \qquad (1.1)$$

and $$\frac{\partial c}{\partial t} = \frac{\partial}{\partial x}\left(D\frac{\partial c}{\partial x}\right) \qquad (1.2)$$

Equation (1.2) becomes

$$\frac{\partial c}{\partial t} = D\frac{\partial^2 c}{\partial x^2}$$

if D is not a function of concentration.

A. Single-phase Diffusion

Consider a semi-infinite diffusion couple in a single-phase binary system (Figure 1.3). If the transformation $\lambda = x/\sqrt{t}$ is applied to Fick's second law (equation 1.2) then the following equation results:

$$-\frac{\lambda}{2}\frac{dc}{dt} = \frac{d}{d\lambda}D\frac{dc}{d\lambda} \qquad (1.3)$$

This has eliminated x and t as independent variables. Hence one concentration profile is applicable at all times in a semi-infinite couple. That is, the profile can be

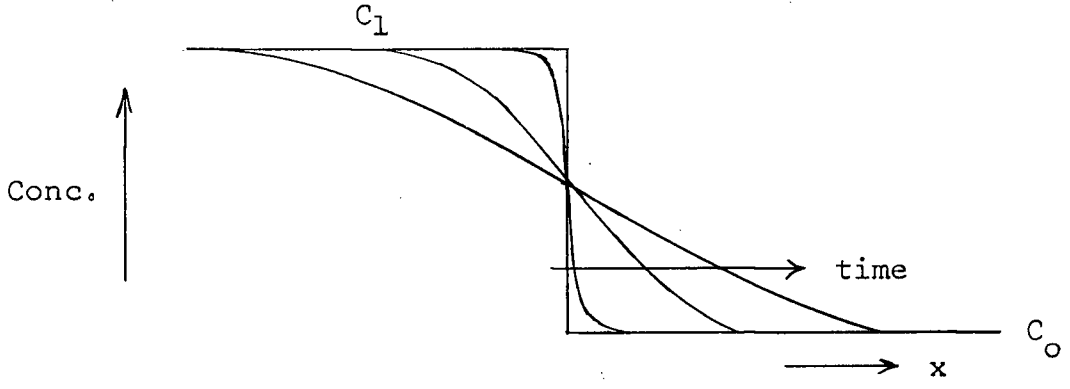

Figure 1.3 Concentration Profiles with Increasing Time in a Single-phase Binary System.

given as $C = C(\lambda)$ instead of a whole series of profiles with $C = C(x,t)$. The equation for this single profile can be found by integrating equation 1.3 twice. If D is taken to be constant then a particular solution to this equation for a semi-infinite diffusion couple is:

$$\frac{C-C_o}{C_1-C_o} = 1/2[1-\text{erf } \lambda/2\sqrt{D}] \qquad (1.4)$$

where $$\text{erf } \lambda/2\sqrt{D} = \frac{2}{\sqrt{\pi}} \int_o^{\lambda/2\sqrt{D}} e^{-\eta^2} d\eta$$

B. Multi-Phase Diffusion

Consider now a diffusion couple composed of two pure metals A and B with no solid solubility in the parent phases but having an intermediate compound γ with a region of solubility from C_1 to C_2 at T_o. After time t a homogeneous region of γ phase extends from x_1 to x_2. In the γ-phase the composition profile will be a portion of an error function of the form

$$C = A - B \text{ erf } \lambda/2\sqrt{D} \qquad (1.5)$$

That is, the profile can be drawn in λ-space (Figure 1.4) and so the growth of the γ-phase will be parabolic. The constants A and B in equation (1.5) may be determined by the boundary conditions at $\lambda = \alpha_1$ and $\lambda = \alpha_2$; namely, $C = C_1$ at $\lambda = \alpha_1$ and $C = C_2$ at $\lambda = \alpha_2$.

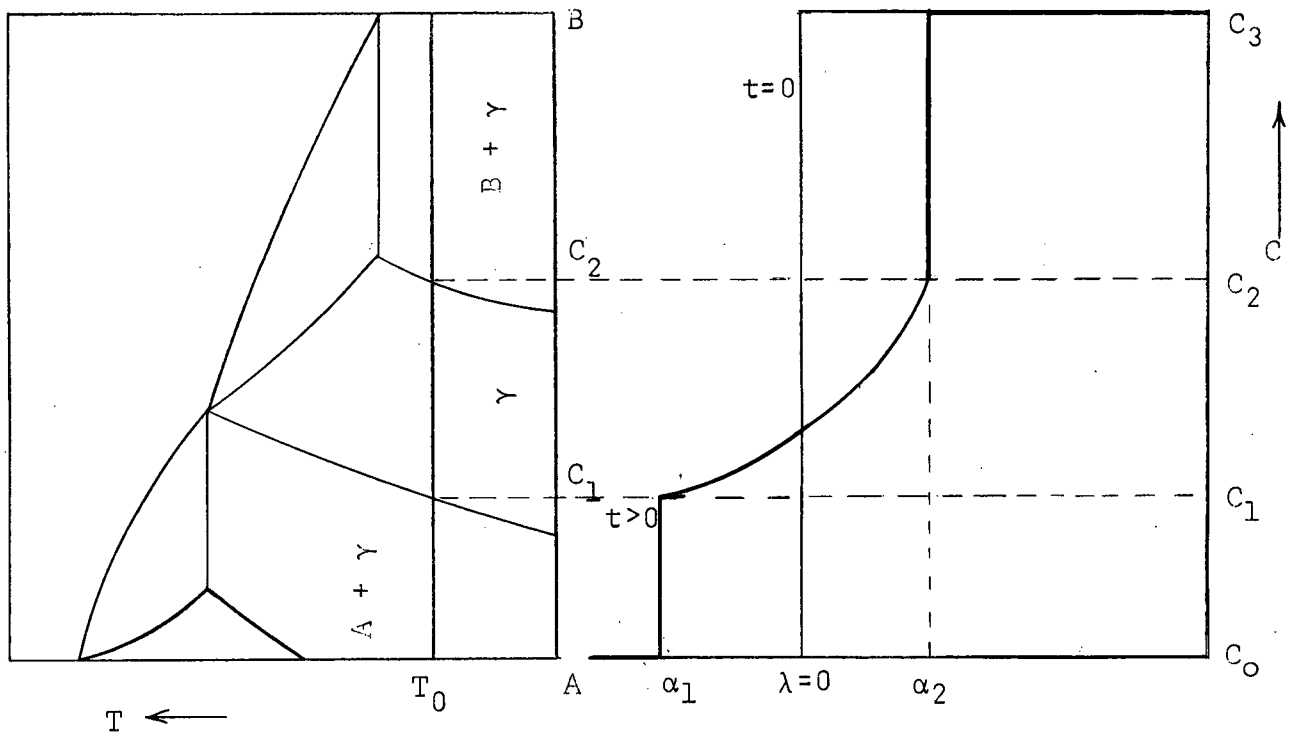

Figure 1.4 Diffusion Couple in an Intermediate Phase System with no Terminal Solid Solubility.

The resulting concentration profile is:

$$C = C_1 + (C_2 - C_1)\left[\frac{\text{erf } \alpha_1/2\sqrt{D} - \text{erf } \lambda/2\sqrt{D}}{\text{erf } \alpha_1/2\sqrt{D} - \text{erf } \alpha_2/2\sqrt{D}}\right] \qquad (1.6)$$

$$C = C_2 + (C_2 - C_1)\left[\frac{\text{erf } \alpha_2/2\sqrt{D} - \text{erf } \lambda/2\sqrt{D}}{\text{erf } \alpha_1/2\sqrt{D} - \text{erf } \alpha_2/2\sqrt{D}}\right] \qquad (1.7)$$

To obtain expressions for α_1 and α_2 mass balance conditions across the interface can be applied and equations (1.6) and (1.7) used to derive the final result.

Simplified Method for Finding α_1 and α_2

If the composition range of the intermediate phase is assumed to be small (5% or less), the concentration gradient in the phase may be taken to be linear to a first approximation. Figure 1.5 shows the resulting profile in λ-space.

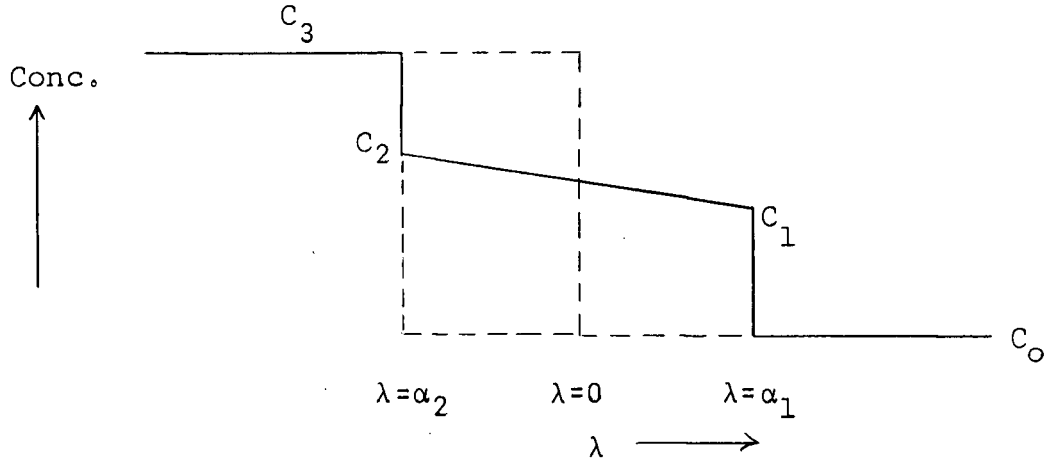

Figure 1.5 Concentration Profile of an Intermediate Phase System in λ-Space.

From this figure it can be seen that

$$\frac{dc}{d\lambda} = - \frac{C_2 - C_1}{\alpha_1 - \alpha_2} \qquad (1.8)$$

The interface mass balance condition at α_1 is that the flux across the boundary in a time dt causes the phase boundary to move a distance $d\xi$ in the direction of the net mass flow. Thus, at the α_1 interface, the condition becomes:

$$- D\left(\frac{\partial c}{\partial x}\right)_\xi dt = (C_1 - C_o)d\xi \qquad (1.9)$$

Setting $\xi = \alpha\sqrt{t}$ and $\lambda = x/\sqrt{t}$ leads to

$$- D\frac{dc}{d\lambda} = (C_1 - C_o)\frac{\alpha_1}{2} \qquad (1.10)$$

Substituting (1.8) into (1.10) gives

$$\alpha_1(\alpha_1 - \alpha_2) = 2D\frac{(C_2 - C_1)}{(C_1 - C_o)} \qquad (1.11)$$

Similarly the mass balance condition at the α_2 interface gives:

$$\alpha_2(\alpha_1 - \alpha_2) = -2D\,\frac{(C_2 - C_1)}{(C_3 - C_2)} \qquad (1.12)$$

Using equations (1.11) and (1.12) it can be found that

$$\alpha_1^2 = \frac{2D(C_2 - C_1)(C_3 - C_2)}{(C_1 - C_o)(C_3 - C_2 + C_1 - C_o)} \qquad (1.13)$$

Thus α_1^2 may be set equal to the diffusion coefficient times some constant γ, say, which depends only on concentration. This may be written as

$$\alpha_1^2 = D\gamma = K_1 \qquad (1.14)$$

where K_1 is henceforth referred to as the diffusion rate constant. Since $\alpha_1^2 = x_1^2/t$, we can write that $x_1 = \sqrt{K_1 t}$. Equation 1.13 shows that x_1 is proportional to both $\sqrt{D}$ and $\sqrt{C_2 - C_1}$. If $C_2 - C_1$ tends to zero - that is, the stoichiometry range of the intermetallic compound tends to zero - then x_1 will become very small. A large value of x_1 under these circumstances would imply an exceptionally large value for D. A similar expression to 1.13 may be derived for α_2^2 giving $x_2 = \sqrt{K_2 t}$.

Effect of Temperature

The diffusion coefficient, D, changes with temperature according to the Arrhenius-type equation

$$D = D_o \exp(-E_1/RT) \qquad (1.15)$$

In most systems having an intermediate phase the composition limits change little with temperature. Thus in equation (1.13) the difference $(C_2 - C_1)$ is not expected to vary significantly with temperature and so the temperature dependence of α_1 and α_2 will be due to the variation of the diffusion coefficient. Even if there is a change in composition range with temperature, a straight line

Arrhenius plot for α_1 and α_2 would still be expected since (C_2-C_1) should theoretically vary with temperature[27] according to an exponential law; namely,

$$(C_2-C_1) = \beta \exp(-E_2/RT) \qquad (1.16)$$

Substituting in this equation using equation (1.13) gives:

$$K_1 = (D\beta\Delta)\exp(-E_2/RT) \qquad (1.17)$$

$$\text{with} \quad \Delta = \frac{(C_3-C_2)}{(C_1-C_o)(C_3-C_2+C_1-C_o)}$$

The terms (C_3-C_2), (C_1-C_o), and $(C_3-C_2+C_1-C_o)$ in this expression will change by negligible amounts compared to (C_2-C_1). Thus it can be seen that

$$K_1 = K_o \exp(-E/RT) \qquad (1.18)$$

where $E = E_1 + E_2$.

In systems having more than one intermediate phase, the motion of the individual phases is still parabolic. Diffusion in such a system will be qualitatively similar to the special case discussed above. A solution to the n-component diffusion couple is complex but has been derived by Buckle[28] and Kidson[29].

1.4 The Structure of Evaporated Thin Films

1.4.1 Thin Film Nucleation[2]

The initial stage of growth of most deposited films consists of the formation of three-dimensional nuclei. The theoretical treatment[30] is concerned with the nucleation of a thin film condensed from the vapour phase on a substrate held at a temperature lower than that of the evaporating source. After impingement on the substrate the vapour atoms can either adsorb and stick permanently to the substrate, they can adsorb and re-evaporate in a finite time, or they can immediately rebound off the substrate. The first two cases are by far the most common.

An atom adsorbed on a substrate can migrate over the surface giving rise to collisions with other atoms, and aggregates of adsorbed atoms can now exist. Aggregates should be more stable toward re-evaporation than single adsorbed atoms, since they are bound to each other by the condensation energy. While the aggregates are very small however, their surface-to-volume ratio is very high and the resulting high total surface energy causes them to have a higher vapour pressure than the bulk material and thus to dissociate again. Consequently there is a size at which the stability of the aggregate is a minimum. Adding another atom to an aggregate of critical size makes it more stable. This may occur by direct impingement and incorporation of atoms from the

gas phase, or by collision with adsorbed atoms diffusing over the substrate surface.

The critical radius r* of a stable aggregate is calculated by considering the total free energy of the aggregate as a function of size. This free energy involves the free energy of condensation, the surface energies of both aggregate and substrate, and the interfacial energy between the aggregate and substrate. It is possible to find both the critical mean linear dimension of the aggregate and the critical free energy of formation (ΔF^*) of the stable aggregate. Figure 1.6 shows the dependence of the free energy of an aggregate on its size.

The relative magnitudes of r* and ΔF^* determine the basic structure of the thin film deposit. Films having a nucleation barrier, that is, a large r* and a high free energy of formation will be coarse-grained having an island structure up to relatively high average film thicknesses. In the low nucleation barrier regime the film is generally much finer-grained since a dense population of small islands grow together at an early stage in the deposition process and become continuous at low average film thicknesses. The tendency to form an island structure is greater in a low boiling-point material due to the weak bonding between atoms and hence the high volume free energy of condensation. Elements such as Cd, Zn, Se, Te, and Sb will therefore remain as island structures up to large film thicknesses

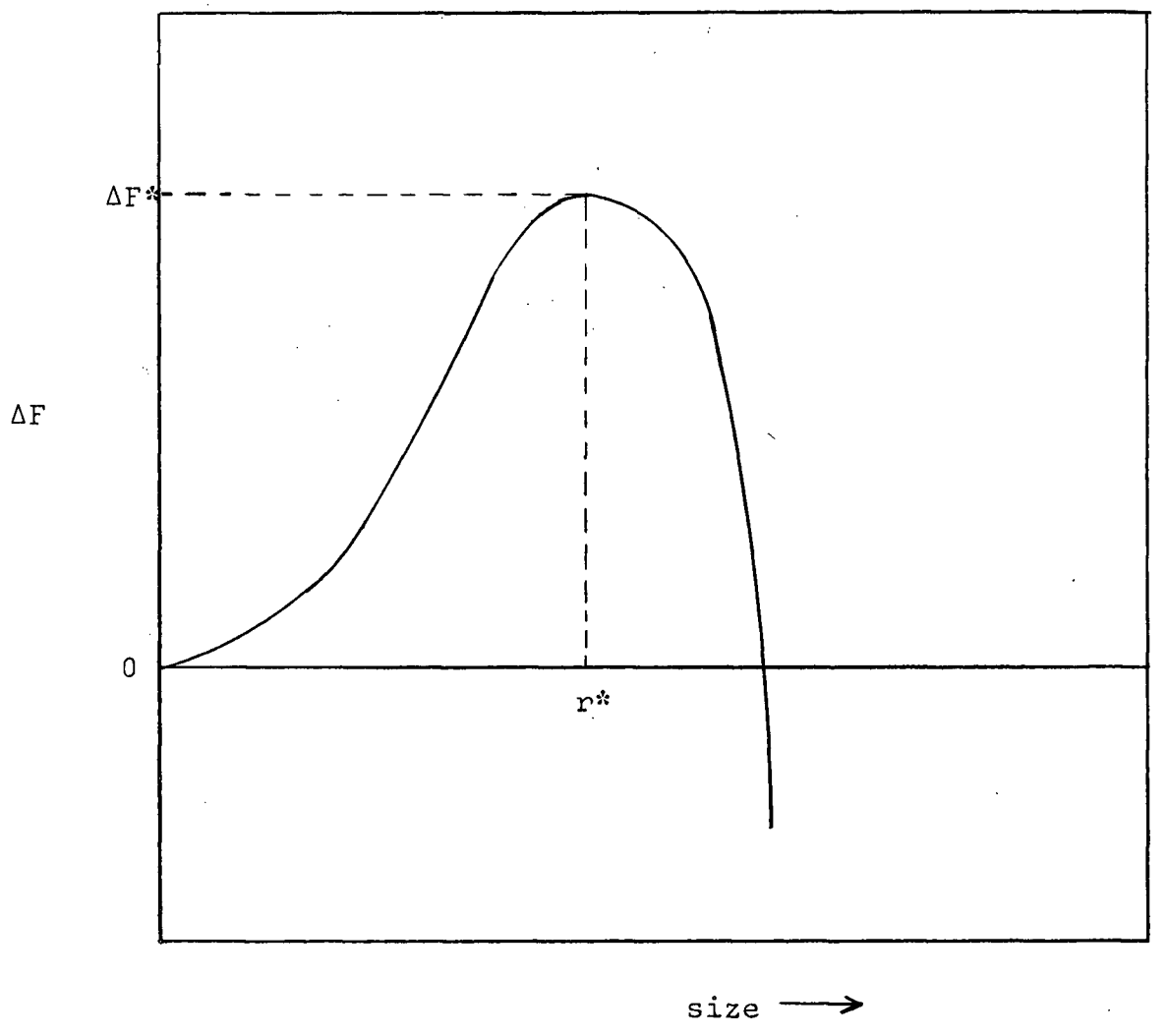

Figure 1.6 The Free energy of Formation of an Aggregate of Film Material as a Function of Size. The aggregate has minimum stability at the critical radius r*.

while Au and Ag, for example, will tend to form continuous films. Other factors promoting the formation of island structures include: (1) a high substrate temperature, (2) a low deposition rate, (3) weak binding forces between film and substrate, (4) a high surface energy of the film material, and (5) a low surface energy of the substrate. These factors, although mentioned only briefly, have a very profound influence on the sub-structure of a thin film[4,5,31].

1.4.2 The Growth of Thin Films[5,32]

The characteristic stages in the growth of a thin film are: (1) the formation of a surface distribution of small three-dimensional nuclei, (2) the growth in size of these nuclei without any increase in their numbers, (3) further increases in size of the nuclei or islands accompanied by a gradual but considerable decrease in their numbers, (4) the formation of a connected network of deposit usually rapidly developing into a channelled structure, (5) a continuous deposit film free of holes (see Fig. 1.7). This sequence of growth events is generally the same for both epitaxial films deposited on single-crystal substrates and polycrystalline films evaporated onto amorphous substrates. The average film thickness of the films at each growth stage are usually different, however. One of the most striking phenomena which occur during the growth of a film is the liquid-like

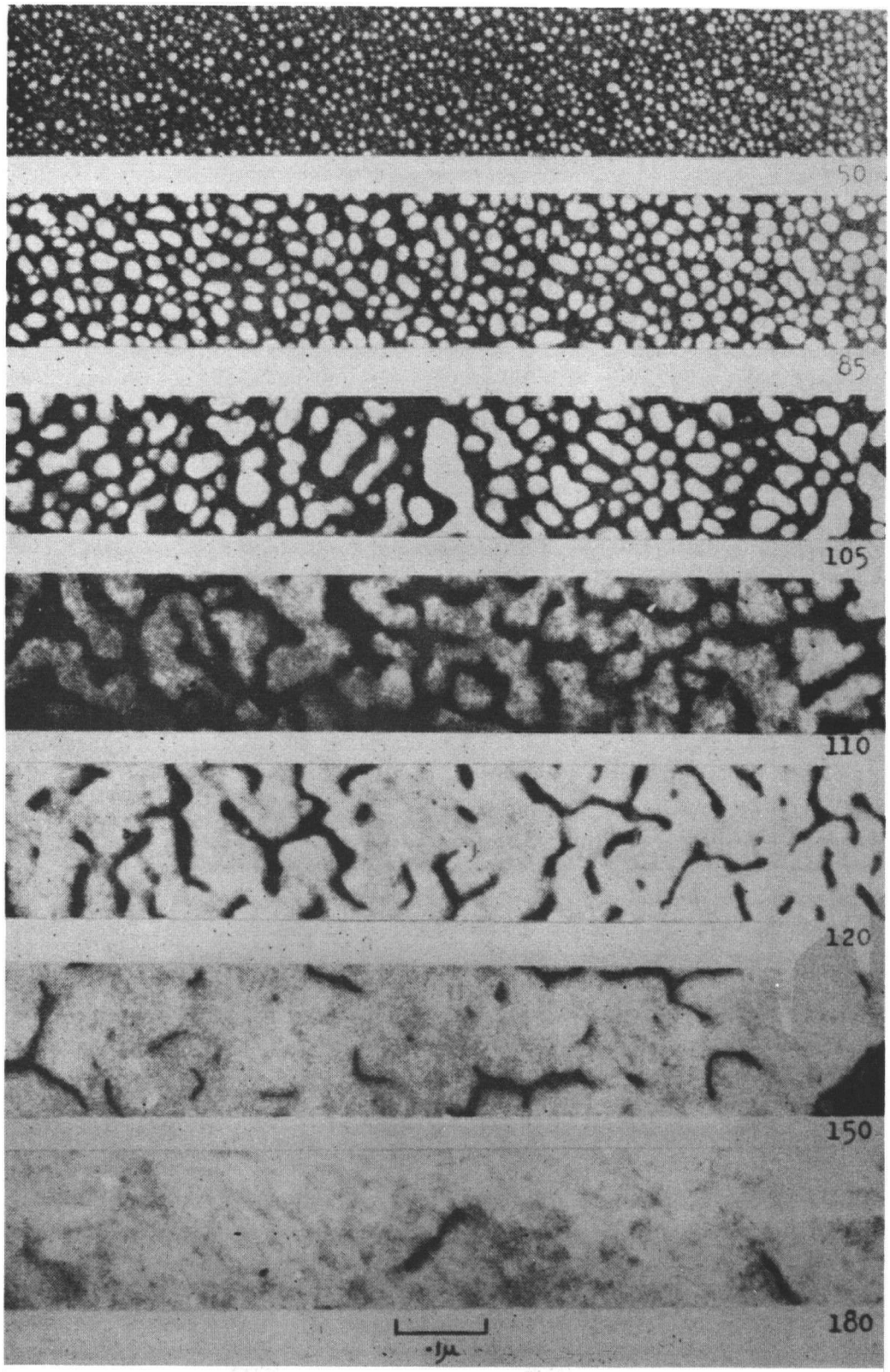

Figure 1.7 Growth of an Ag Film (after Sennett and Scott[33])

coalescence of randomly oriented nuclei and islands which takes place as the nuclei or islands touch one another.

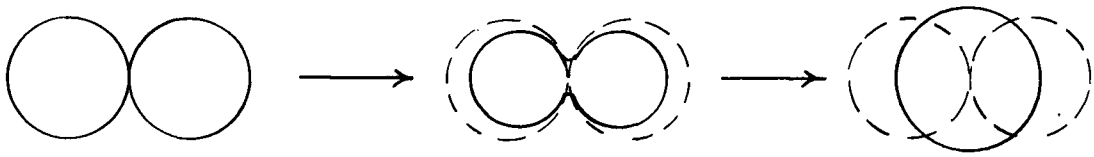

Figure 1.8 Manner of Coalescence of Two Small Rounded Nuclei. (Pashley[32])

The effect is illustrated in Figure 1.8 for the case of nuclei which have round profiles. When the islands are small (say less than 200 Å across) the complete coalescence appears to take place instantaneously and the compound island has a greater thickness than the two initial islands. The composite island has a single orientation that may differ from the orientations of the parent islands. The mechanism of coalescence is completely analogous to that of sintering and is explained in terms of the surface mobility of deposit atoms over the deposit (rather than the substrate) with the driving force for the transfer of material between islands being the surface

energy. As the coverage of the substrate becomes high, the islands have increasing difficulty in assuming their favoured crystallographic shapes, and an open network structure is eventually formed. Finally the elongated channels in the network become filled in and a continuous film is formed.

The three predominant deposition parameters are chamber pressure, deposition rate and substrate temperature. While most of the investigations of the effect of these variables on a deposit have been done for single-crystal films[32,34], there is some evidence available for polycrystalline films as well[5,32]. The chamber pressure determines the quantity of residual gases present during evaporation. Adsorbed impurity gas atoms on the substrate can decrease surface mobilities and result in small grain sizes. The deposit film may be porous and highly disordered if gas atoms are trapped by the deposit or impure if any residual gases with a high chemical affinity for the film are present. With increasing substrate temperature the size of the crystallites (islands) increases due to a higher surface mobility of the deposit atoms and the grain size of the deposit becomes larger. For a given substrate temperature the grain size of a polycrystalline film is usually finer and less agglomerated the higher the rate of deposition. This is because highly mobile surface atoms at high deposition rates become buried in random sites by successively arriving atoms before finding

appropriate lattice sites.

1.4.3 The Properties of Thin Films

A. Lattice Defects

The main classes of lattice defects may be listed as follows: (1) dislocation lines, (2) stacking faults, (3) microtwins, (4) aggregation of point defects, (e.g. dislocation loops and stacking-fault tetrahedra). At the stages before a continuous hole-free film is formed, there are few dislocations, and the initial nuclei are completely free of dislocations[5,32]. The way in which the dislocation density increases during growth of the film is shown in Figure 1.9. Appreciable numbers of dislocations appear only when the network stage of growth is reached. Five proposed mechanisms for the intro-

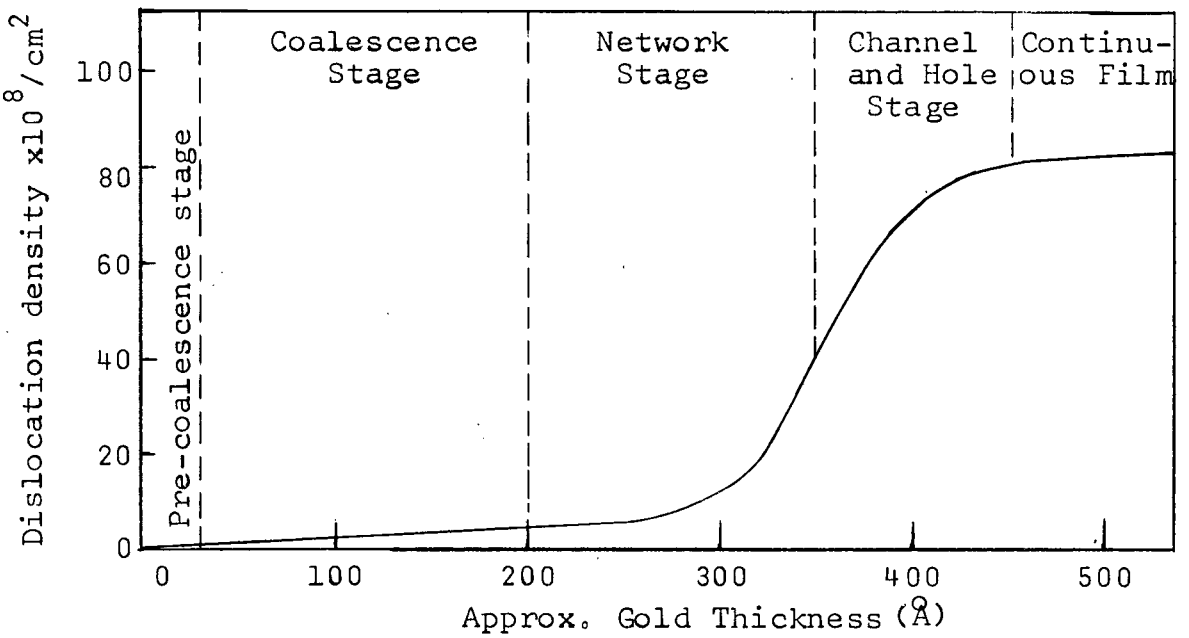

Figure 1.9 The Density of Dislocations (per unit area of substrate) in a Gold Deposit.

duction of growth imperfections are:

(1) The extension of imperfections already existing at the substrate surface.

(2) The formation of imperfections to accommodate any orientation differences between joining nuclei.

(3) The formation of imperfections to accommodate displacement misfits between joining nuclei.

(4) The formation of point defects and their aggregation to form dislocation loops and other imperfections.

(5) Plastic deformation of the film at various stages of growth.

B. Stresses in Thin Films

Vacuum deposited films can be in a state of high mechanical stress. The magnitude of the stress can be very high and in some instances exceeds the normal bulk yield stress of the material[7]. The origin of this stress is not clearly understood. There are two components of the stress, the first due to any temperature differences between substrate and deposit during deposition (thermal stress) and the second any additional stress due to structure (intrinsic stress). Intrinsic stress can be generated by enclosed gas atoms or impurities, by freezing-in of lattice defects during condensation, or by surface effects due to the small thicknesses involved (for example, surface tension). Also, oxides or other

chemically bound surface layers can contribute to the stress in a manner similar to the interface between substrate and film[31,35]. Stress resulting from lattice disorders which accounts for most of the intrinsic stress on a film can be relieved by annealing or by the choice of a higher deposition temperature.

CHAPTER 2

EXPERIMENTAL PROCEDURE

2.1 Vacuum Equipment

Thin film depositions were carried out in a CVC-14 vacuum unit capable of an ultimate pressure of 5×10^{-8} Torr in the working chamber. Modifications were made to the basic system so that four evaporation sources were available. An aluminum masking plate was installed at a distance of 25 cm. above the base-plate giving an effective source-to-specimen spacing of 22 cm. A rotation seal was machined so as to impart both a lifting and rotation motion to all specimen holders. This enabled specimens to be set in place on a mask directly above any one of four sources during a single pump-down. A 1/8" diameter Al wire was installed in the bell jar at a distance of 1 1/2" from the specimen plane to provide glow-discharge cleaning during the roughing part of the pump-down cycle. This wire was inserted into one of the main base-plate plugs. Prior to evacuation of the vacuum chamber, an 85 mm. glass cylinder was placed around each evaporation source so as to prevent contamination of

other sources and samples. Slides were attached to the specimen holder with scotch tape. Glass cover slides .0015" thick were used for masking. A mask could be in any desired shape depending on the experiment. Figure 2.1 shows the details of the vacuum equipment.

2.2 Film Deposition

2.2.1 Sample Preparation

Specimens were prepared on glass microscope slides. Each slide was rinsed with a detergent solution, polished with lens tissue, and subjected to the breath test* before being inserted into the vacuum chamber. To complete the cleaning process[36] the slide was exposed to a glow discharge inside the vacuum system for 10 minutes during the first part of the pumping cycle. The evaporations were carried out in a vacuum of 2×10^{-6} Torr using resistance heated .010" molybdenum boats. The substrates, mounted 22 cm. above the evaporation sources, could be rotated so as to lie directly above each source in turn. It was calculated[30] that at this source to specimen distance the variation in thickness across the slide would be less than 2%.

In kinetic studies two diffusion couples were evaporated onto a single microscope slide using suitable

---

* Breath test: Slide is clean to within one or two monolayers of contamination when a breath mark on it disappears rapidly.

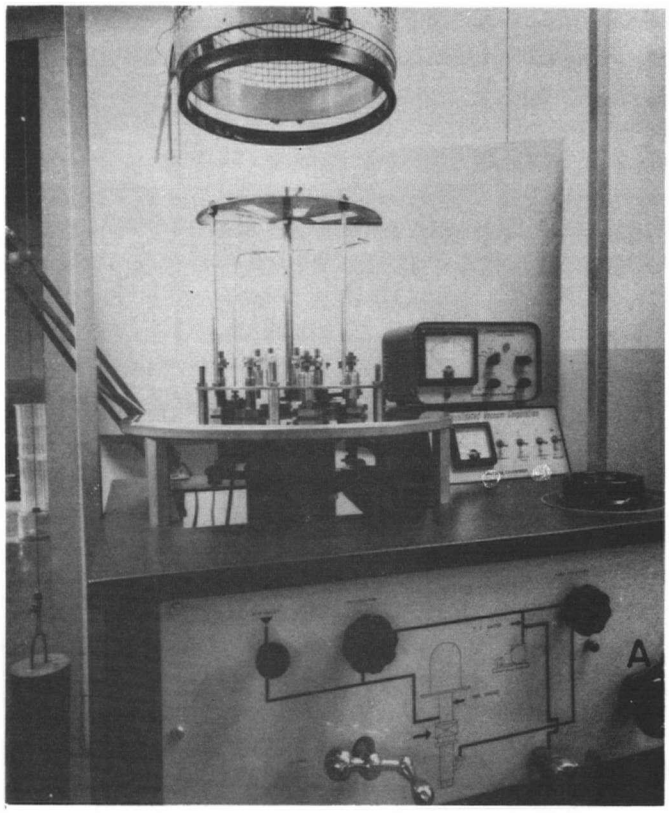

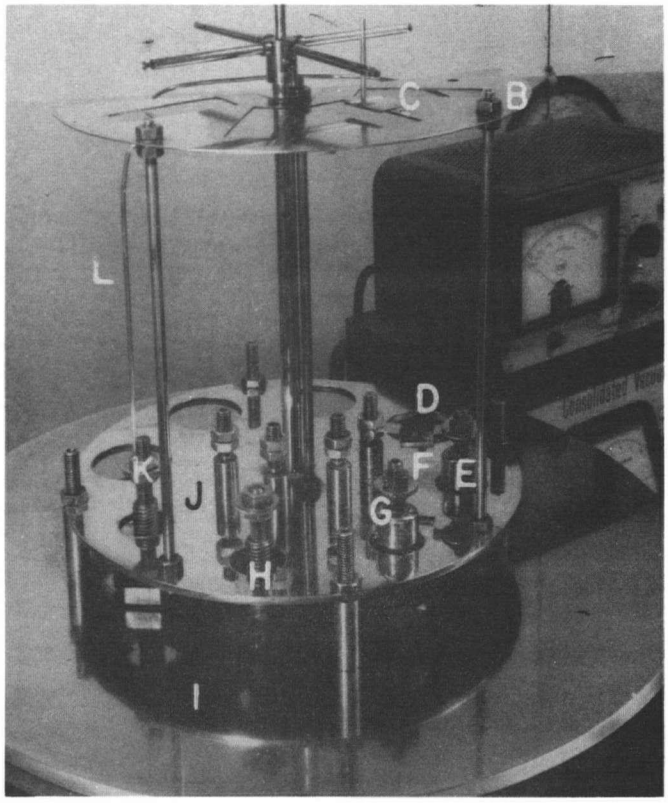

LEGEND

A evaporation source selector switch

B masking plate

C specimen holder

D rotation control

E #4 evaporation source

F Mo boat

G #3 evaporation source

H #2 evaporation source

I main base plate

J brass base-plate

K #1 evaporation source

L glow discharge ring

Figure 2.1 Vacuum Equipment

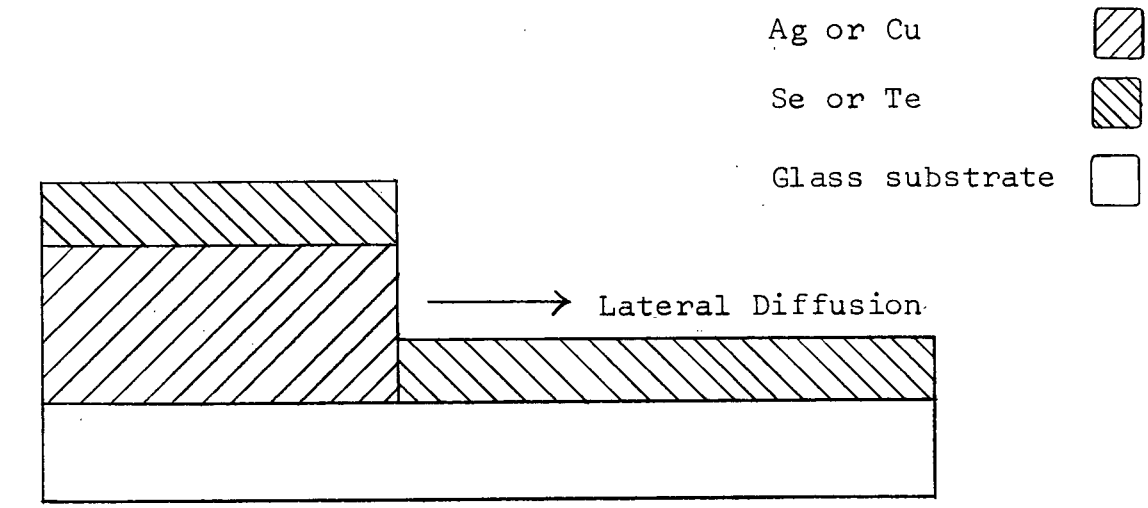

(a)

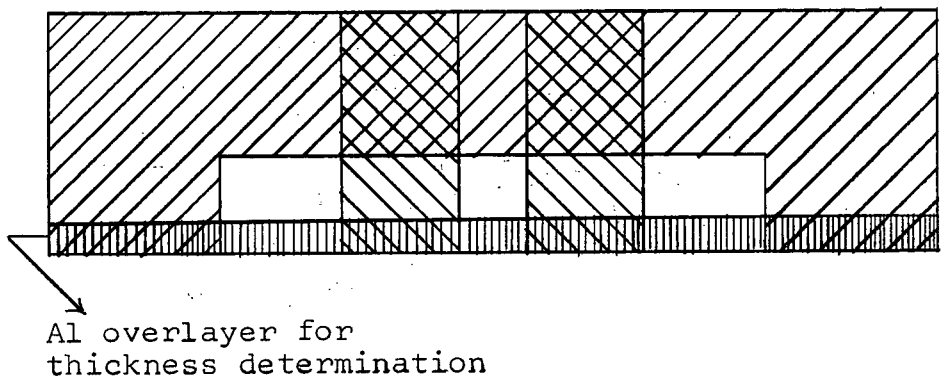

(b)

Figure 2.2 Main Evaporation Configuration

masks above each source. Figure 2.2 (a) shows the main experimental configuration used to observe lateral diffusion and Figure 2.2 (b) shows the layout of samples on the microscope slide substrate. A film of Ag or Cu was first deposited over part of the slide and allowed to cool for a minimum of 15 minutes in order to ensure that the substrate would be at room temperature for successive evaporations. The slide was then rotated into place over two Te or two Se sources in succession and evaporation across the existing Ag or Cu step was carried out. A time of 3 minutes was allowed between the two evaporations.

2.2.2 Film Thicknesses

For purposes of measurement of film thicknesses an opaque strip of Al was evaporated across the film steps at the clear edge of the slide (Figure 2.2 (b)). The method of Fizeau fringes of constant thickness as described by Tolansky[37] was used to determine the film thickness. In this technique a partially silvered (4-6% transmission) optical flat is brought close to the Al over-layered step. If the relative positions of slide and flat are adjusted so as to form a wedge shaped air gap, and the interferometer is illuminated by a beam of parallel monochromatic light, a series of dark fringes can be made to run in straight lines perpendicular to the steps on the opaque film. These fringes trace out the points of equal air

gap thickness and their separation corresponds to an increase in gap thickness of $\lambda/2$ where λ is the wavelength of the light. The fringes show a displacement as they pass over the step edge and measuring this as a fraction of the fringe spacing gives the film thickness in units of $\lambda/2$. Figure 2.3 shows the interferometry arrangement and some typical fringe systems observed.

2.2.3 Temperature Tests

Temperature tests in the range 30-100°C were carried out in a water bath controlled to $\pm$ 1.5°C by insertion of the sample slide into a 1" diameter test-tube immersed in the water. The test-tube was sealed with a rubber stopper to reduce convection heat losses. Tests at 0°C were carried out in an ice-water mixture. Thermometer readings were made on the bath every hour during a run as a check on the temperature controller.

2.2.4 Measurement of Diffusion Rate Constants

The diffusion rate constant was determined by measuring the width (x) of the lateral diffusion zone as a function of time. Measurements were made using a calibrated travelling eyepiece on a metallurgical microscope.

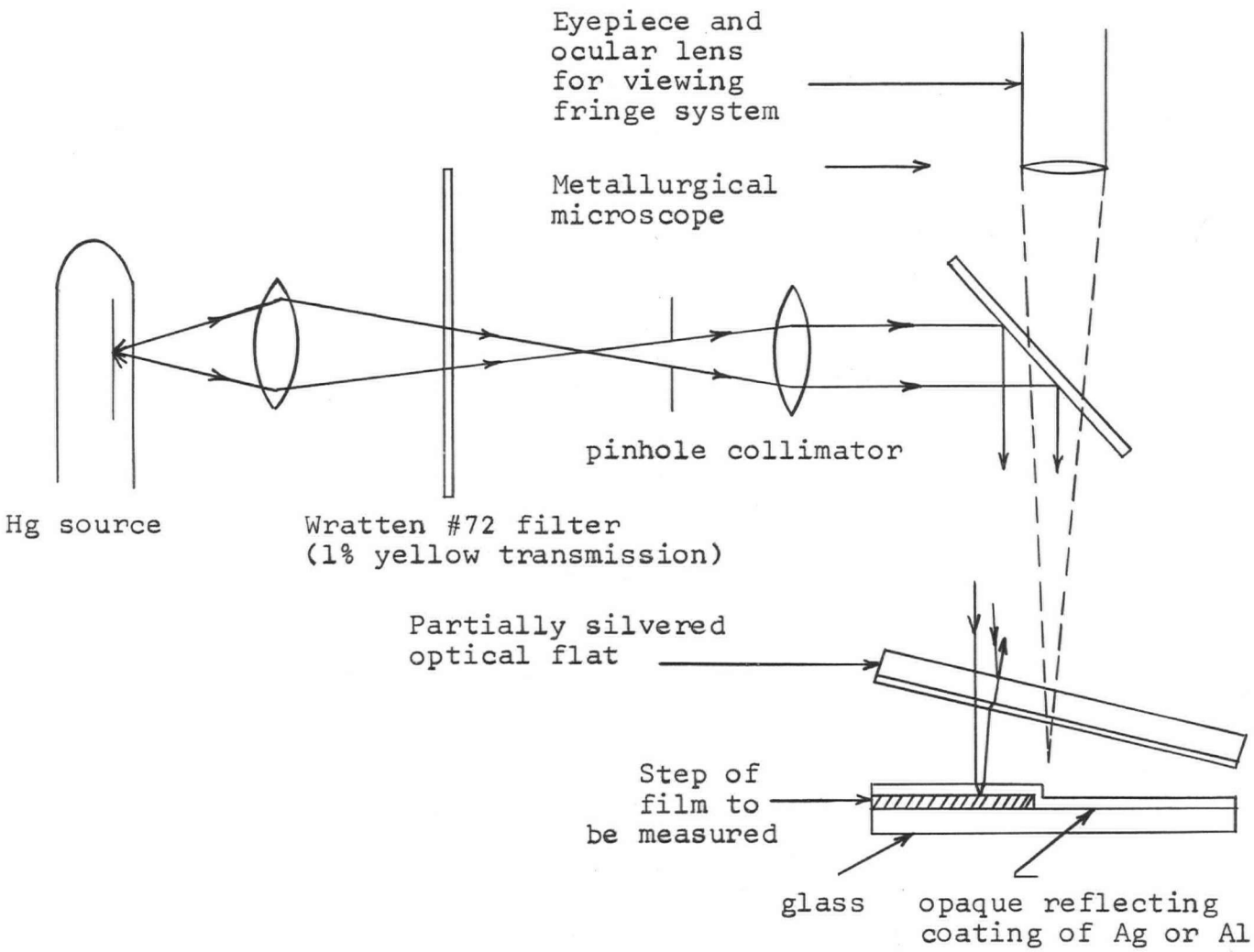

Observed Fringe Patterns

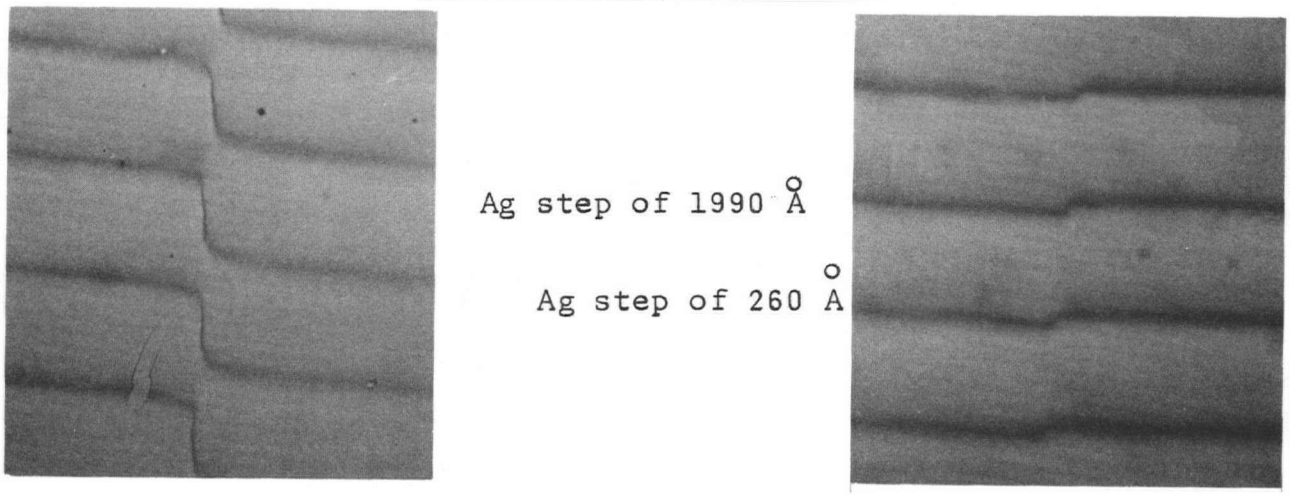

Figure 2.3 Measurement of Film Thicknesses

2.2.5 Electron Microscopy

A thin evaporated carbon film floated onto a 150 mesh specimen grid in distilled water provided a substrate for an evaporated diffusion couple that could be studied by transmission electron microscopy. The specimen grid with its attached carbon support film was taped by one edge to a microscope slide and a diffusion couple was deposited on it in the configuration shown in Figure 2.4. The slide was masked so as to facilitate film thickness measurements. A cooling time of at least 15 minutes was allowed between the two required evaporations.

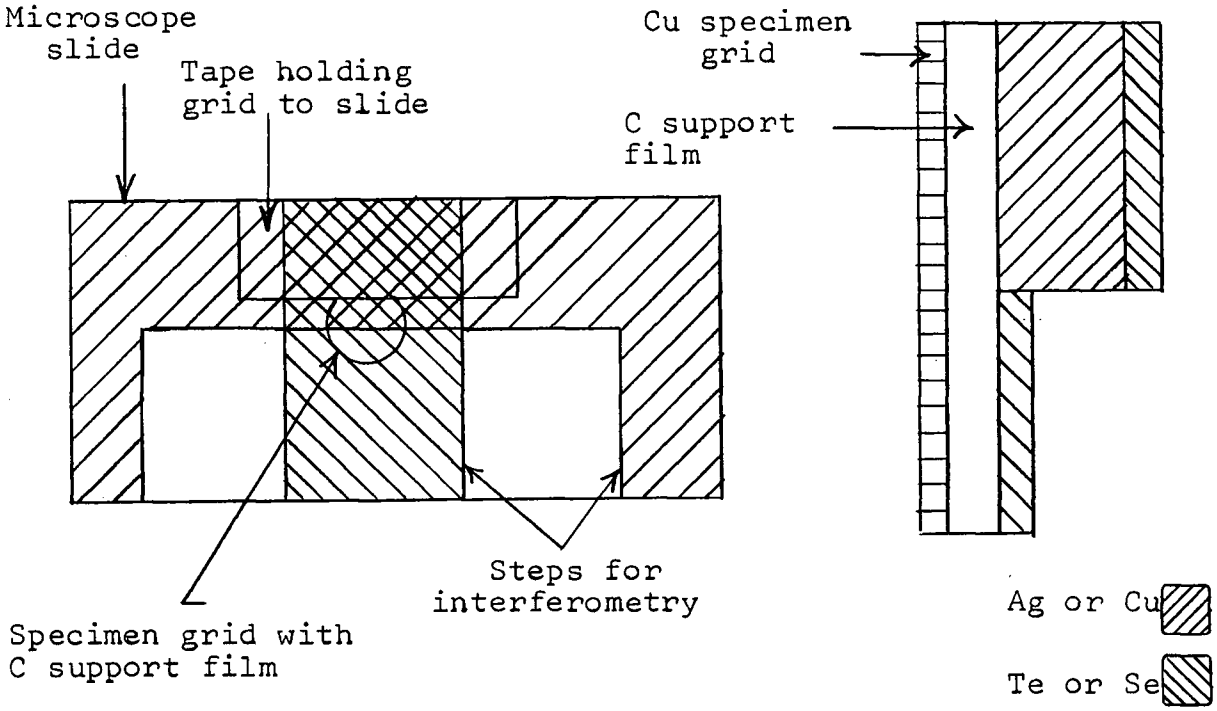

Figure 2.4 Evaporation Configuration for Electron Microscopy Specimens.

2.3 Different Evaporation Configurations

Three other evaporation configurations in Cu-Te were investigated to see if any lateral diffusion occurred. The geometries involved are shown in Figure 2.5. The occurrence of lateral diffusion in 2.5 (a) or (b) - that is, the advance of a diffusion zone into the pure Cu film - would be due to the diffusion of the Te into Cu. In samples prepared in these two configurations no lateral diffusion was ever observed either by optical or electron microscopy even after annealing at 50°C for 2-3 hours. The reason that diffusion in this direction is not observed is probably due to the development of Kirkendall porosity (see page 7, Introduction) on the Cu/Cu-Te interface causing its rupture.

The geometry of 2.5 (c) should be exactly equivalent to that described in Section 2.1. Diffusion of Cu into the pure Te film should result in the formation and growth of a lateral diffusion zone. While there was some indication that lateral diffusion was proceeding immediately after the diffusion couple formation, the inevitable result of forming a sample in this way was that the entire Cu side became detached from the glass substrate and lifted away from the surface. With the resulting discontinuity between Cu-rich side and Te, diffusion could not proceed. The immediate and rapid loss of adhesion was probably due to both the poor adhesion

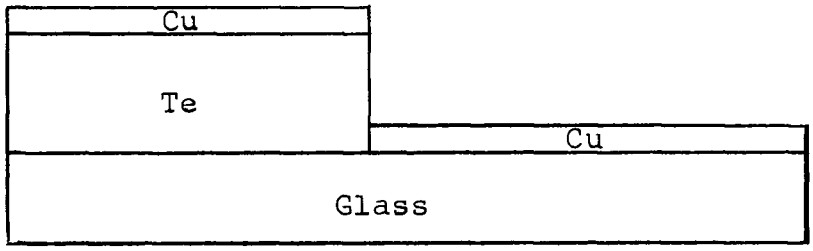

(a)

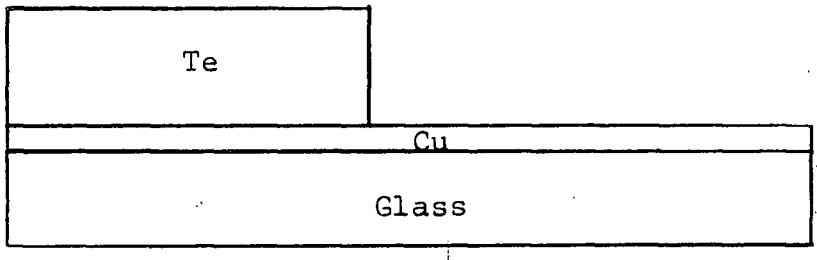

(b)

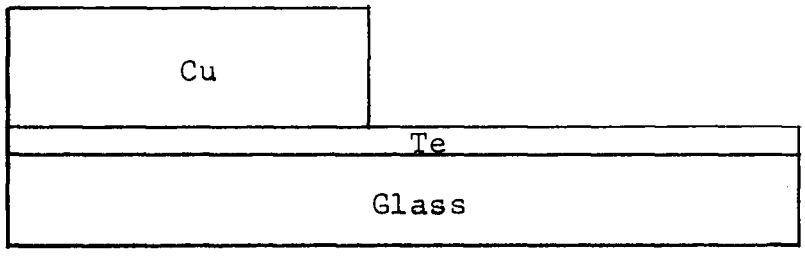

(c)

Figure 2.5 Alternative Evaporation Geometries

of the intermetallic compound produced by downward diffusion on the Cu side (which extends right to the glass surface) and the aggregation of the Te substrate film during the deposition of Cu. The evaporation of Cu requires a high power input to the source for sufficient lengths of time to produce 40-50°C temperature increases at the substrate. It was observed that the application of a thin Cr substrate to the glass before evaporating Te and Cu seemed to stabilize the Cu side for about 15 minutes during which time a thin lateral zone developed. At longer periods, however, the Cu side peeled off and diffusion ceased. Because of this adhesion problem - common to all four systems - a study of diffusion in this configuration was extremely difficult and further work was not attempted.

2.4 Other Systems

Table 2.1 lists 18 systems in which room temperature lateral diffusion was looked for without success. For a system X-Y, the evaporation configuration was as shown in the table and was generally arranged so that the faster diffusing atom would be in a position X. This was to avoid the development of porosity at the boundary of the diffusion zone. In all the additional systems investigated it was concluded that no lateral diffusion took place because the expected diffusion coefficients at room temperature were too small. Table 2.2 lists the expected diffusion coefficients as found in thin films (after Brown[9] where available) in

Table 2.1 Other Systems in which the Possibility of Lateral Diffusion Was Investigated

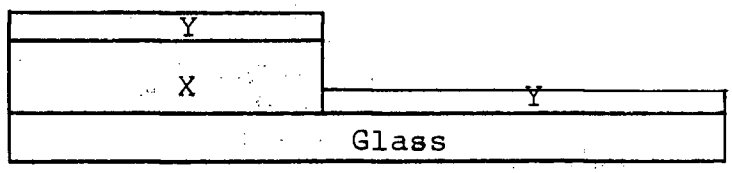

Pb-Te	Pb-Se	Ag-Cd	Ag-Sb	Cu-Sn
Al-Te	Al-Se	Cu-Cd	Cu-Sb	Au-Pb
Fe-Te	Bi-Se			Cu-Ge≠
Bi-Te				Cu-Al
Cd-Te				Ag-Al**
Au-Te				

≠ Annealed at 200°C for 4 hours

** Observed at 600°C in electron microscope hot-stage.

TABLE 2.2

Expected Diffusion Coefficients in some Possible Thin Film Diffusion Systems

System	Faster Diffusing Atom	T(°C)	D (cm^2/sec)
Ag-Al	Ag	21	$3x10^{-22}$
Cu-Al	Cu	21	$8.4x10^{-29}$ ≠
Ag-Cd	Ag	21	$1.5x10^{-16}$
Au-Pb	Au	21	$2.17x10^{-15}$
Cu-Sn	Cu	21	$1.13x10^{-36}$
Cu-Cd	Cu	21	$5x10^{-16}$ ≠
Au-Te	Au	90	$2x10^{-16}$
Cu-Ge	Cu	700	$3x10^{-5}$ ≠

≠ Bulk diffusion data[39].

some of these systems. At higher temperatures movement of the phase boundary interface would be expected but this was never observed even in the electron microscope hot stage due to interface rupture, diffuse interfaces, aggregation, oxidation, etc.

CHAPTER 3

LATERAL DIFFUSION IN Ag-Se

3.1 Introduction

Figure 3.1 shows the equilibrium phase diagram for Ag-Se[40]. At low temperatures only the phase Ag_2Se is thermally stable and it is expected that diffusion in the Ag-Se system will result in its formation. Ag_2Se undergoes an allotropic transformation at about 130°C. The low temperature β modification has been described as having either an orthorhombic or monoclinic structure while the α modification, stable above 130°C, has a CaF_2 structure[41].

Pure bulk Se has several allotropic forms[42,43]. The two most important modifications are the hexagonal, the most common form stable below the melting point, and the amorphous form which is induced by supercooling liquid Se. All of the evaporated thin films of Se observed in this work were amorphous in nature. The colour of the Se deposits varied from light orange for the very thin films (< 100Å) to deep red for the very thick films (> 4000 Å).

The experimental configuration of all Ag-Se thin film diffusion couples investigated is shown in Figure 3.2.

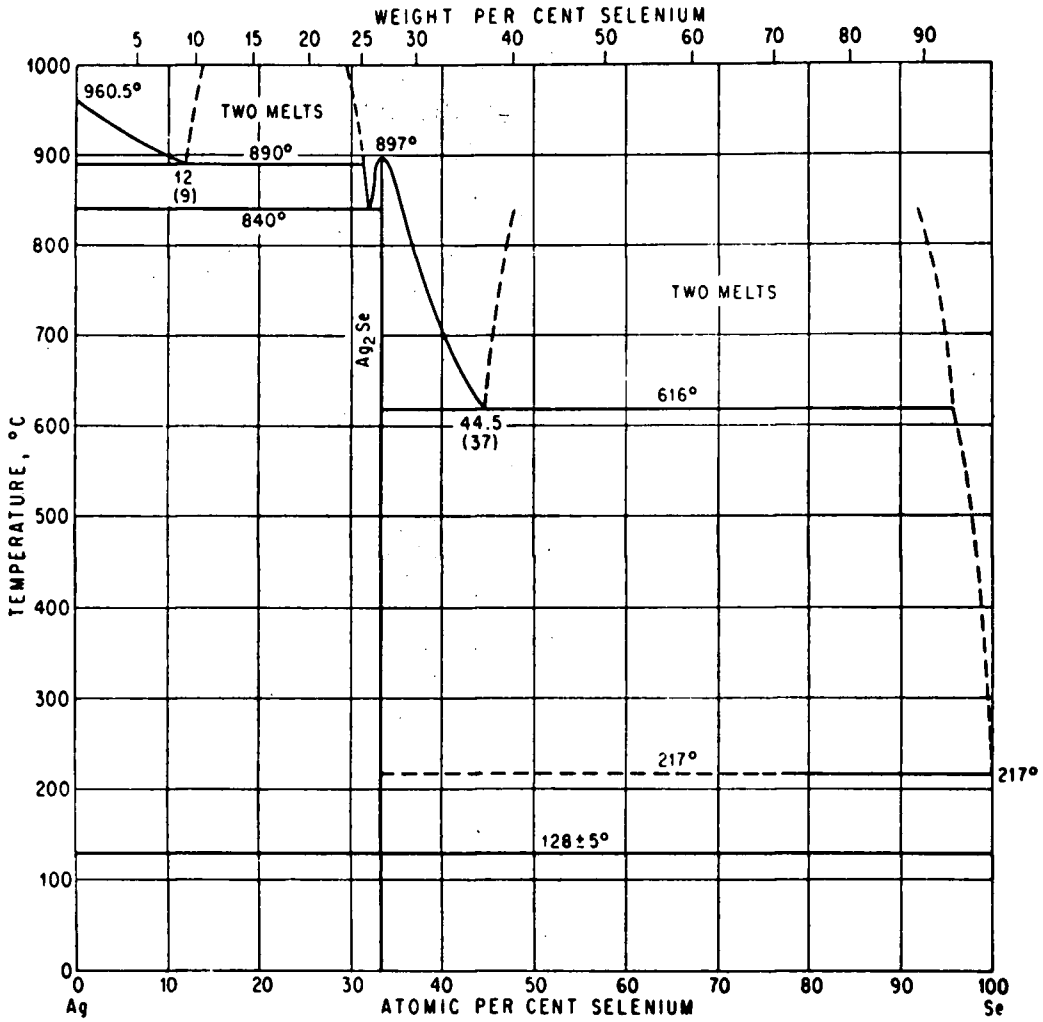

Figure 3.1 Equilibrium Phase Diagram for Ag-Se (Hansen[40]).

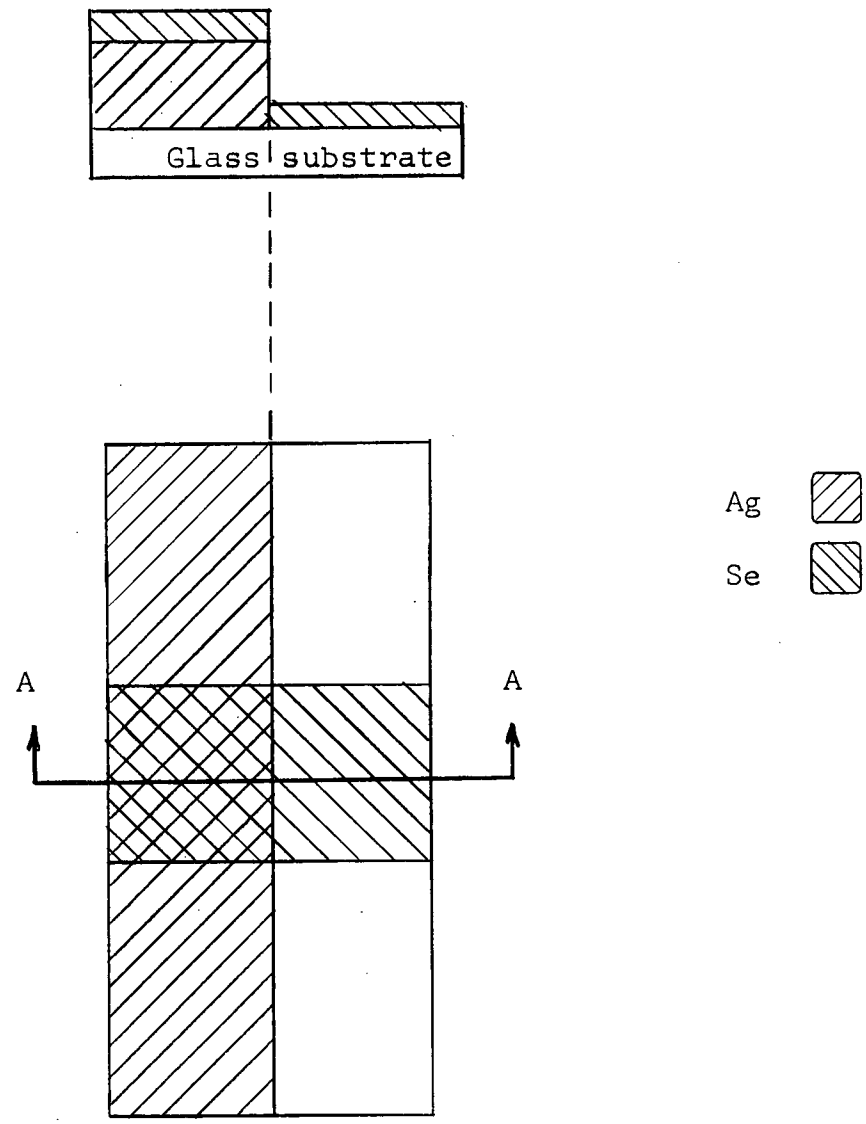

Figure 3.2 Ag-Se Diffusion Couple

Evaporation of the Se across the Ag step resulted in the immediate formation of the intermetallic compound Ag_2Se on the Ag side of the couple. During deposition this was evidenced by an immediate colour change ranging from blue-purple for very thin Se films to light grey for thick Se films. A white diffusion zone was observed at the interface A (figure 3.2) immediately after the sample was removed from the vacuum chamber. The growth of the diffusion zone proceeded rapidly at room temperature (21 $\pm$ 3°C) with a planar phase boundary interface advancing into the pure Se. The interface was seen to remain planar even after a long ageing time (750 hours).

3.2 Diffusion Kinetics

3.2.1 Growth Rate

A typical plot of the diffusion zone width x as a function of time is shown in Figure 3.3. In Figure 3.4, x is plotted against $\sqrt{t}$ and the linear dependence illustrates that the phase boundary motion obeys the parabolic law $x^2=Kt$ where K is the diffusion rate constant. Virtually all of the diffusion zones measured in the Ag-Se system exhibited this parabolic behaviour. As discussed in the "Introduction", parabolic growth is characteristic of diffusion control.

The series of photographs in Figure 3.5, made on an optical microscope, shows the growth of the Ag_2Se phase from t= 0 to t = 4 hours. The white band appearing between the diffusion zone and the Ag-Se region of the diffusion

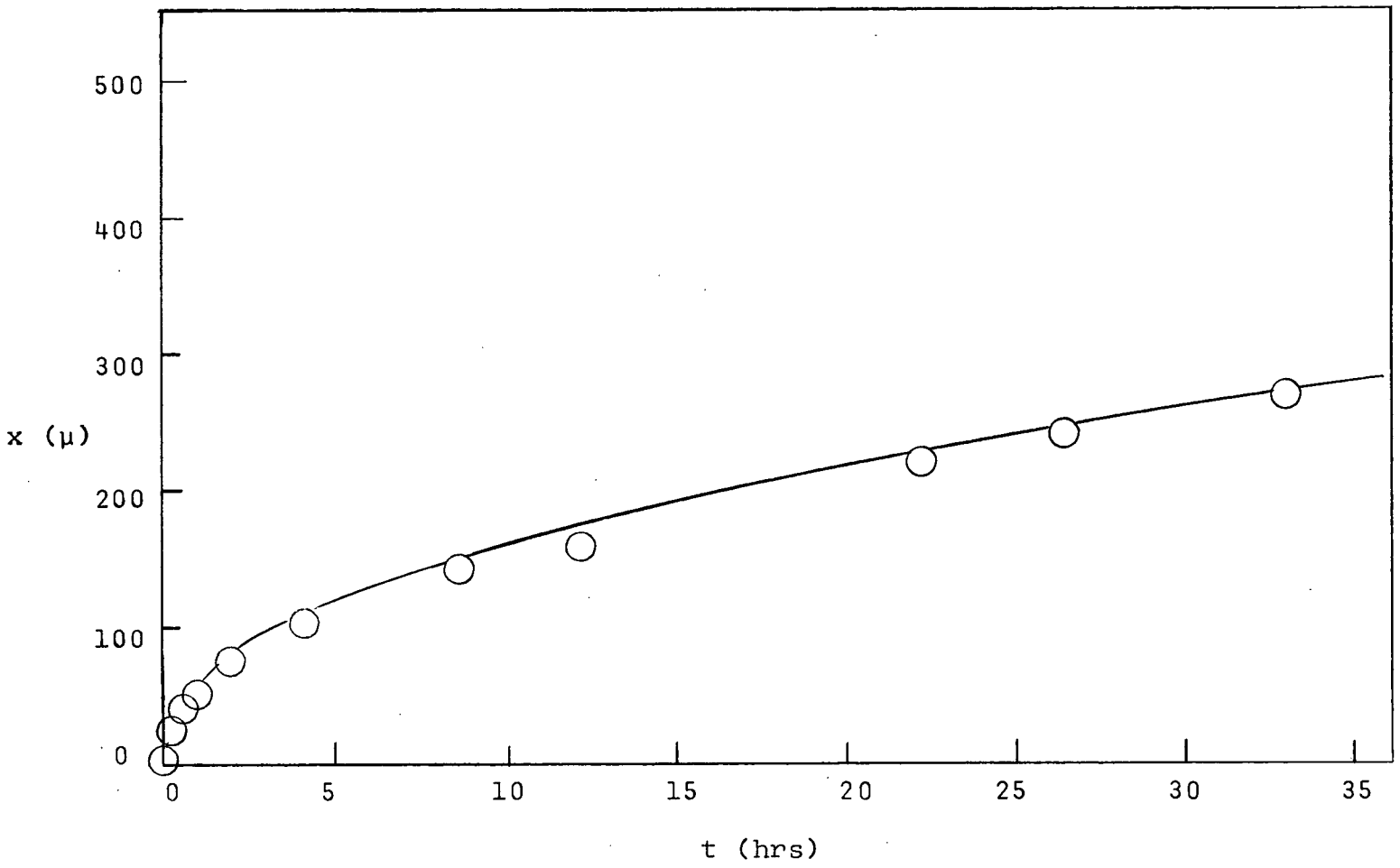

Figure 3.3 Typical Plot of x versus t at Room Temperature

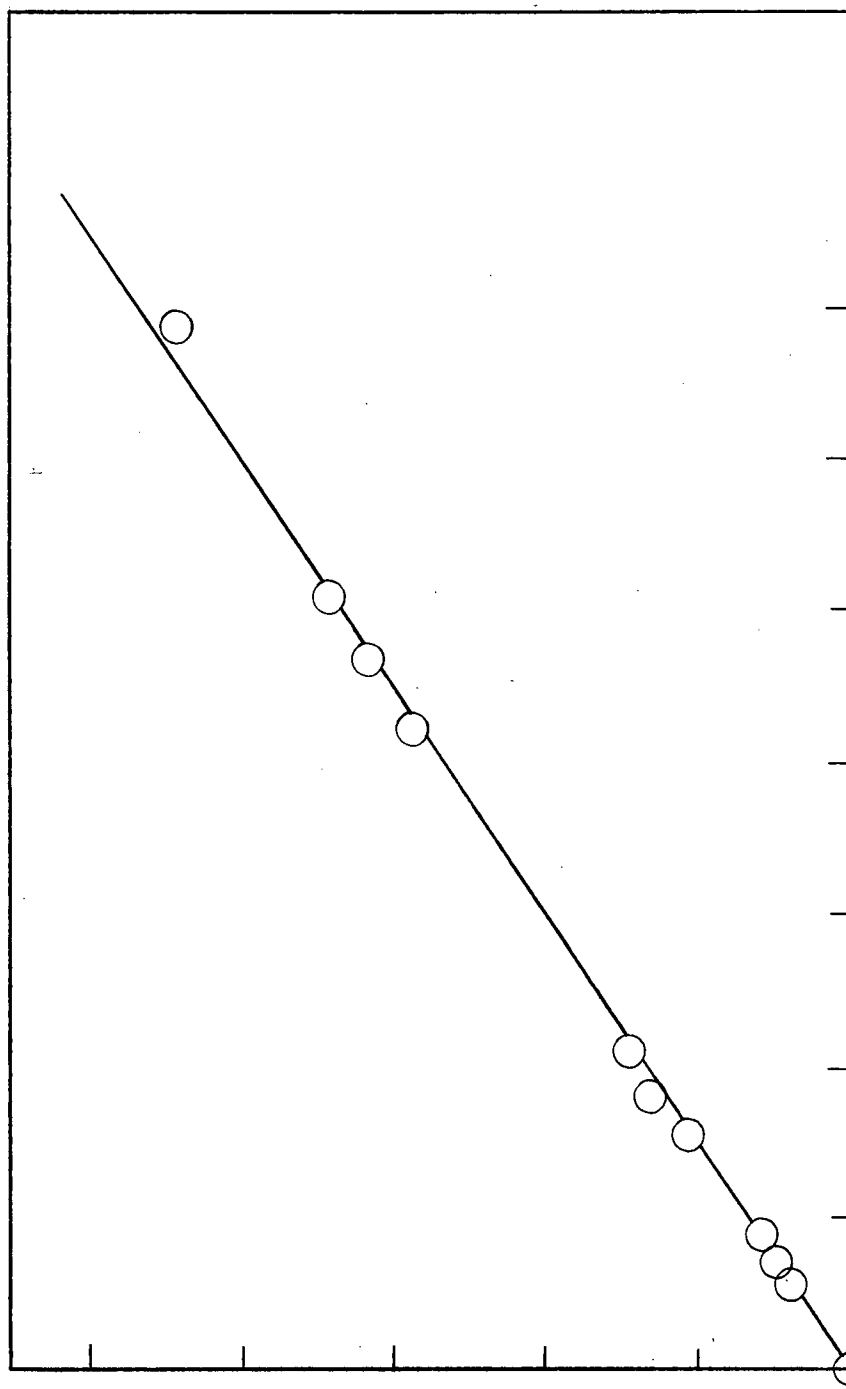

Figure 3.4 Plot of x versus $\sqrt{t}$

t_{Se} = 660 Å

t_{Ag}/t_{Se} = 6.8

Legend

A Se

B White Zone

C Ag+Se

D Diffusion Zone

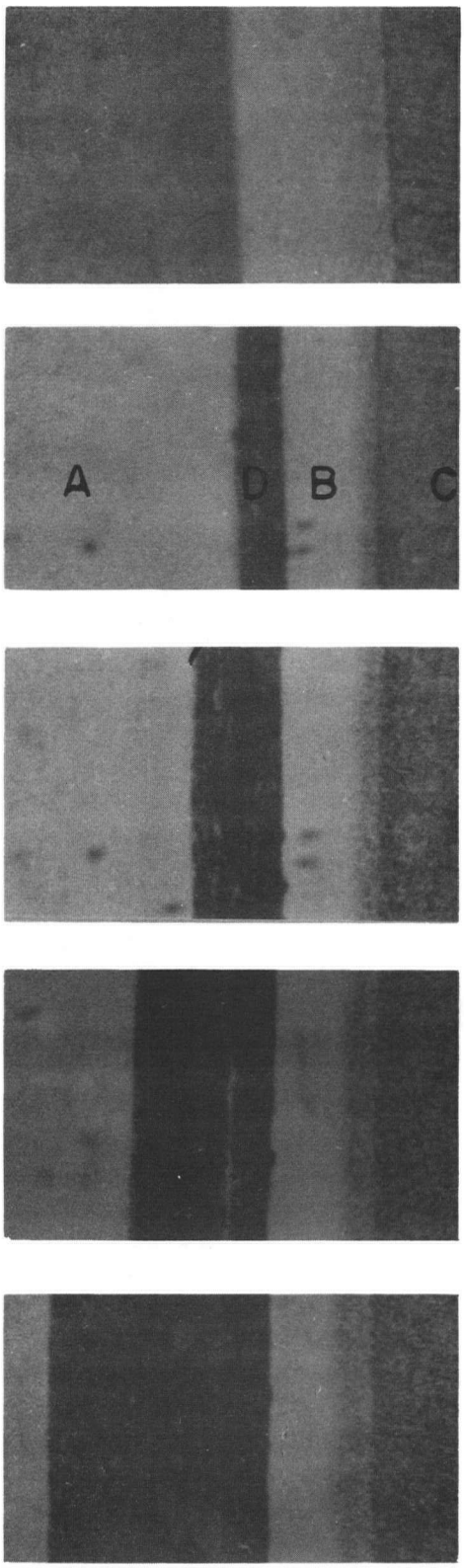

t = 0

t = 0.5 hr.

t = 1 hr.

t = 2 hr.

t = 4 hr.

Figure 3.5 Growth of a Diffusion Zone in Ag-Se (x188)

couple has been called a "white Zone". This region will be discussed in the Appendix where it is shown that the "white zone" is of no significance in the lateral diffusion process.

3.2.2 Effect of Se Thickness on the Rate Constant

Figure 3.6 shows a series of x versus $\sqrt{t}$ plots for Ag-Se diffusion couples in which the Se thickness ranged from 0 to 1300 Å. In every case parabolic growth was observed indicating diffusion control. In Figure 3.7 the rate constant, K, determined from the growth kinetics of samples in which t_{Se} was varied from 0 to 2260 Å is plotted as a function of Se thickness. The ratio of Ag to Se thickness (t_{Ag}/t_{Se}) was greater than 1.1 in all these samples. The reason for excluding samples in which $t_{Ag}/t_{Se} < 1.1$ will be discussed in the next section.

These results show that in the Se thickness regime 200 to 2260 Å, the rate constant has a constant value of 1.1×10^{-8} cm^2/sec. Between 0 and 200 Å, the rate constant rises sharply to reach a maximum at about 150 Å then drops to the constant value above 200 Å. It appears, therefore, that the diffusion rate is enchanced in the thickness regime 90 to 170 Å. This maximum in the curve attains a value only 3.5 times greater than the constant rate constant value and appears to be a genuine effect since similar peaks were also found in the other three systems investigated, and in the Te systems a much larger difference between peak and constant rate values was observed.

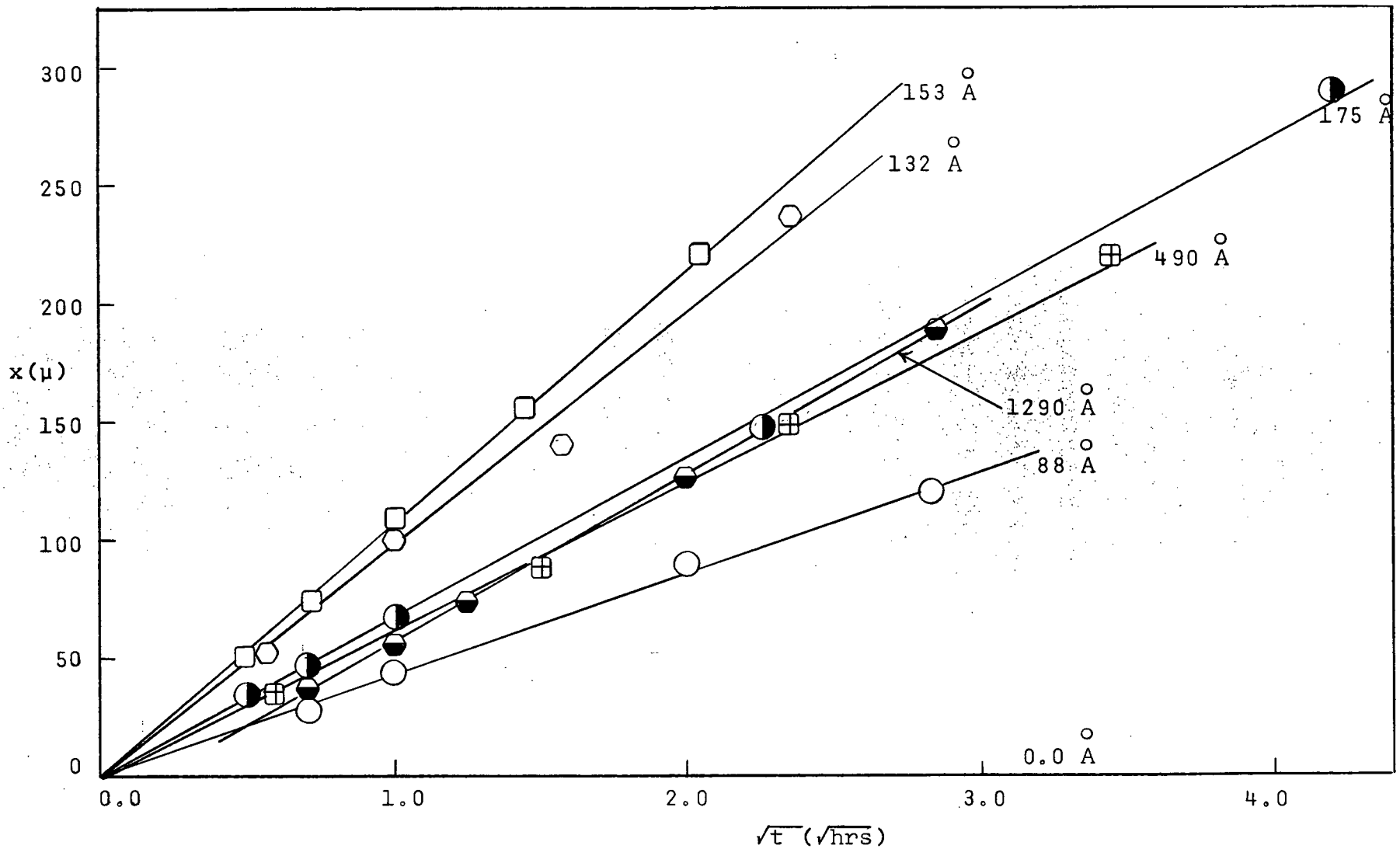

Figure 3.6 Effect of Se Thickness on Growth Rate

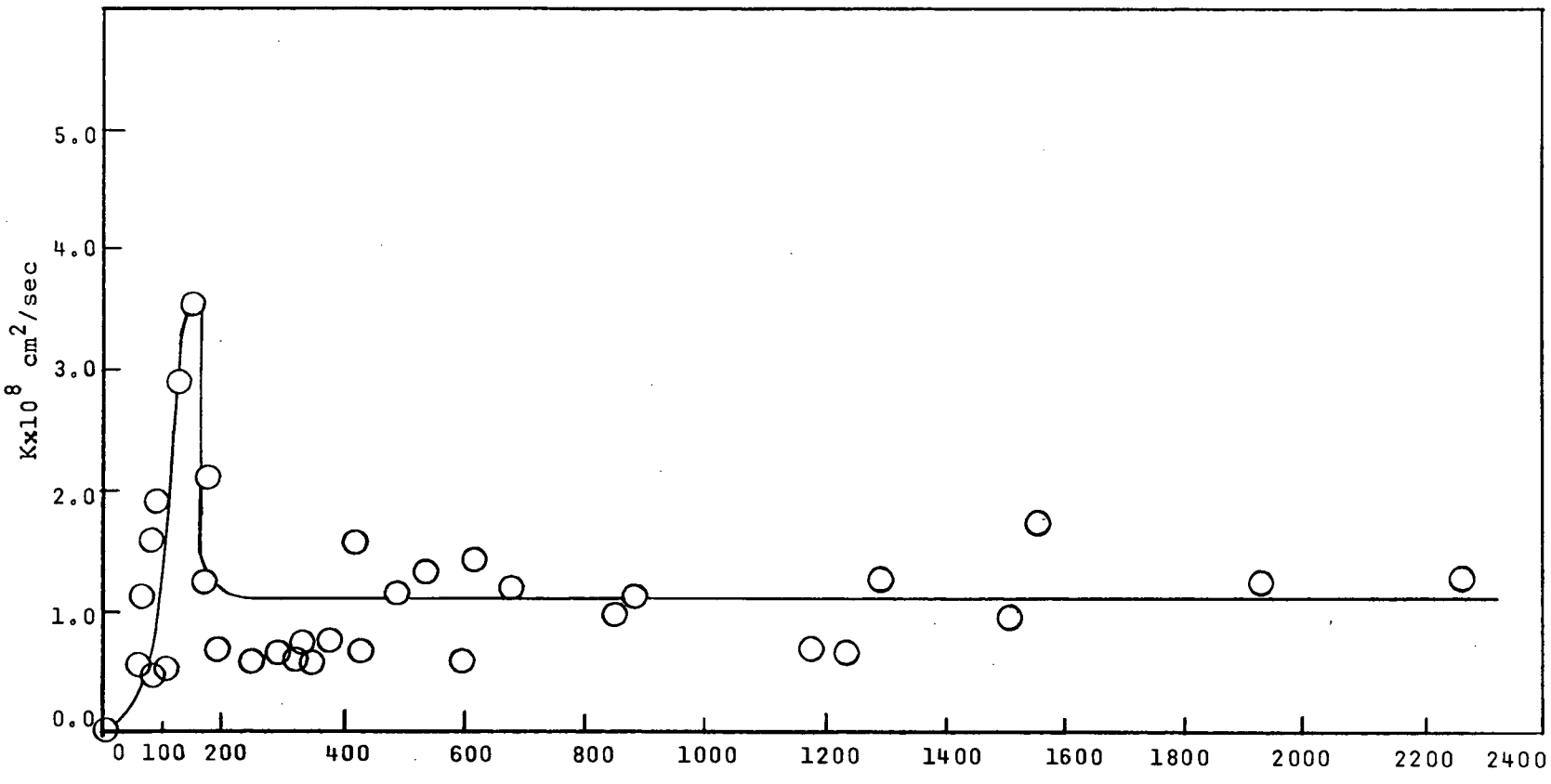

Figure 3.7 Rate Constant as a Function of Se Thickness

3.2.3 The Structure of Se Films

A suggested explanation of the faster diffusion rate at low Se thickness is that a disproportionate number of high-diffusivity paths are present in these films. An electron microscopy study of very thin Se films was carried out to see if, in fact, high-diffusivity channels did exist in the amorphous Se films.

Although the general growth stages of a thin film have been well documented for such metals as Au and Ag (see Introduction, page 21), no specific reference to Se could be found in the literature. Initially, thin Se films between 50 and 300 Å were examined by transmission electron microscopy both at room temperature and liquid nitrogen temperature using the microscope cold stage. In the thickness range 50 to 90 Å the Se films appeared to consist of massive, disconnected islands with some tendency to be coalesced at higher thicknesses (~ 100 Å). There appeared to be no material present between the islands, however. Cr-shadowed carbon replicas were then made of the same Se films observed by transmission electron microscopy. Electron micrographs showed that at t_{Se} = 50 Å, the Se film consisted of large islands 2000 to 5000 Å in diameter with a fine inter-island substructure in evidence. At 90 Å coalescence of the large Se islands had begun and the substructure between the islands was well defined. This inter-network layer was calculated to be about 30 Å thick. Figure 3.8 shows both the transmission and replica electron microscopy results for very

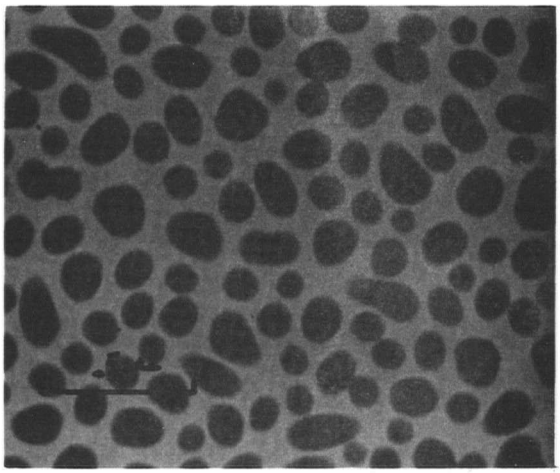

(1) 50 Å Se film (transmission)

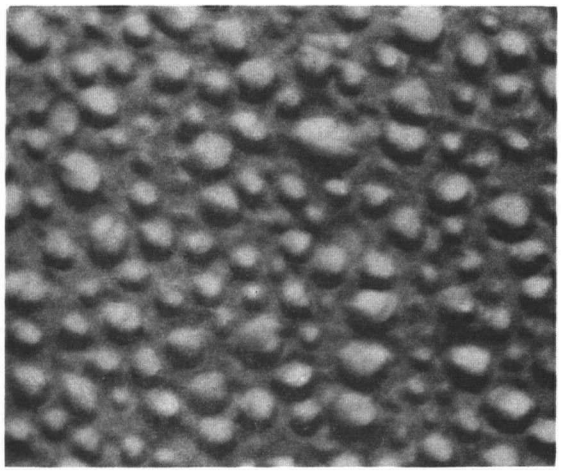

(2) 50 Å Se film replica

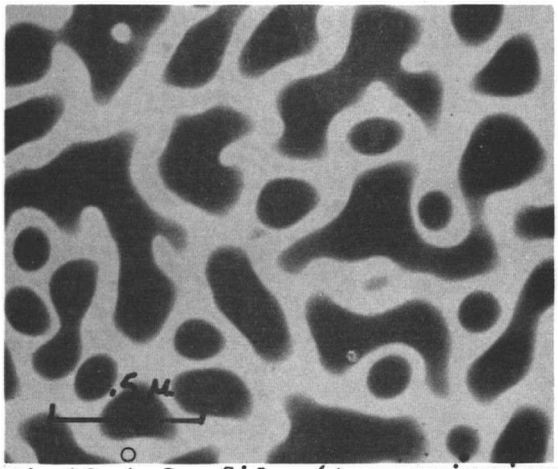

(3) 90 Å Se film (transmission)

(4) 90 Å Se film replica

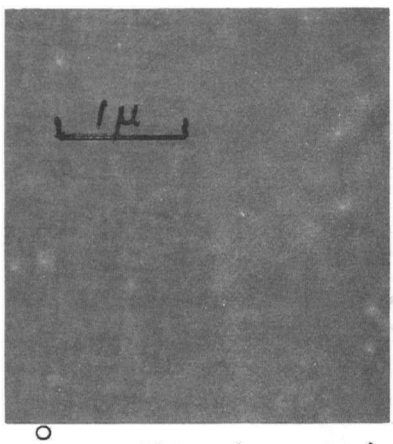

(5) 300 Å Se film (transmission)

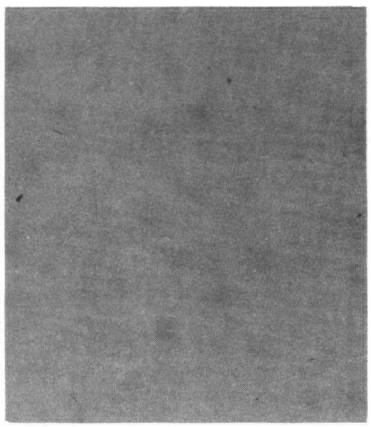

(6) Cr-shadowed glass surface (replica)

Figure 3.8 Structure of Se Films

thin Se films. In both cases the size of the Se aggregates is equivalent indicating that the isolated islands in the transmission micrographs are not the result of melting by the electron beam and that the microstructure of the Se films is not influenced by the substrate (glass versus carbon). Also shown in Figure 3.8 is an electron micrograph of a Cr-shadowed replica of a glass surface. The absence of any fine structure indicates that the substructure seen in the Se replicas is due strictly to the structure of the Se film and not to irregularities on the glass substrate. The micrograph of a 300 Å Se film characterizes continuous Se films; the large islands present during the early growth stages are faintly visible within the amorphous material.

The effect of a very thin Se film possessing a structure like that shown in Figure 3.8(4) on the diffusion zone interface is shown in the series of optical micrographs in Figure 3.9. Up to 150 Å the phase boundary interface consists of many minute projections suggesting the tendency for diffusion to proceed slightly faster in the inter-island channels. A calculation of the wavelength of the interface fluctuations made from Figures 3.9 (1), (2), (3) shows that it is approximately 3000 to 5000 Å which is approximately the same as the particle size indicated in the electron micrographs. By contrast the interface in Figure 3.9 (4) where t_{Se} = 900 Å is very planar. The Se film at this thickness is continuous having the microstructure

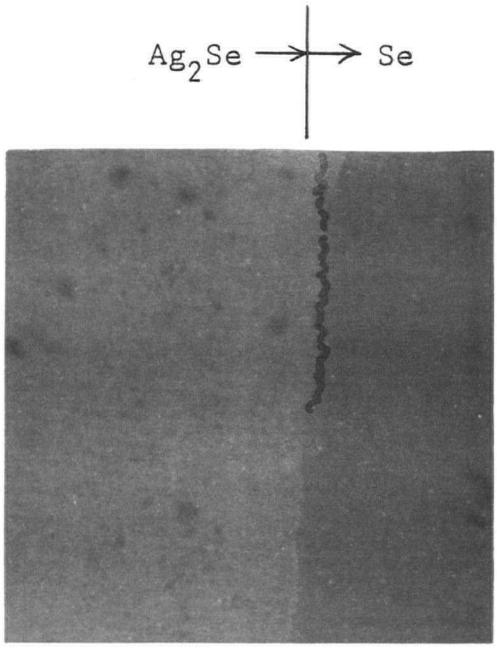

(1) t_{Se}=85 Å (x600)

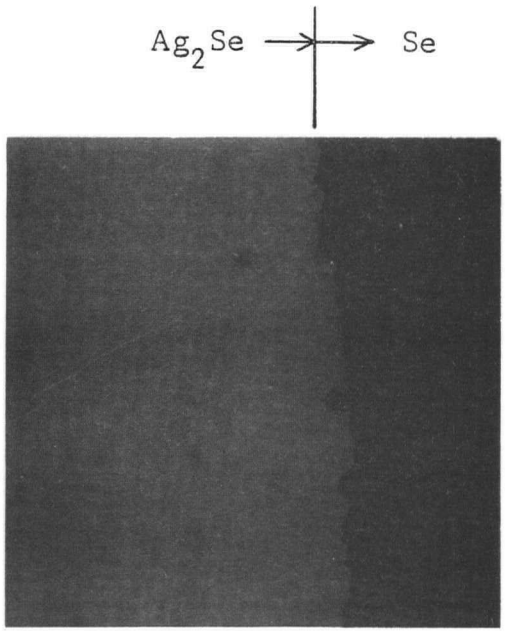

(2) t_{Se}=85 Å (x1500)

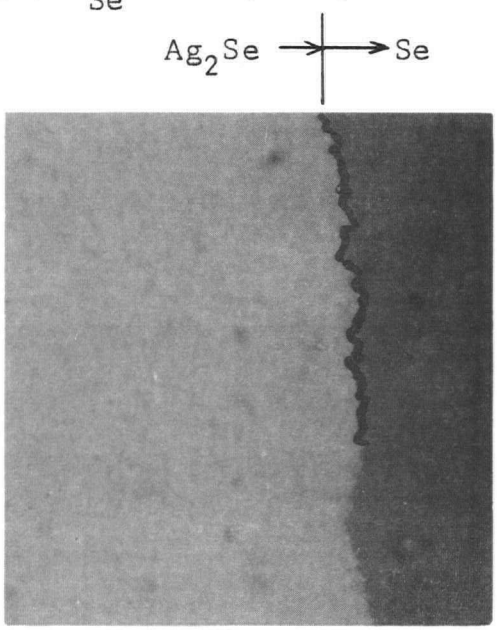

(3) t_{Se}=130 Å (x600)

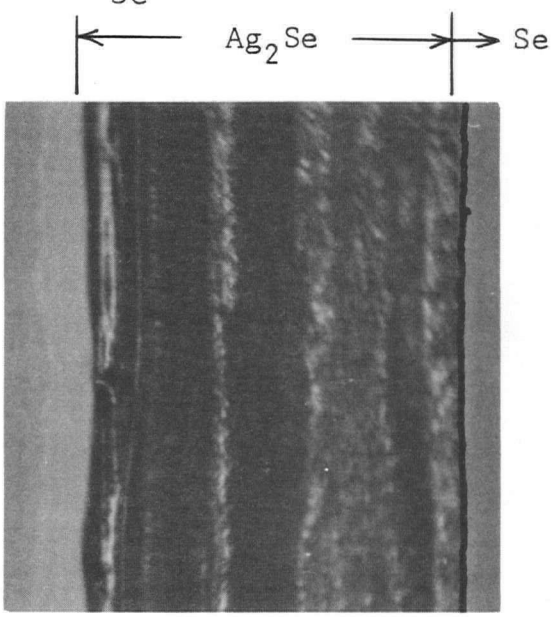

(4) t_{Se}=900 Å (x600)

Figure 3.9 Appearance of Phase Boundary at Varying Se Thickness

shown in Figure 3.8 (5).

The electron microscope results on very thin Se films lead to the suggested growth sequence shown in Figure 3.10. Enhanced short circuit diffusion occurs mainly in the network stage of growth when the inter-island substructure is very thin but still continuous. The substructure part of the film is likely a region of high disorder containing a large number of grain boundary-like regions. Diffusion in the substructure is probably analogous to grain boundary diffusion. In terms of Fischer's model[18] (Figure 3.11) the inter island film would correspond to a grain boundary although, of course, it is very much wider. The large islands would be equivalent to bulk material. Even though grain boundary diffusion in bulk metals is about 10^6 times greater than in the lattice the effect is fairly small because lateral diffusion from the grain boundary into the lattice essentially "damps" the faster diffusion process taking place in the boundary.

3.2.4 Effect of Thickness Ratio on the Rate Constant

Figures 3.12 and 3.13 show the effect of the ratio of Ag to Se on the ratio constant for Se films greater than 200 Å thick. It can be seen that below a ratio of 1.1, the diffusion rate constant is zero while at values of t_{Ag}/t_{Se} greater than 1.1, the rate constant tends to a constant value of 1.1×10^{-8} cm^2/sec. The value of t_{Ag}/t_{Se} above which diffusion occurs and below which diffusion does not occur

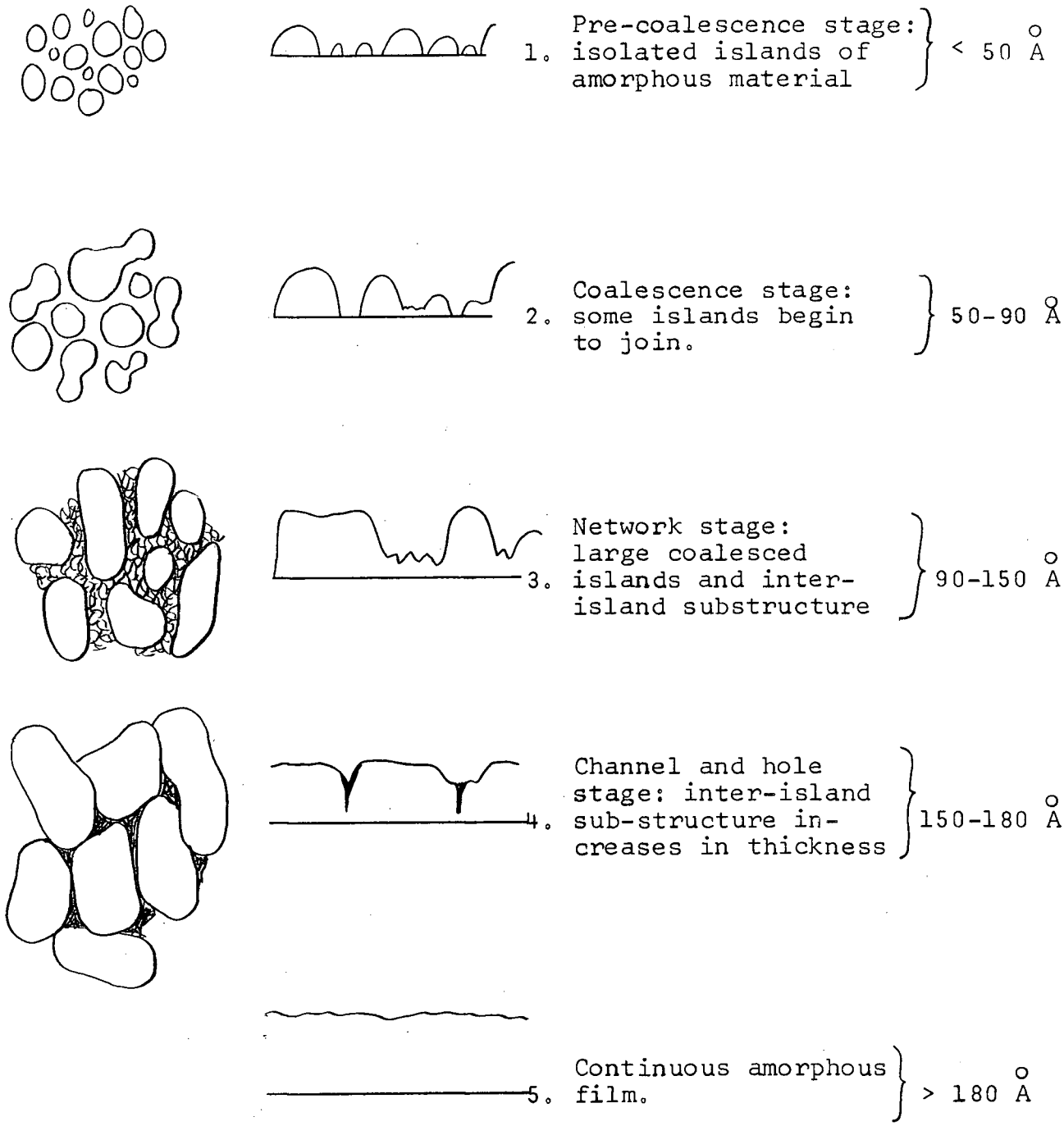

Figure 3.10 Stages in the Formation of a Continuous Amorphous Se Film.

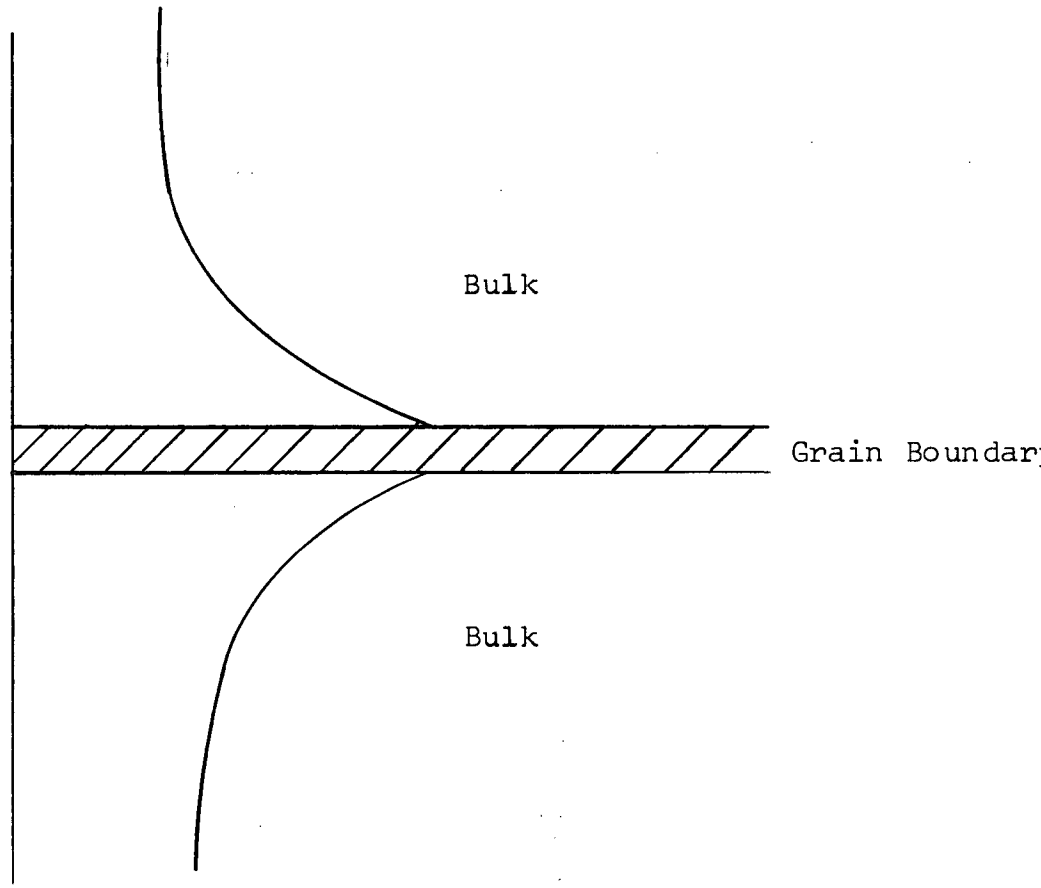

Figure 3.11 Fischer's Model for Grain Boundary Diffusion.

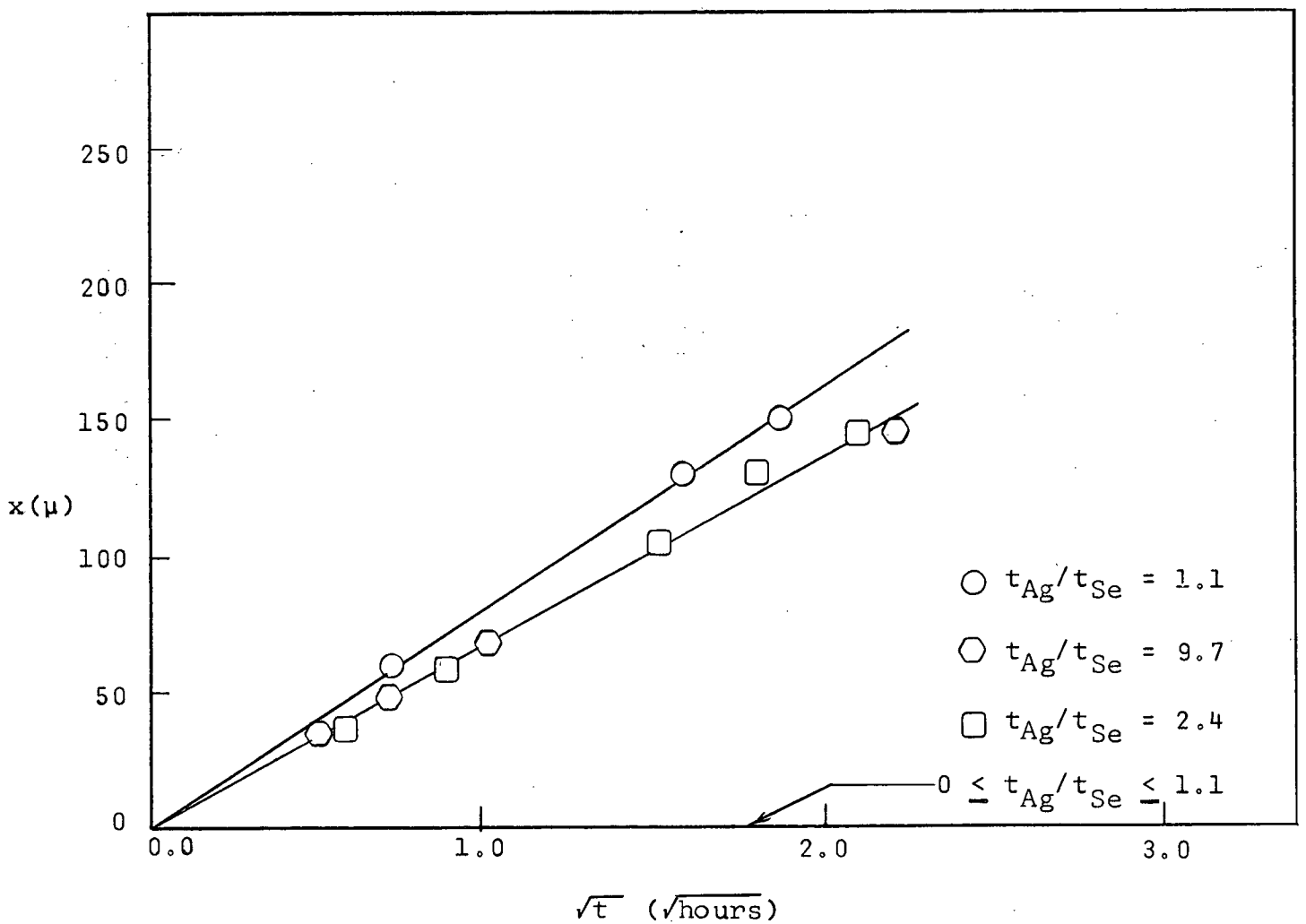

Figure 3.12 Effect of Thickness Ratio on Growth Rate

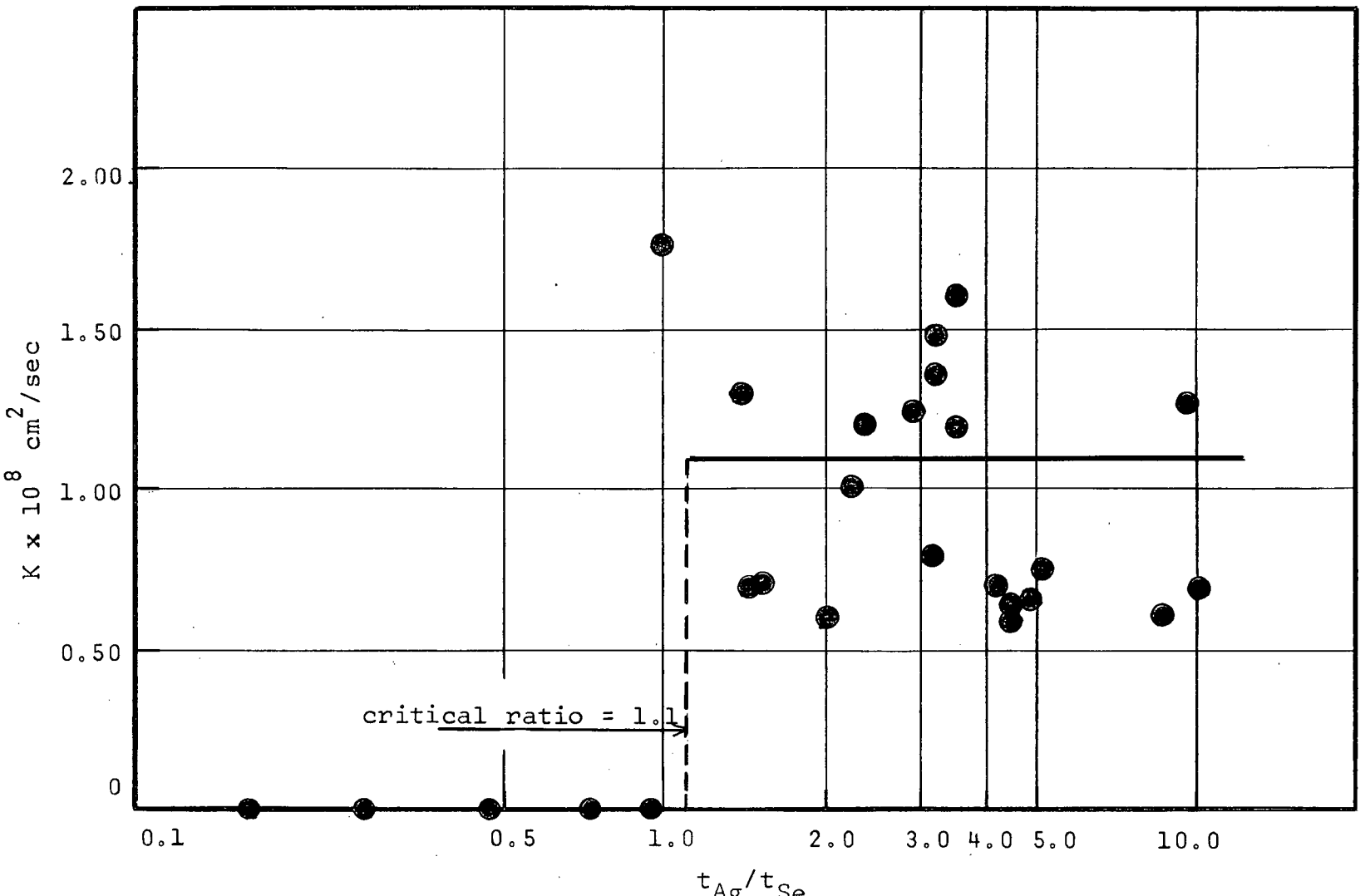

Figure 3.13 Growth Rate as a Function of Thickness Ratio

has been called the critical ratio (R_c). An investigation of the critical ratio value over a range of Se thicknesses showed that it was independent of the absolute Se thickness. The result of this study is shown in Table 3.1.

TABLE 3.1

Critical Ratio Dependence
on the Absolute Se Thickness

R_c	t_{Se} (Å)
.95-1.15	125
1.1±.1	390
1.03±.1	740
1.11±.1	1570

The origin of a critical ratio of Ag to Se which must be exceeded in order for diffusion to proceed is due primarily to the stoichiometry in the Ag-Se overlap region of the diffusion couple.

3.2.5 Theoretical Determination of the Critical Ratio

Consider the thin film diffusion couple M-Y shown in Figure 3.14 where M is the faster diffusing species. In rapidly diffusing systems such as Ag-Se a diffusion reaction occurs very quickly in the region where Y overlaps M to form

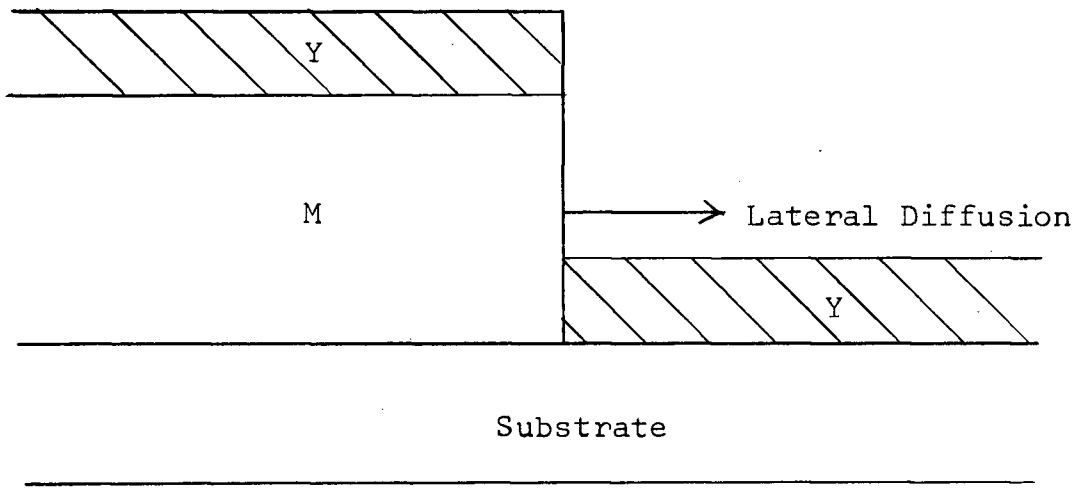

Figure 3.14 Theoretical Diffusion Couple M-Y

a compound M_xY, say. Knowing the exact composition of this diffusion compound it is possible to calculate on the basis of stoichiometry the ratio of thickness of M to Y at which the entire volume of M will be used up in forming M_xY. When this occurs there is no excess M available to diffuse laterally. Consider, now, a unit area (1 cm^2); the critical ratio is the ratio of t_M (M thickness) to t_Y (Y thickness) at which the entire volume of M in this unit area combines with a sufficient amount of Y to form M_xY. The molar volume (α) is given by

$$\alpha = \frac{\rho}{A} \tag{3.1}$$

where ρ = density and A = atomic weight in grams/mole. In dealing with thin films it is assumed, therefore, that the bulk and thin film densities are equivalent. In unit area there will be t_M cm^3 of M and t_Y cm^3 of Y. Neglecting any volume change in Y as M diffuses into it, the critical thickness ratio $R_c = (t_M/t_Y)_{crit}$ which must be exceeded for any excess M to be left for lateral diffusion is given by:

$$\frac{\text{Moles/cc of M} \times (t_M)_{crit}}{\text{Moles of M reacting to give } M_xY}$$

$$= \frac{\text{Moles/cc of Y} \times (t_Y)_{crit}}{\text{Moles of Y reacting to give } M_xY} \tag{3.2}$$

If α_M and α_Y are the molar volumes of M and Y respectively and β_M, β_Y are the number of moles of M and Y required to form M_xY, then we may write that

$$\left(\frac{t_M}{t_Y}\right)_{crit} = R_c = \frac{\beta_M}{\beta_Y} \times \frac{\alpha_Y}{\alpha_M} \qquad (3.3)$$

To correct for any volume expansion or contraction of Y as M diffuses in to form M_xY, it is necessary to multiply the value of R_c obtained from equation (3.3) by the ratio

$$\frac{\frac{1}{\alpha_{M_xY}}}{\frac{x}{\alpha_M} + \frac{1}{\alpha_Y}} \qquad (3.4)$$

where x is the stoichiometric ratio between M and Y in the compound M_xY. Notice that the units of $1/\alpha$ are cm^3/mole and that α_{M_xY} is the actual molar volume of the compound M_xY as defined in equation (3.1). For Ag_2Se, the only intermetallic compound in the Ag-Se system, a theoretical value for R_c of 1.05 is obtained using equations (3.3) and (3.4). This is in good agreement with the observed experimental value of $1.1 \pm .1$. The close agreement between theoretical and experimental values of R_c found in Ag-Se appeared to justify the application of the theory to predicting the intermediate compound formed in the other three systems in which more than one intermetallic phase is stable at room temperature.

3.2.6 Temperature Dependence of the Rate Constant

The temperature dependence of the rate constant for samples having $t_{Se} > 180$ Å and $t_{Ag}/t_{Se} > 1.1$ in the temperature range 0-55°C was determined. Figures 3.15 and 3.16 show the results of the study. The upper limit of the temperature range was kept below 60°C since Se films heated above this temperature became aggregated*. The Arrhenius-type expression obtained for the rate constant K from Figure 3.15 was

$$K = 67 \exp[-\frac{12000}{RT}]$$

To see if the diffusion process in thin films was comparable to that which occurs in bulk couples, the diffusion rate constant was measured at 50, 100, and 130°C in bulk diffusion couples of Ag and crystalline Se. Since diffusion rates in this system are controlled by the diffusion of silver through the crystalline Ag_2Se diffusion zone, the use of crystalline Se rather than the amorphous material should not have affected the results. Some couples were made using amorphous Se, but even at temperatures as low as 50°C, the Se became plastic and flowed after short

---

*NOTE: The false origin in the 3°C test was due to the inclusion of the white zone width in the diffusion zone width. This was necessary because the exact start of the diffusion zone was not well defined in this specimen.

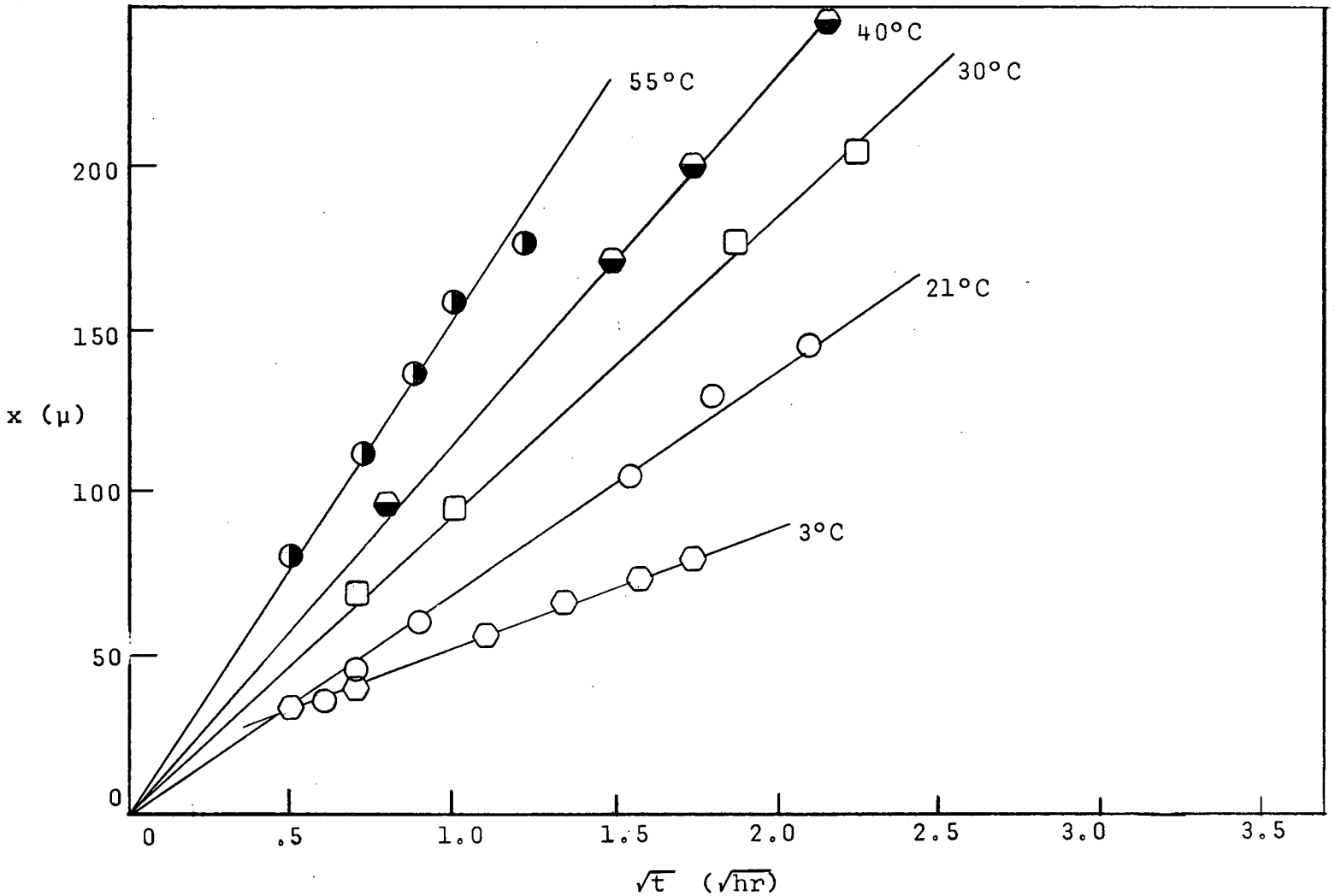

Figure 3.15 Temperature Dependence of the Rate Constant in Ag-Se

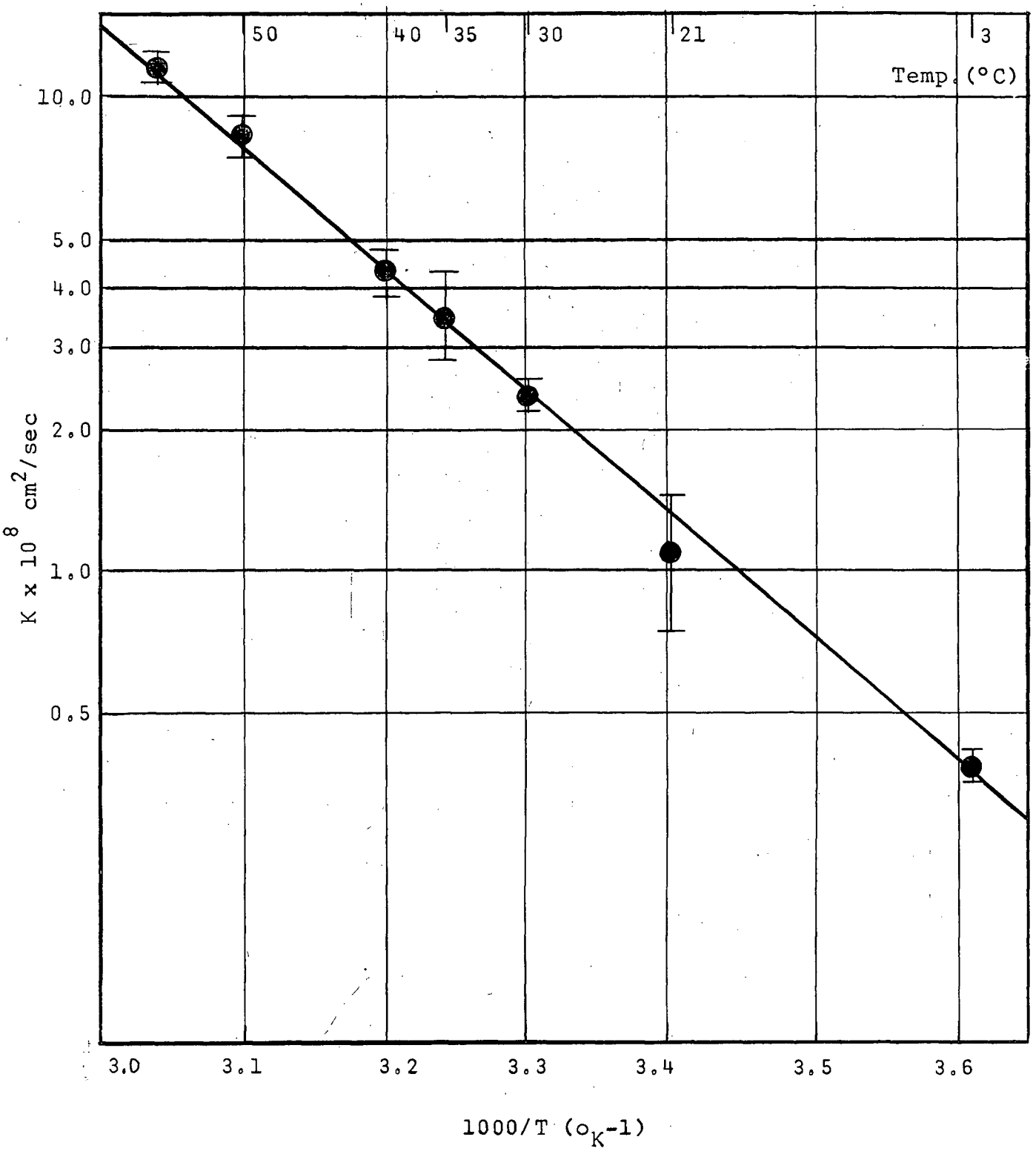

Figure 3.16 Arrhenius Plot for Ag-Se

annealing times (2-4 hours). The results of the bulk temperature study are plotted in Figure 3.17 along with the thin film data. From this graph the temperature dependence of the rate constant for bulk couples is found to be

$$K = 24 \exp[-\frac{17600}{RT}]$$

The large difference in growth rates between bulk and thin film couples (about 3 orders of magnitude) and the difference in activation energies implies that the diffusion mechanism is not the same. It would seem likely that some form of short-circuit diffusion process is operative in thin films which results in a lower activation energy.

3.3 Electron Microscopy

The advance of the Ag_2Se phase boundary was observed directly in the electron microscope. The interface appeared to be quite planar even at high magnification and its motion was rapid. Although the Se film in front of the diffusion zone was amorphous in nature, the diffusion zone itself was crystalline with elongated or columnar grains aligned parallel to the interface growth direction. Figure 3.18 shows a series of electron micrographs made of the moving phase boundary as it swept across the field of view. The elapsed time between micrographs 1 and 3 in this figure was about 4 minutes. This figure illustrates

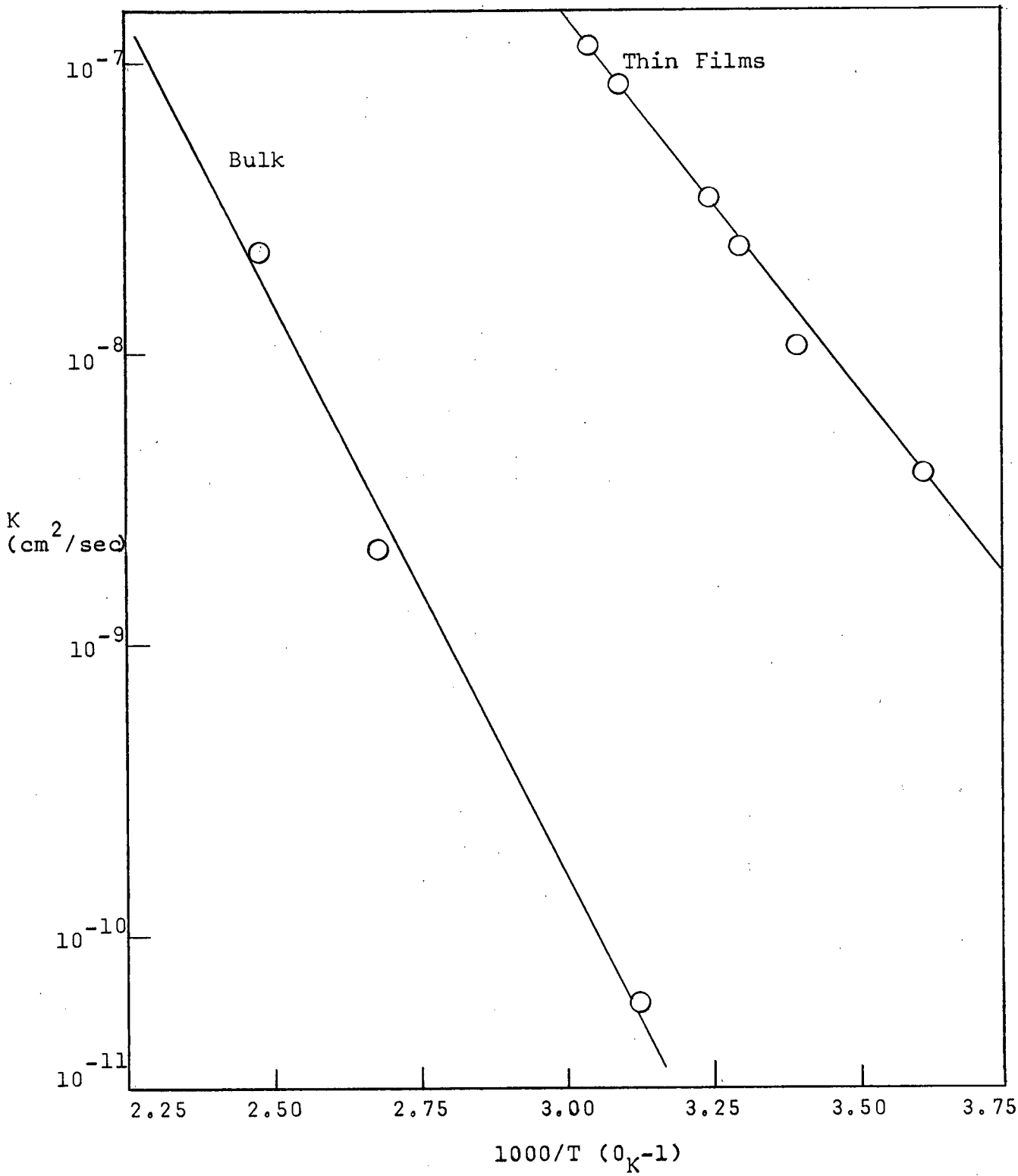

Figure 3.17 Comparison of Thin Film to Bulk Temperature Dependence.

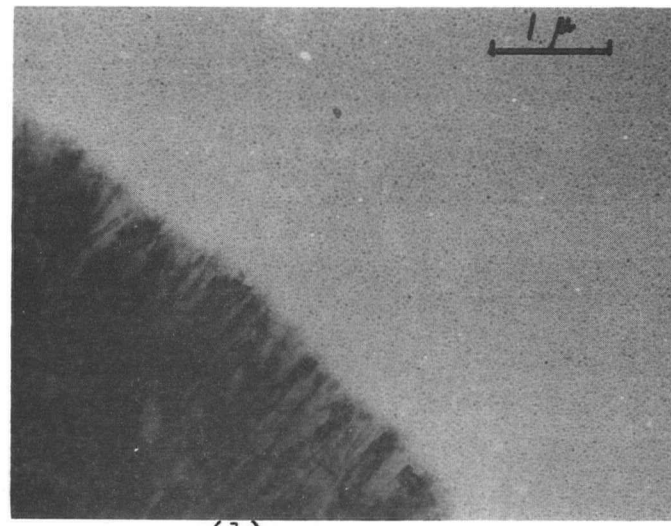

(1)

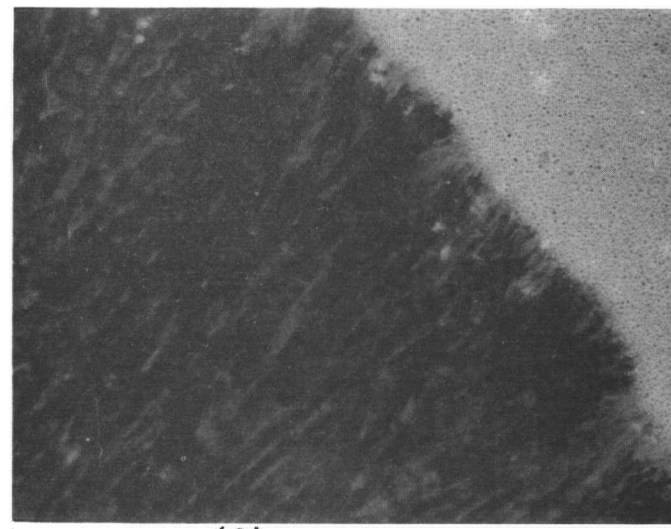

(2)

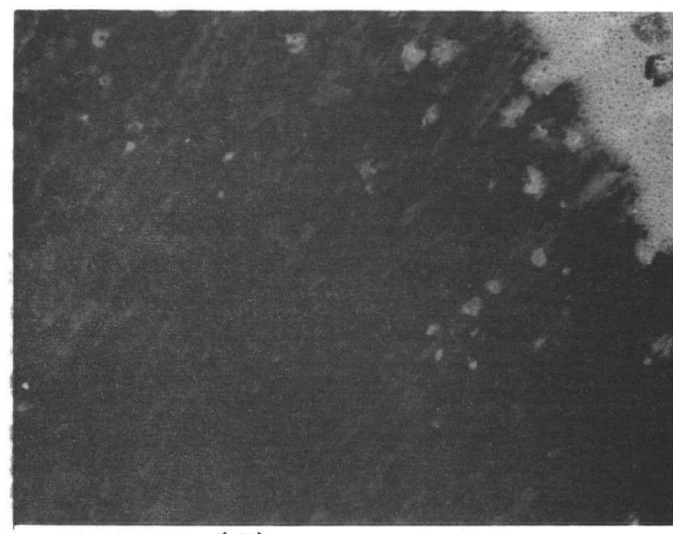

(3)

Figure 3.18 Advance of the Phase Boundary in Ag-Se

one of the major difficulties encountered in the electron microscopy of Se films; namely, that the heating of the film by the electron beam is sufficient to produce aggregation of the Se. In photographing the moving interface it was impossible to prevent aggregation even when very low illumination levels were used. Aggregation of the Se accounts for the minute black specks seen in the micrographs of Figure 3.18. The white areas in 3.18 (2), (3) appear after the electron beam induces a localized temperature increase and are probably depleted regions produced by Se aggregation or re-evaporation. This explanation is substantiated by the coincidence of the white areas in Figure 3.18 (2) and 3.18 (3).

The general appearance of the diffusion zone and phase boundary interface at high magnification is shown in Figure 3.19. The major contributing factor to the contrast between the dark diffusion zone and the light Se is the difference in thickness resulting from volumetric expansion of the Se when Ag diffuses in to form Ag_2Se. The volume change brought about in this case is about 57%. It should also be pointed out that this volumetric expansion causes the diffusion zone to become quite rumpled and distorted and to become partially detached from its underlying substrate. Evidence of this distortion is provided by the large number of bend and thickness contours seen in Figure 3.19 (a). A further contribution to contrast between the

(a) Appearance of the Ag_2Se diffusion zone

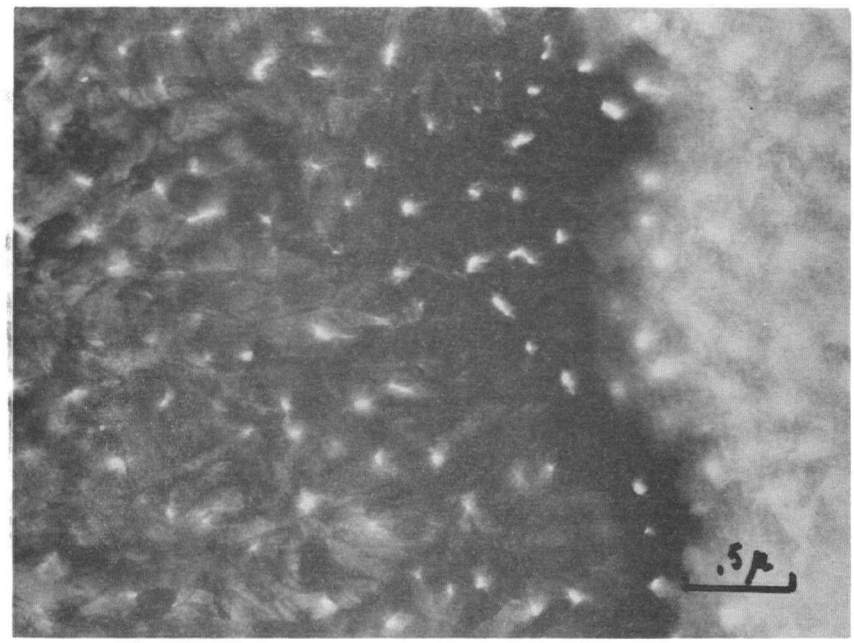

(b) Phase Boundary interface showing elongated grains in the diffusion zone

Figure 3.19 Diffusion Zone in Ag-Se

diffusion zone and pure Se may be the large difference in atomic scattering factors[44] of Ag and Se.

Selected area diffraction patterns were made of the diffusion zone. Subsequent analyses showed that the d-spacings calculated from the pattern rings were in good agreement with the known d-spacings of β-Ag_2Se, the low temperature modification. Figure 3.20 shows a typical set of diffraction results.

While the electron microscopy results enabled the composition of the diffusion zone to be determined and while the direct observation of the moving phase boundary was in itself interesting, particularly since relatively little is known about the actual motion of phase boundaries, the results provided little information concerning the mechanism for diffusion in Ag-Se.

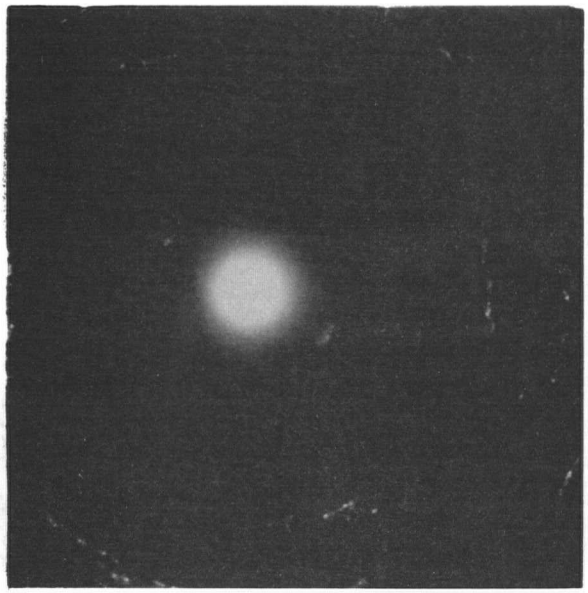

(a) S.A.D. of diffusion zone in an Ag-Se thin film couple

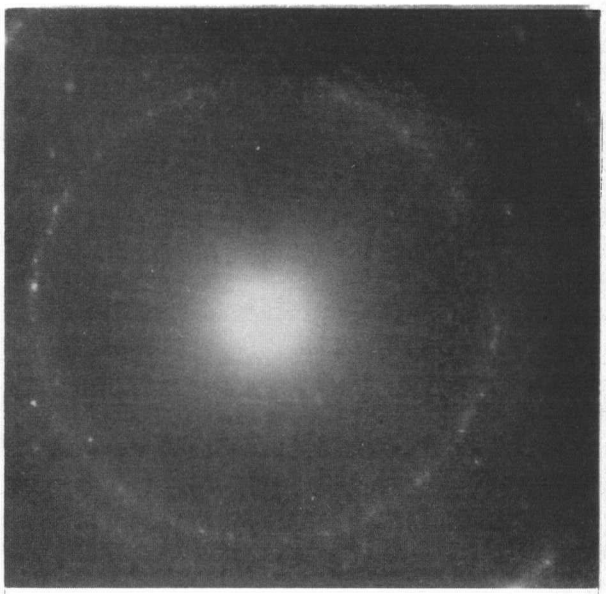

(b) Au Standard

Calculated d-spacings (Å)	d-spacings for β-Ag_2Se (Å)
7.25	--
4.32	4.15
3.76	3.77
3.42	3.30
2.84	2.89
2.76	2.72
2.66	2.67
	2.57
2.20	2.23
2.10	2.11
2.04	2.07
	2.00
1.84	1.87
1.77	1.82

Figure 3.20 Selected Area Diffraction Pattern of Diffusion Zone

CHAPTER 4

LATERAL DIFFUSION IN Cu-Te

4.1 Introduction

The equilibrium phase diagram for Cu-Te is shown in Figure 4.1. Unlike Ag-Se, in which only one intermetallic phase is thermally stable at room temperature, Cu-Te has at least 3 possible stable phases at room temperature. The main intermetallic compounds are Cu_2Te, $Cu_{2-x}Te$ with $x \sim 0.6$ (Cu_4Te_3), and CuTe. In addition Hansen[40] has pointed out the possible existence of a phase (X) whose composition lies at about 36-37 at. % Te. It is shown in section 4.3 that the diffusion of copper along a Te film results in the formation of only one phase, $Cu_{2-x}Te$. This phase has a defect structure of the Cu_2Sb type (tetragonal) and undergoes a polymorphic transformation at about 367°C. The phase diagram indicates that $Cu_{2-x}Te$ ranges in composition from $Cu_{1.35}Te$ to $Cu_{1.41}Te$ so that $0.59 < x > 0.65$.

At temperatures below the melting point Te has a stable hexagonal form[42,43]. The structure is highly anisotropic due to different bonding perpendicular and parallel to the c-axis. This anisotropy is reflected in

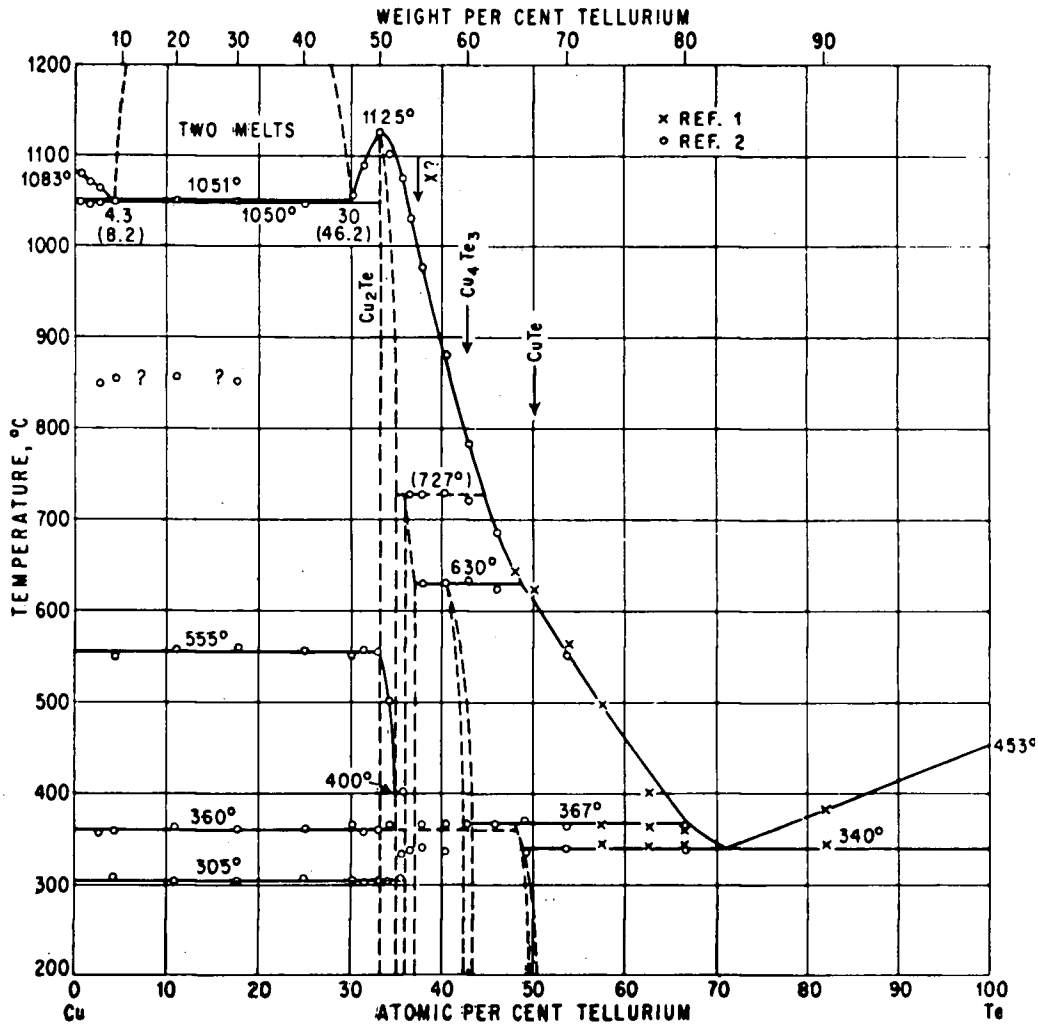

Figure 4.1 Equilibrium Phase Diagram of Cu-Te (after Hansen[40])

both the linear expansion coefficient, which is negative parallel to the c-axis, and positive perpendicular to it, and the electrical resistivity which attains a value twice a as great in the parallel direction as in the perpendicular. Figure 4.2 is a selected area diffraction pattern made on a pure evaporated Te thin film. The d-spacings calculated from this pattern are in good agreement with the known d-spacings for hexagonal Te. Because of the crystalline nature of all Te films encountered in this work, the results obtained in Cu-Te, although completely analogous to those for Ag-Se, will be discussed in some detail.

4.2 Kinetics

4.2.1 Growth Rate

Figure 4.3 is a typical plot of the diffusion zone width as a function of $\sqrt{t}$ obtained for the diffusion of Cu into Te. The linear dependence shows a parabolic growth law which implies that growth is diffusion controlled.

4.2.2. Effect of Te Thickness on the Kinetics

Figures 4.4 and 4.5 illustrate the effect of Te thickness on the growth rate for samples having $t_{Cu}/t_{Te} > R_c$. Beyond Te thicknesses of about 200 Å, the diffusion rate constant has a constant value of 2.1×10^{-9} cm^2/sec. In thinner films, however, the growth rate is much faster and approaches a value of 9×10^{-9} cm^2/sec at a thickness of 110 Å.

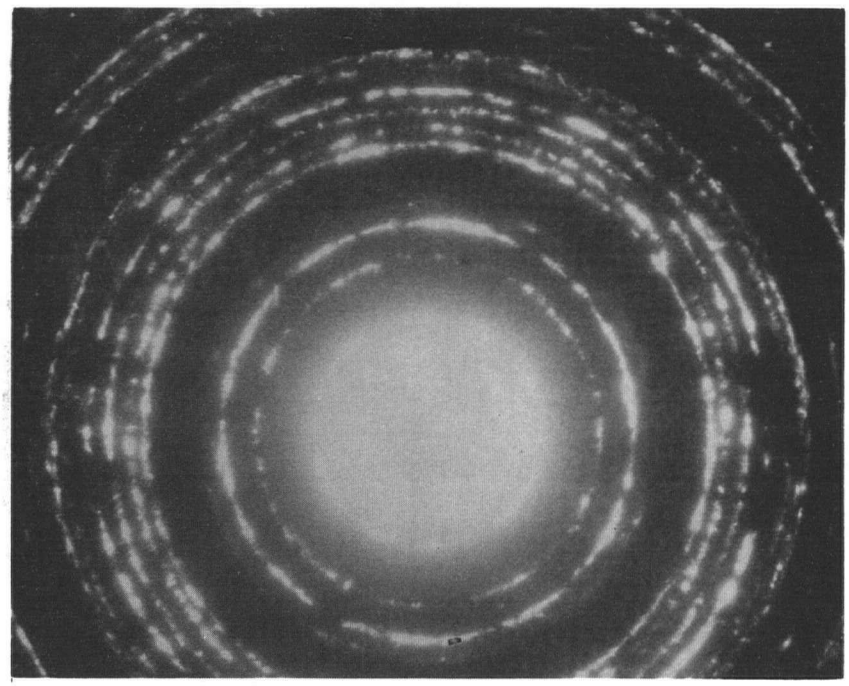

Figure 4.2 Selected Area Diffraction Pattern of Pure Te

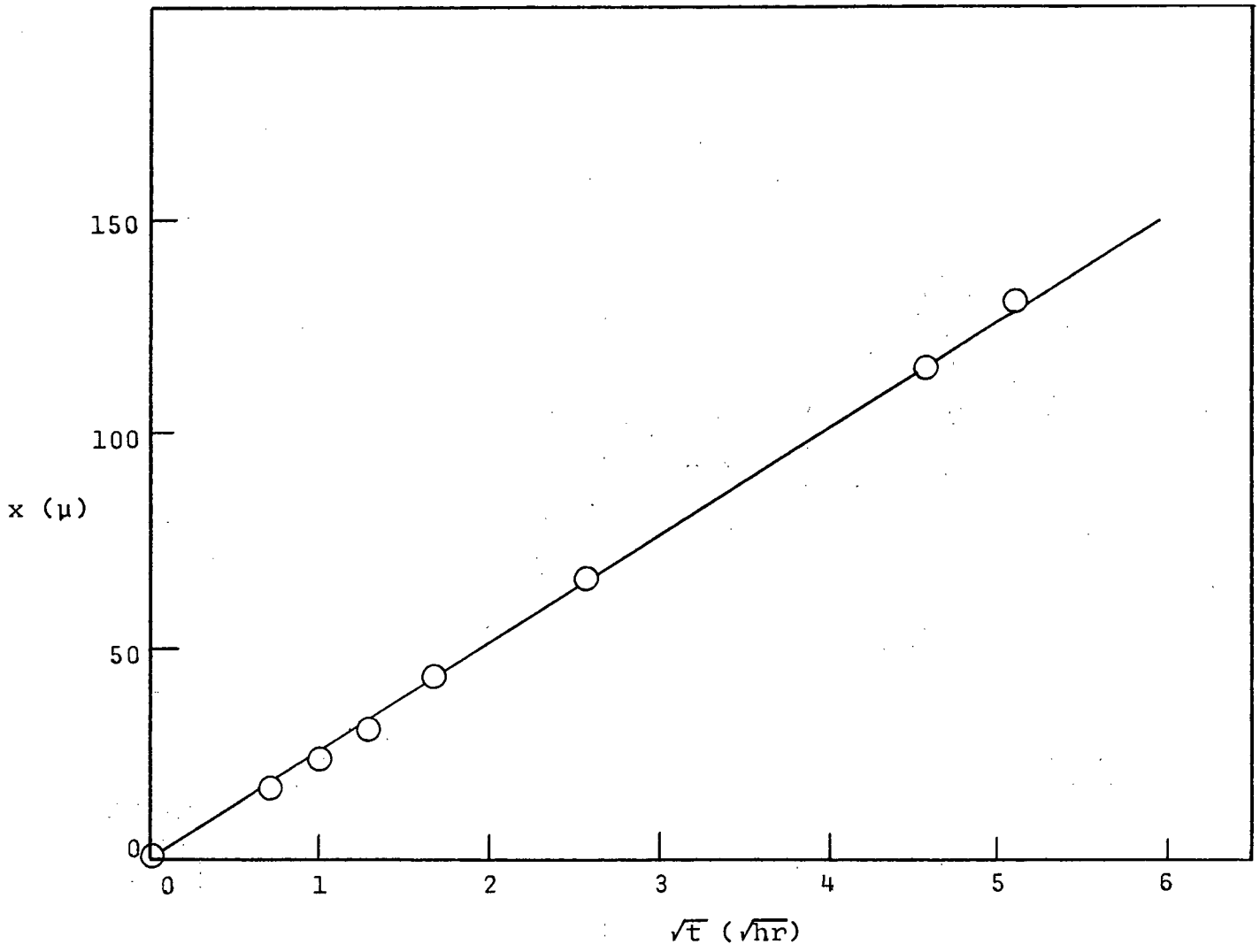

Figure 4.3 Typical Plot of x versus $\sqrt{t}$ in Cu-Te.

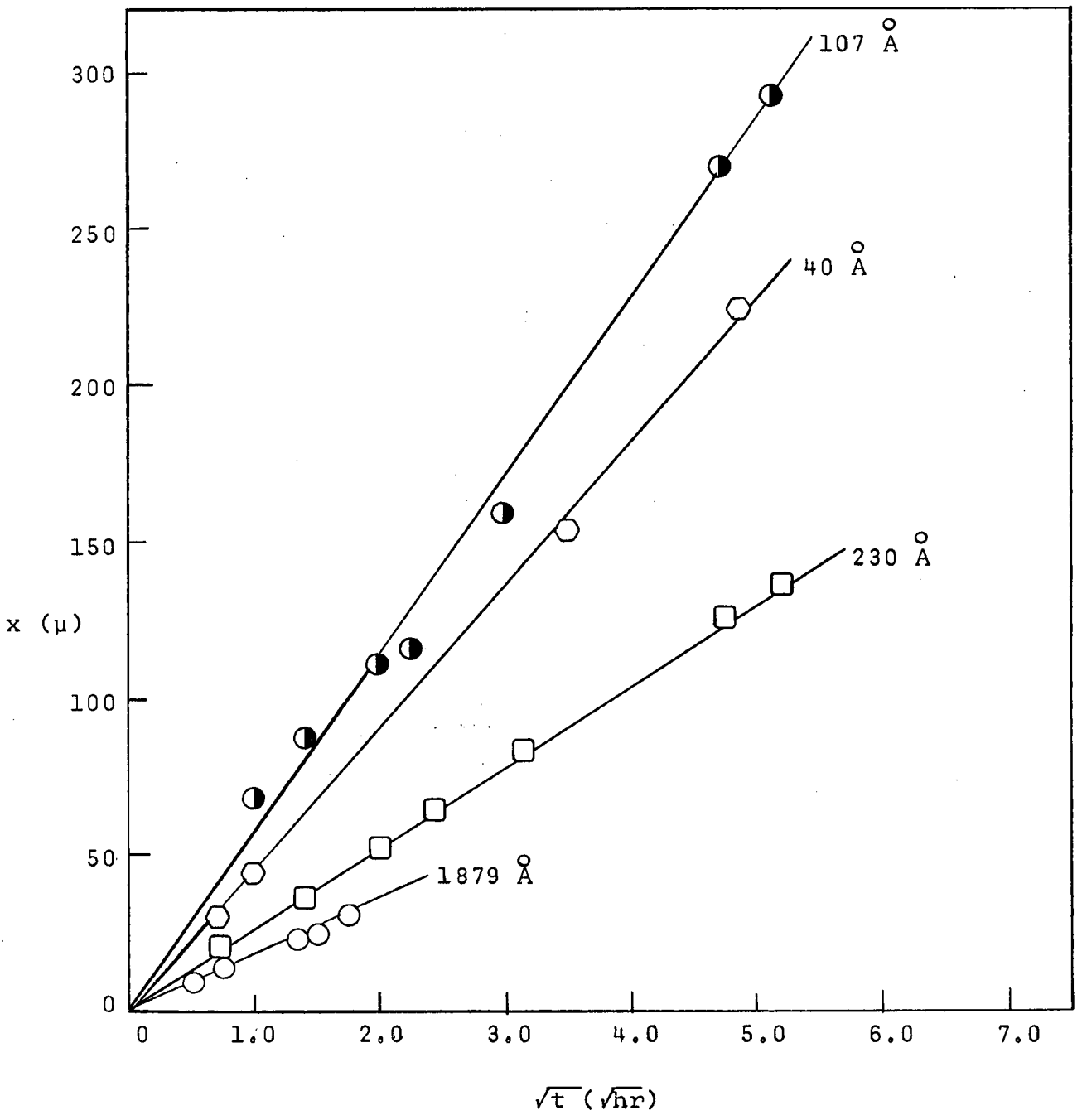

Figure 4.4 Effect of Te Thickness on Kinetics

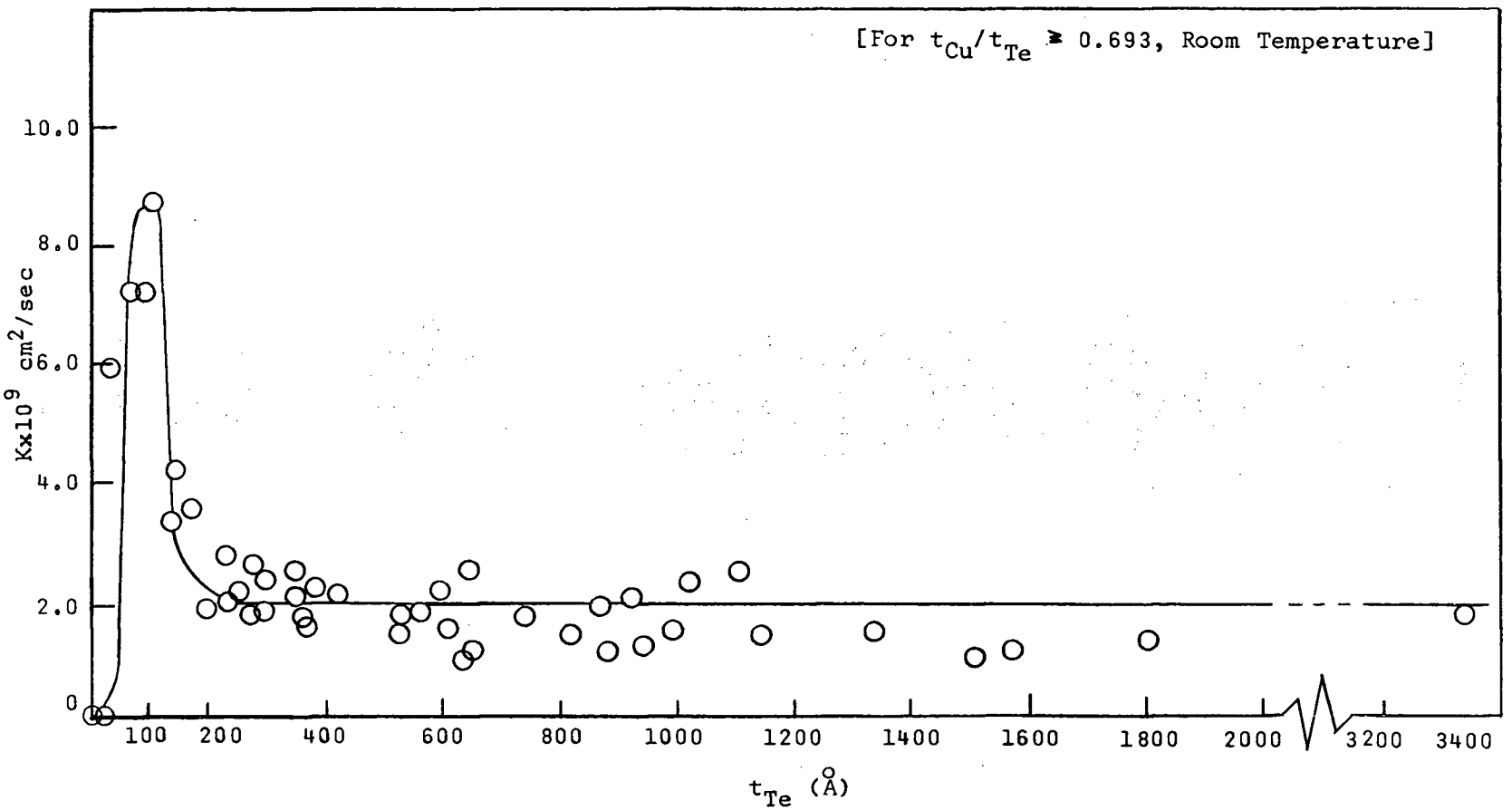

Figure 4.5 Rate Constant as a Function of Te Thickness

4.2.3 The Structure of a Te Film

The early growth stages of a Te film before it becomes continuous account for the apparent peak in the rate constant versus Te thickness graph. The steps in the formation of the Te film closely parallel those of a Se film as discussed in section 3.2.3, but a major difference is that the islands of Te observed in the pre-coalescence stage (see page 25 of Introduction) are randomly oriented crystallites about 200 Å in diameter rather than the large (2000 - 5000 Å diameter) amorphous islands observed in Se films. A transmission electron microscopy investigation of the microstructure of Te films 50 - 1200 Å thick was carried out. The results of this study, shown in Figure 4.6, suggest that enhanced diffusion occurs when the Te film is in the network and channel stages of growth. In this thickness regime, between 90 and 130 Å, the Te film consists of coalesced islands with a highly disordered inter-island network, probably analogous to grain boundaries, where diffusion can occur more rapidly. The exact mechanism is probably similar to that which occurs in Ag-Se as discussed in section 3.2.3. Film continuity and the onset of a definite grain structure is seen at about 200 Å and persists up to the thickest film studied - 1200 Å. The microstructure of Te films greater than 400 Å thick closely resembles that of bulk material except that films between 400 and 900 Å are characterized by numerous thickness contours.

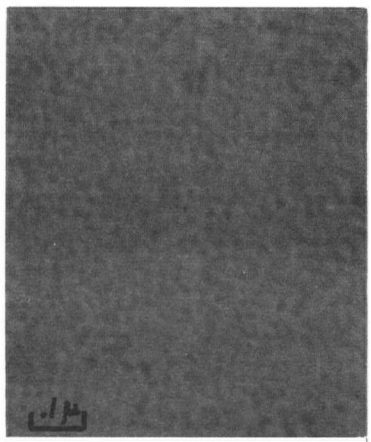

(a) Pre-coalescence stage; t_{Te}=20 Å, K=0

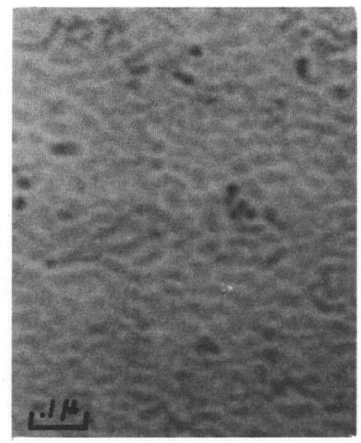

(b) Coalescence-network stage; t_{Te}=90 Å; K>0 and large

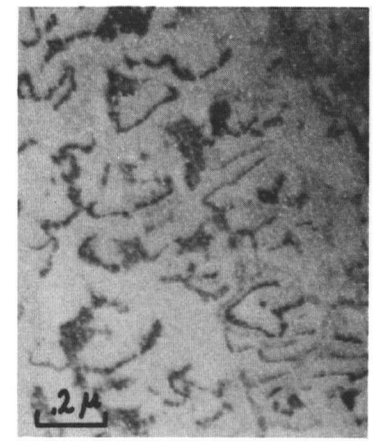

(c) Hole and channel stage; t_{Te}=130 Å; K>0 and large

(d) Continuous film; grains begin to form; t_{Te}=200 Å
$K=2.1\times10^{-9}\ cm^2/sec$

(e) t_{Te}=600 Å
Note ~~thickness~~ INCLINATION contours
$K=2.1\times10^{-9}\ cm^2/sec$

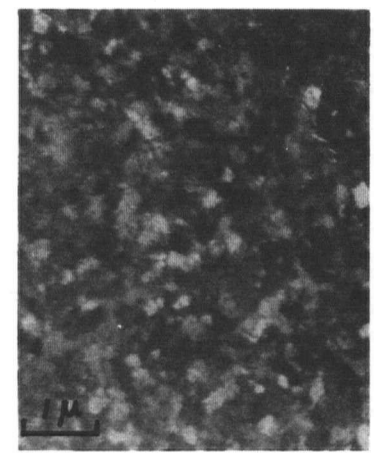

(f) t_{Te}=1200 Å
Note absence of ~~thickness~~ INCLINATION contours
$K=2.1\times10^{-9}\ cm^2/sec$

Figure 4.6 The Growth of a Te Thin Film

4.2.4 Critical Ratio

Figure 4.7 shows a plot of the room temperature diffusion rate constant as a function of the ratio of Cu to Te thickness (t_{Cu}/t_{Te}) for couples in which $t_{Te} > 180$ Å. This figure indicates that the critical ratio (R_c) is 0.63; that is, when $t_{Cu}/t_{Te} > 0.63$ diffusion proceeds at a constant rate of about 2.1×10^{-9} cm^2/sec while for $t_{Cu}/t_{Te} < 0.63$, diffusion does not occur. The theoretical values of R_c for each of the three intermetallic phases in Cu-Te were calculated using the methods outlined in section 3.2.5. Table 4.1 lists the theoretical values for each phase. From this it would appear that the growing phase should have the composition Cu_2Te. As will be discussed in section 4.3, the phase forming in the diffusion zone was positively identified by electron diffraction analysis as $Cu_{2-x}Te$. The reason why the critical thickness ratio is in error in this system is uncertain, since the technique yielded excellent results in the other systems investigated. The value for the critical ratio is not dependent on the absolute thickness of the Te film (see Table 4.2) and so is independent of the film structure. The actual percentage error is fairly small (~ 30%) and it is perhaps unfortunate in this system that the three intermetallic compounds occur at fairly equivalent compositions.

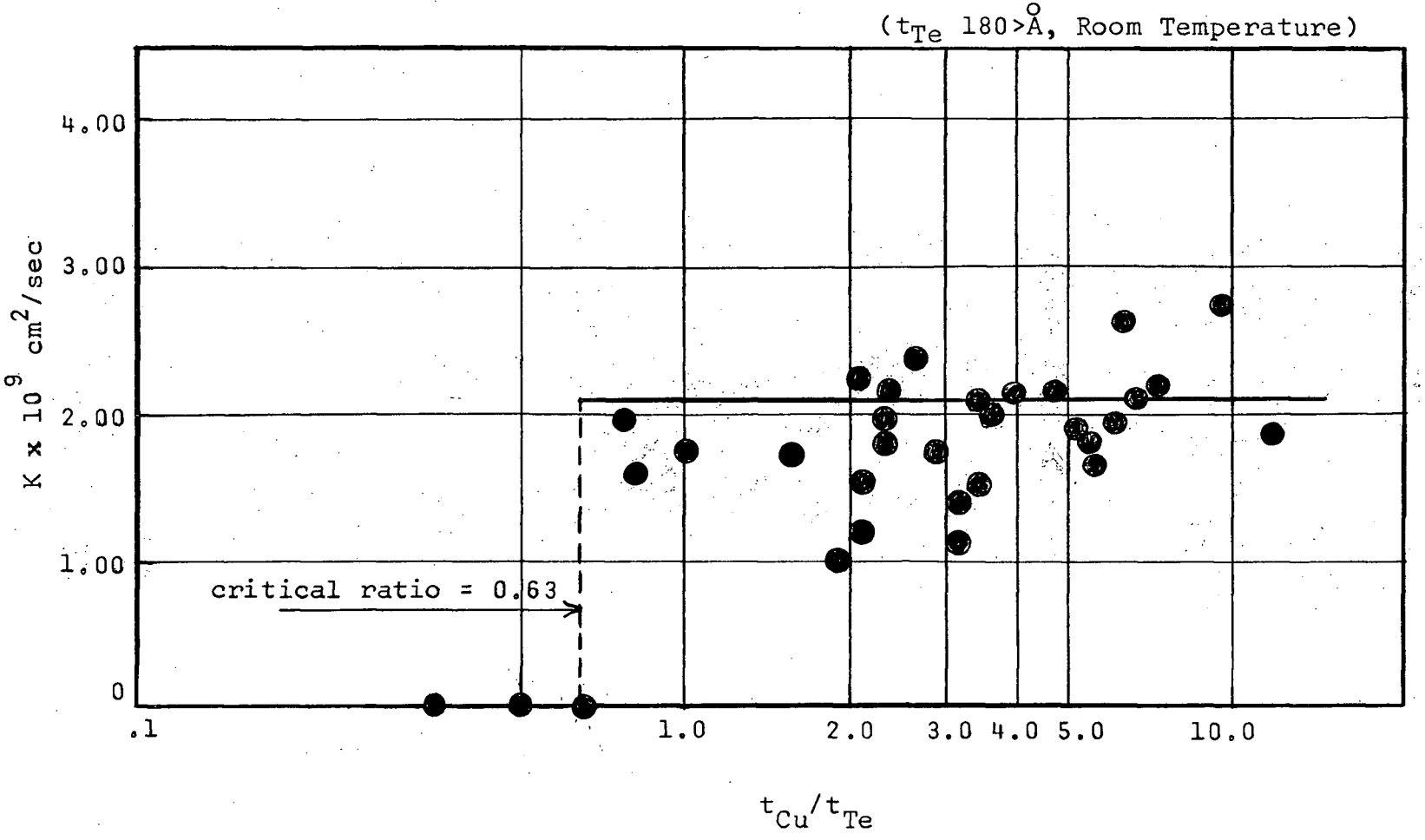

Figure 4.7 Rate Constant as a Function of Thickness Ratio

TABLE 4.1

R_c for Intermetallic Phases in Cu-Te

Phase	R_c
Cu-Te	0.35
$Cu_{2-x}Te$	0.47
Cu_2Te	0.63

TABLE 4.2

Critical Ratio as a Function of Absolute Te Thickness

R_c	t_{Te}(Å)
0.58-0.70	270
0.66±0.1	800
0.62±0.1	3350
0.63±0.1	5000

4.2.5 Temperature Dependence of the Rate Constant

The temperature dependence of the rate constant for film couples having $t_{Te} > 180$ Å and $t_{Cu}/t_{Te} > R_c$ was determined over the range 0-100°C. Since Te tends to be far less aggregated on a glass substrate than does Se[31], it was possible to extend the temperature range of investigation in both Cu-Te and Ag-Te up to 100°C without encountering aggregation problems. Figure 4.8 shows the Arrhenius plot obtained. From this graph the dependence of the diffusion rate constant on temperature was found to be

$$K = .0017 \exp[-\frac{7800}{RT}]$$

Also shown in Figure 4.9 is the Arrhenius plot obtained by

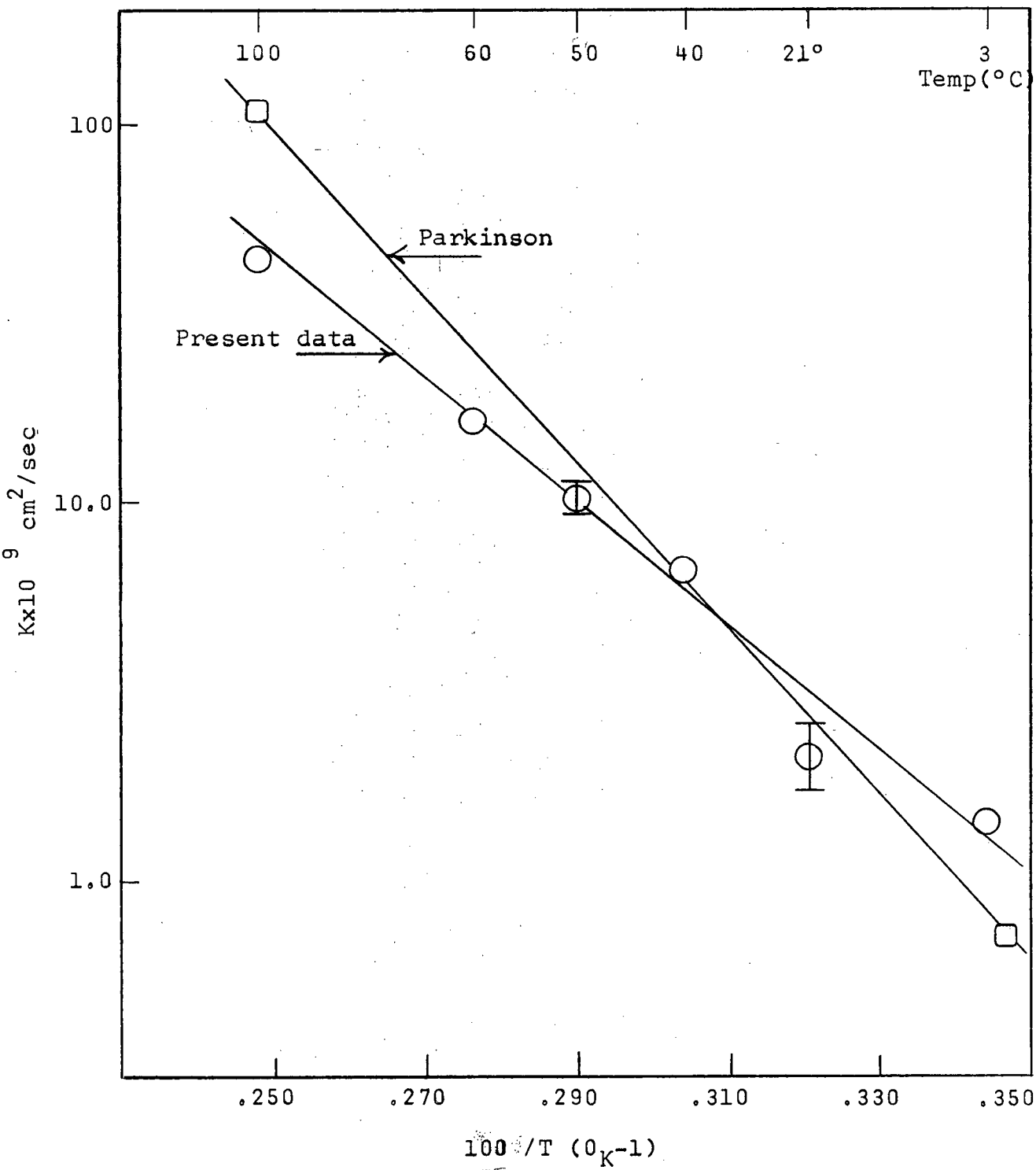

Figure 4.8 Arrhenius Plot for Cu-Te

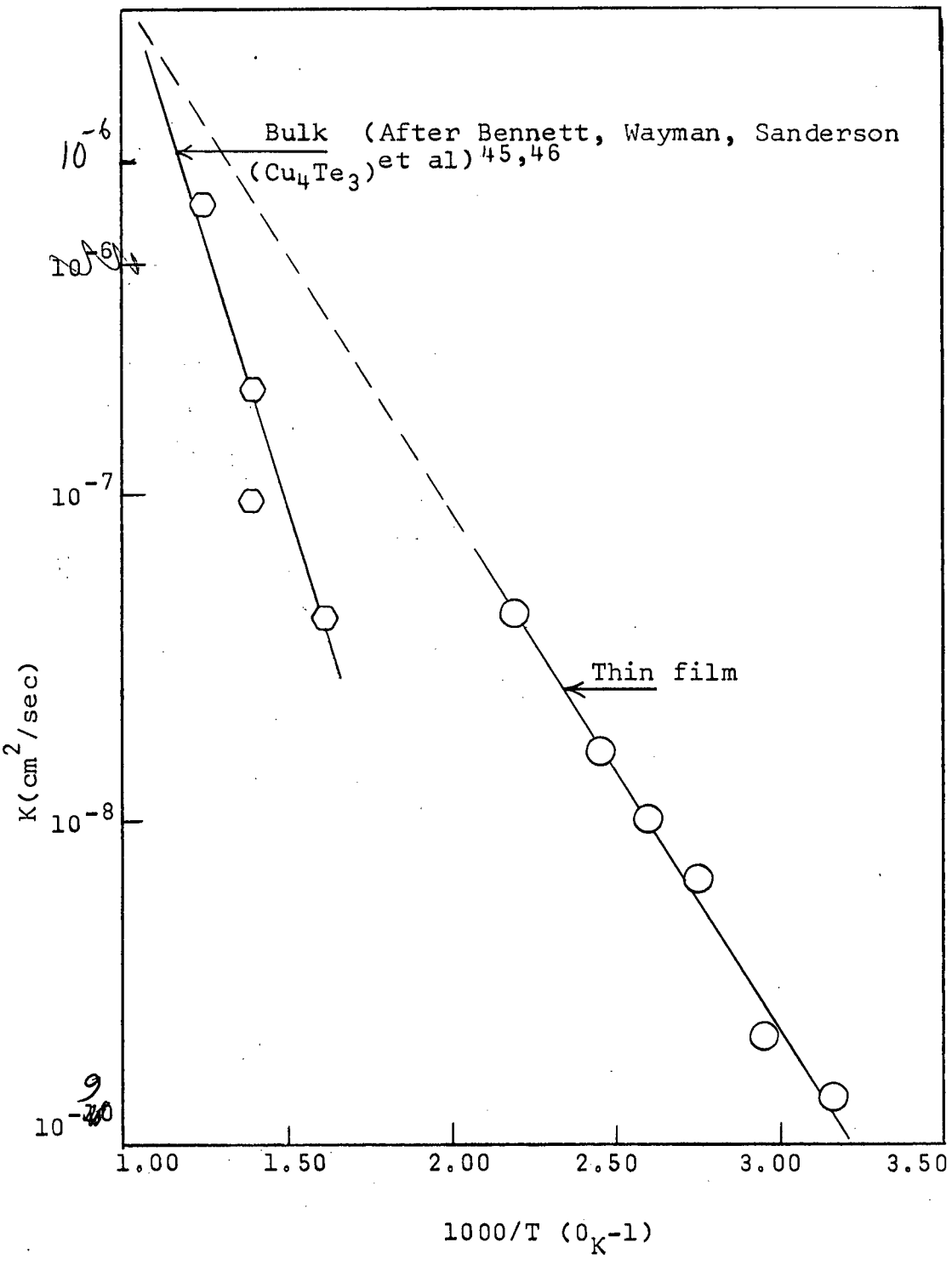

Figure 4.9 Comparison of Bulk to Thin Film Temperature Dependence

Parkinson[16] for Cu-Te thin films. His results gave

$$K = .0755 \exp[-\frac{10000}{RT}]$$

in the temperature range 0-105°C. The agreement between the two sets of results is somewhat disappointing since basically the same technique was used in both instances. It is felt that the results obtained in the present investigation are probably more reliable since a more complete range of temperatures has been used and the effects of thickness ratio and Te film thickness have been properly understood.

Figure 4.9 shows an Arrhenius plot of the rate constant for growth of $Cu_{2-x}Te$ in bulk Cu-Te couples as found by Wayman and Bennett[45], Sanderson, St. John, and Brown[46]. This system is one in which diffusion is sensitive to any compressive stress applied to the diffusion zone. The work of Sanderson et al has shown that during diffusion a third phase, Cu_2Te, appears in the diffusion zone in addition to $Cu_{2-x}Te$ and Cu-Te, if the magnitude of the applied stress is great enough. At zero applied stress Cu_2Te is not detected. In the thin film couples studied, only the phase $Cu_{2-x}Te$ was ever present. The absence of any Cu_2Te indicates that the thin film couples were comparable to bulk couples at "zero pressure". Therefore, a valid comparison between the temperature dependence of the growth rates of $Cu_{2-x}Te$ in bulk and thin films can be made.

If the Arrhenius plot for bulk specimens in Figure

4.9 is compared to the thin film curve, it can be seen that although the activation energies are quite different, the diffusion rate constants in bulk and thin film couples are quite comparable in the 300-450°C temperature range. The convergence of the two curves at these temperatures suggests that some short circuit diffusion mechanism such as grain boundary diffusion is operative at lower temperatures (see Figure 1.2). The activation energy predicted by the bulk graph is 15000 cal/mole, nearly twice as great as the thin film activation energy of 7800 cal/mole. This is again indicative of a short circuit mechanism in the thin films.

4.3 Electron Microscopy

The advance of a phase boundary along a Te film suggests a somewhat different picture from that presented by the Ag-Se system due to the crystalline structure of the Te. As viewed by transmission microscopy, the phase boundary motion is still quite rapid but the phase interface in general is seen to be more irregular at high magnification. This is illustrated in Figures 4.10 and 4.11 which show respectively the interface motion along a Te film 490 Å thick and one of only 200 Å thickness. An interesting feature of the latter series of micrographs is that the Te film is still so thin that a well-defined grain structure is not present. The total elapsed time between pictures #1 and #4 in both series is about 6 minutes. All of the micro-

(1)

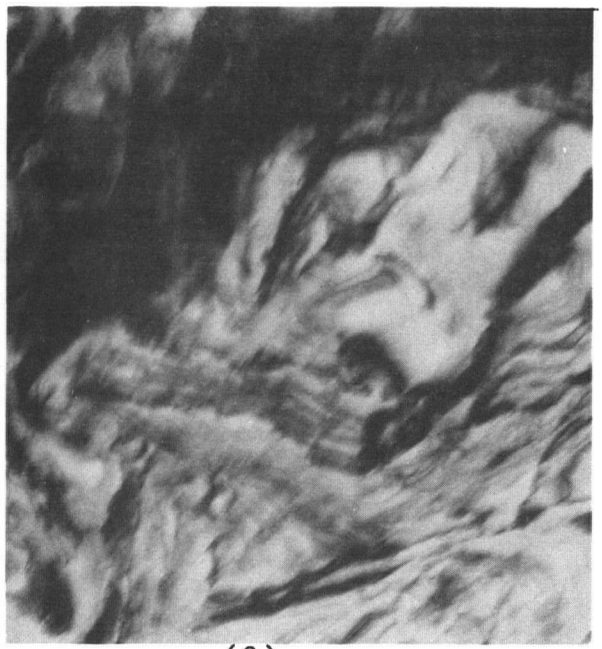

(2)

(3)

(4)

Figure 4.10 Motion of the $Cu_{2-x}Te$ Phase Boundary (x22,000)

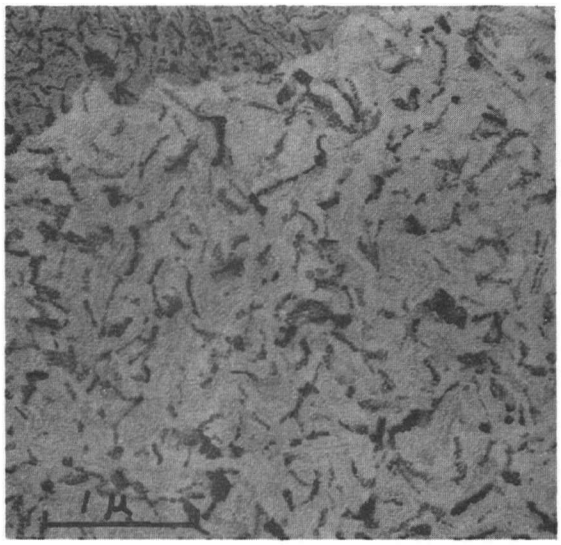

(1)

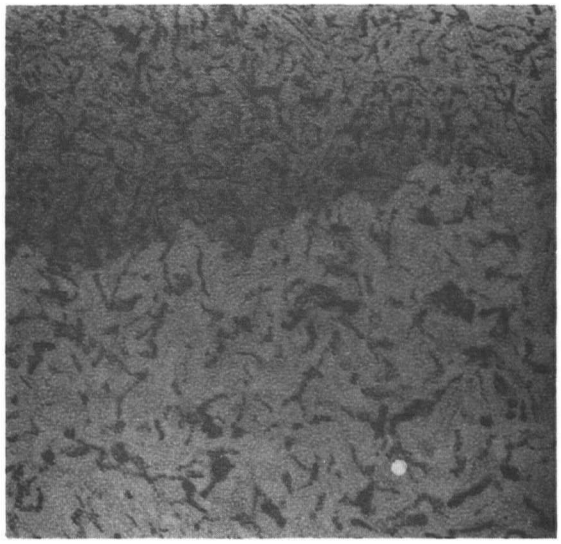

(2)

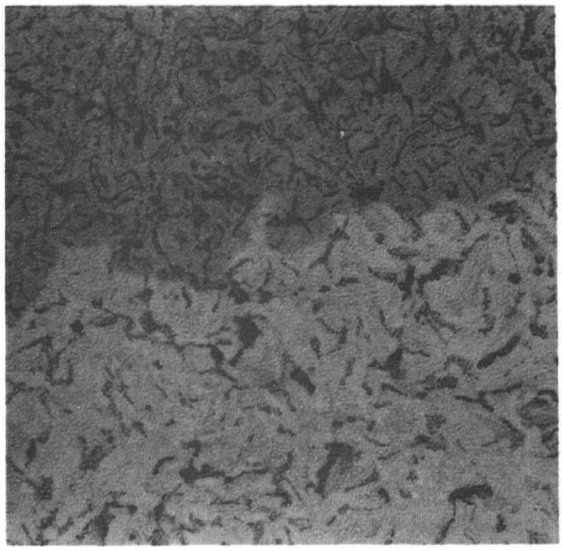

(3)

(4)

Figure 4.11 Diffusion into a 200 Å Te Film

graphs indicate that the grains in the diffusion zone are equiaxed rather than columnar as in Ag-Se. The micrographs of Figure 4.12 are enlargements of the phase boundary interfaces of the previous two figures. Figure 4.12 (b), in particular, suggests that there is some tendency for the advancing phase boundary to surround some of the Te grains. This phenomenon is more clearly demonstrated in Figure 4.13 and its accompanying schematic sketch (Figure 4.14) which depicts the surrounding of a Te grain by the advancing phase boundary. These observations suggest that there is a tendency for grain boundary diffusion to occur in Cu-Te.

The results of an electron diffraction study of the diffusion zone in Cu-Te showed that only the phase $Cu_{2-x}Te$ was formed during diffusion. A typical selected area diffraction pattern and the calculated d-spacings obtained from it are shown in Figure 4.15.

Electron microscopy results on the motion of the $Cu_{2-x}Te$ phase boundary suggest that grain boundary diffusion is important in the room temperature diffusion process which occurs in Cu-Te. Grain boundary diffusion would account for the irregular nature of the phase boundary interface. The equiaxed grain structure of the diffusion zone suggests that its formation may be due to lateral diffusion from the grain boundaries into the pure Te grains. Also the peak in the growth rate at a Te thickness of about 110 $\mathring{A}$ is in agreement

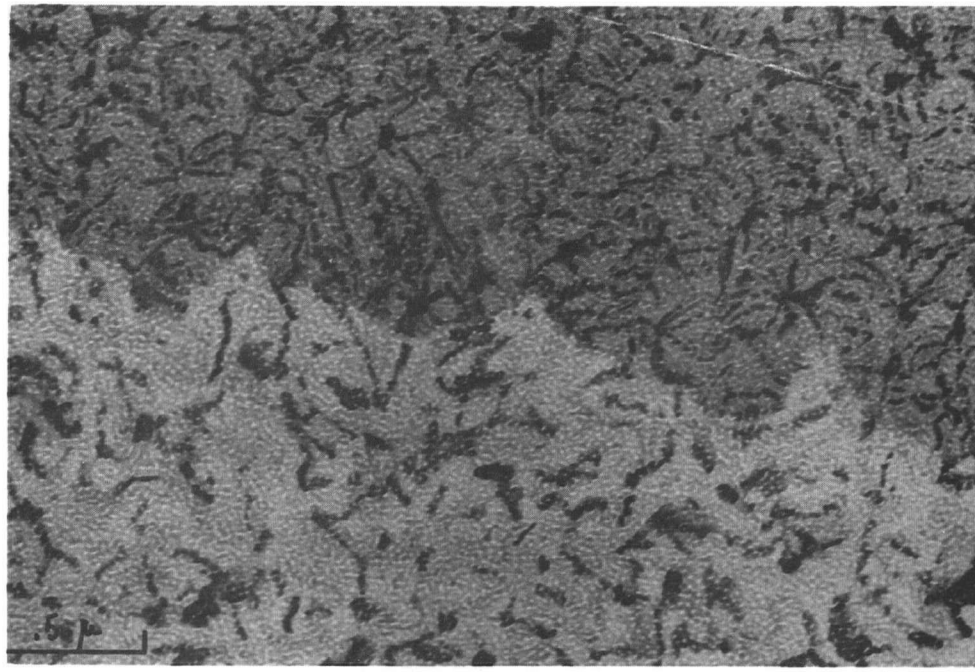

t_{Te} = 200 Å

(a)

t_{Te} = 490 Å

(b)

Figure 4.12 Phase Boundary Interfaces at High Magnification

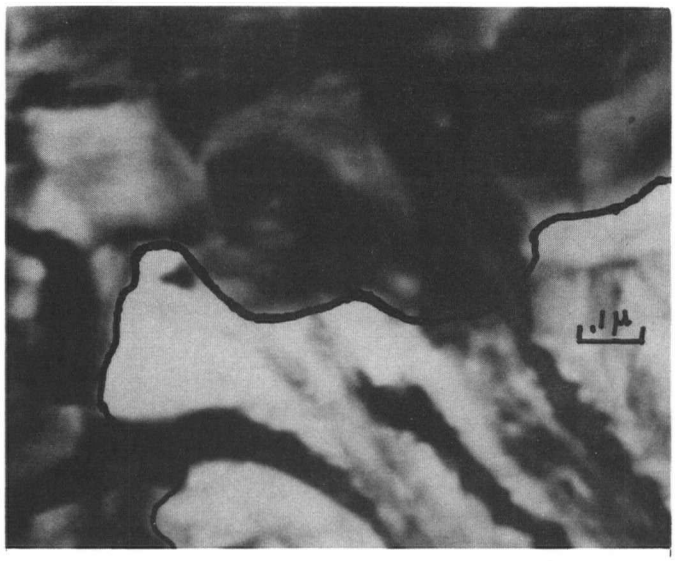

(1)

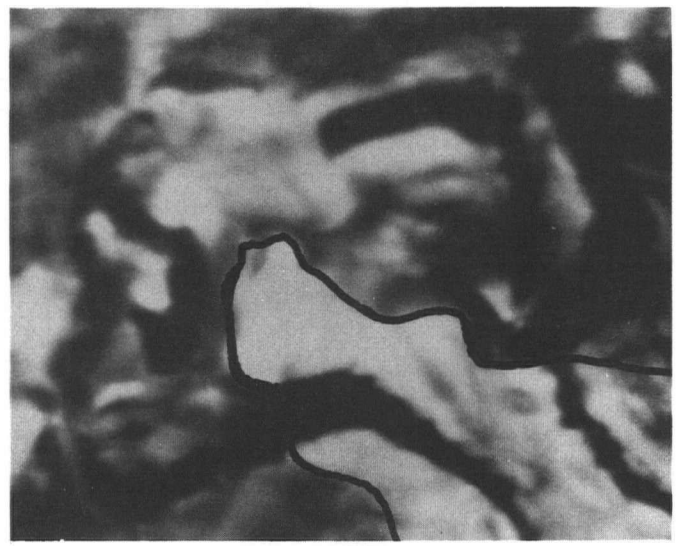

(2)

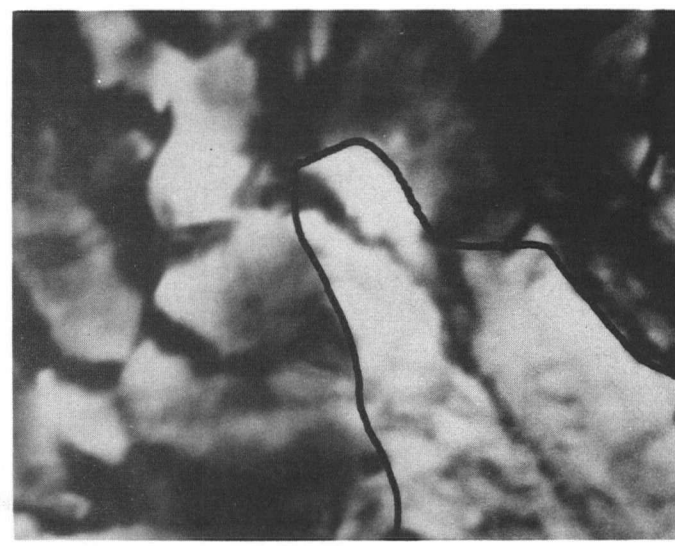

(3)

Figure 4.13 The Surrounding of a Grain of Te by the Diffusion Zone Interface

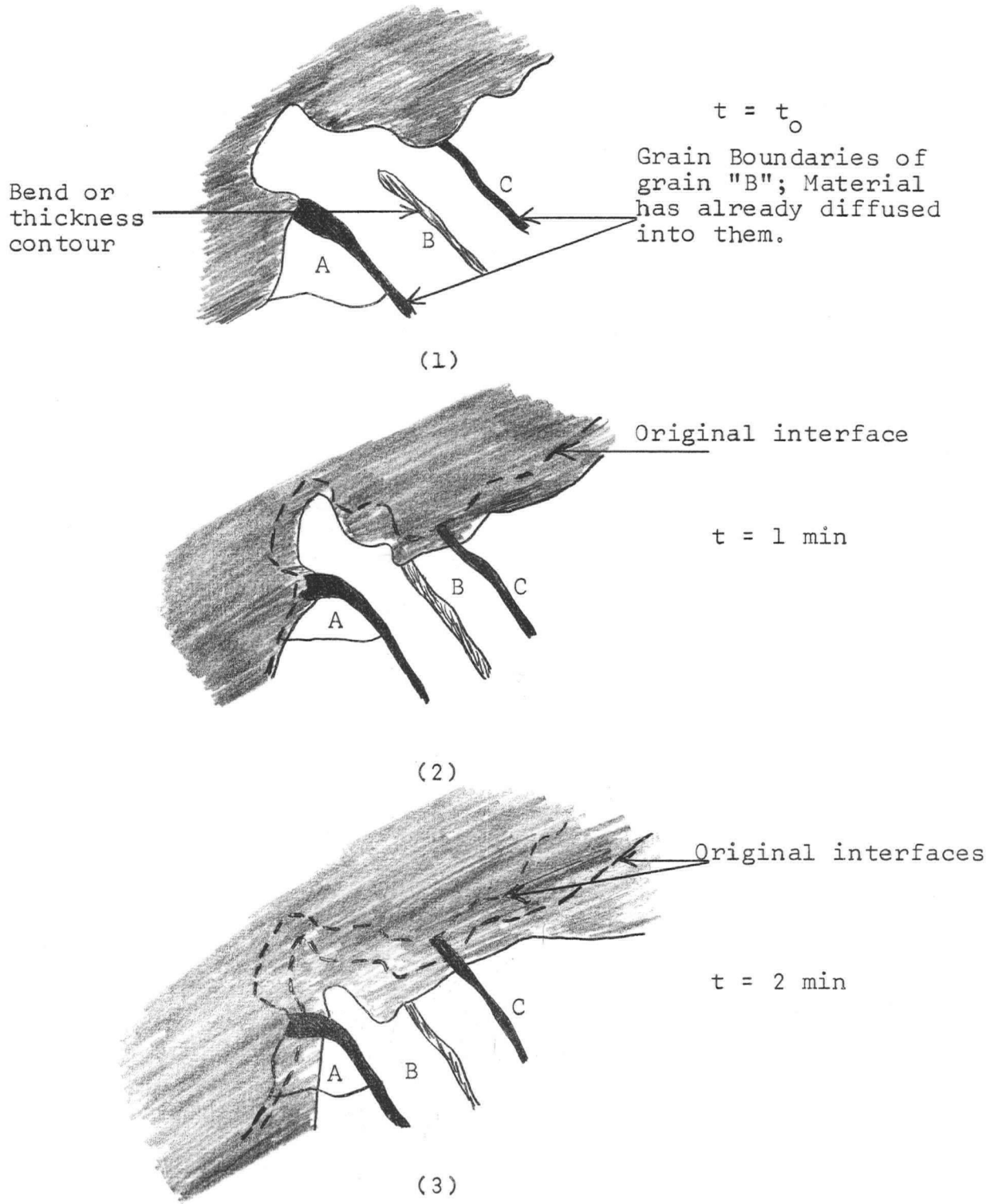

Figure 4.14 Schematic Sketch of the Surrounding of a Te Grain by the Phase Boundary Interface

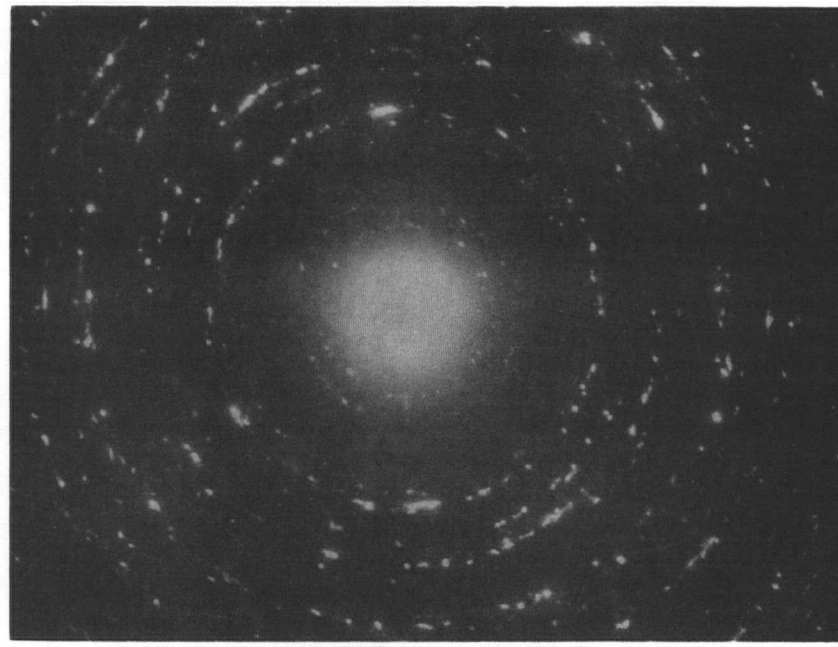

(a) S.A.D. of diffusion zone of Cu-Te thin film couple

Calculated d-spacings (Å)	d-spacings for $Cu_{2-x}Te$ (Å)
8.29	
7.82	
6.08	6.05
3.70	
3.42	3.35
2.88	2.81
2.62	2.54
2.48	2.42
2.11	2.07
1.85	1.82
1.76	1.70

Figure 4.15 Selected Area Diffraction Pattern of the Diffusion Zone of a Cu-Te Thin Film Couple

with a grain boundary mechanism. No quantitative estimate of the relative rates of grain boundary to volume diffusion could be made on the basis of the electron micrographs. Nevertheless, the microscopy results provide strong evidence to support the idea that grain boundary diffusion is an important mechanism in thin film Cu-Te couples.

CHAPTER 5

LATERAL DIFFUSION IN Ag-Te

5.1 Introduction

The overall results found in the Ag-Te system closely paralleled those of Cu-Te and for this reason they will be reviewed only briefly. The equilibrium phase diagram, seen in Figure 5.1[40], shows that two intermetallic phases, Ag_2Te and $Ag_{5-x}Te_3 (x \sim 0.2)$, may be thermally stable at room temperature. The phase Ag_2Te undergoes a polymorphic transition between 135 and 149°C. The low temperature modification, β-Ag_2Te[47], with which we are concerned here, is reported by Hansen[40] to possess an orthorhombic structure. $Ag_{5-x}Te_3 (x \sim 0.2)$, the other stable phase in this system, has a hexagonal structure.

5.2 Kinetics

In all diffusion zones studied in Ag-Te the phase boundary motion was found to be parabolic. The rate of advance of the interface was quite rapid - nearly an order of magnitude greater than in Cu-Te - and the interface itself was observed to remain very planar even when the diffusion

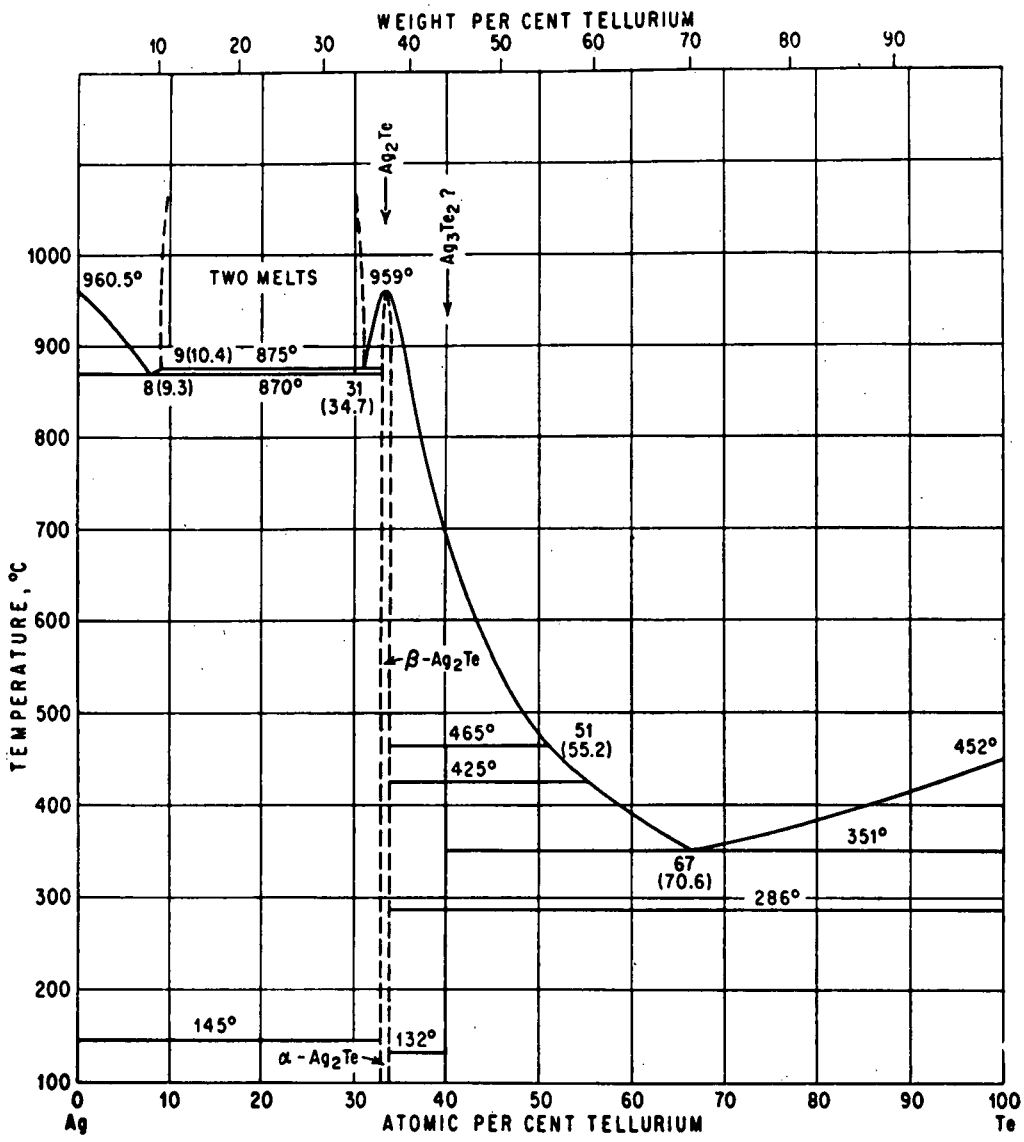

Figure 5.1 Equilibrium Phase Diagram of Ag-Te (after Hansen[40])

zone width was 700-800 μ.

For Te thicknesses between 50 and 180 Å (with $t_{Ag}/t_{Te} > R_c$) the diffusion rate constant attained substantially higher values than at greater thicknesses. Between 200 and 1750 Å the rate constant tended to a constant value of about 1.9×10^{-8} cm^2/sec. Figure 5.2 illustrates the experimental dependence of the rate constant on the Te thickness. The peak value observed lies at about 80 Å and is over twenty times the constant value found at thicknesses of 200 Å and greater. This is a much larger effect than that seen in any of the other three systems investigated. It is probably due to the network structure of very thin Te films which gives high diffusion rates between islands as discussed in section 4.2.3. Figure 5.3 shows the dependence of the rate constant on the Ag to Te thickness ratio (t_{Ag}/t_{Te}) for couples in which $t_{Ag} > 180$ Å. The critical ratio was found to be 1.0 ± 0.1. This agrees closely with the theoretical value of 1.00 which would be given by the phase Ag_2Te. If $Ag_{5-x}Te_3 (x \sim 0.2)$ were the intermetallic phase formed during diffusion, the calculated critical ratio would be 0.715, in poor agreement with the experimental value. The results indicated, therefore, that the composition of the diffusion zone was Ag_2Te. A determination of the critical ratio at tellurium thicknesses of 105 and 2730 Å gave the same value of 1.0 ± 0.1. The critical ratio was thus taken to be independent of the Te film thickness over the thickness range under investigation.

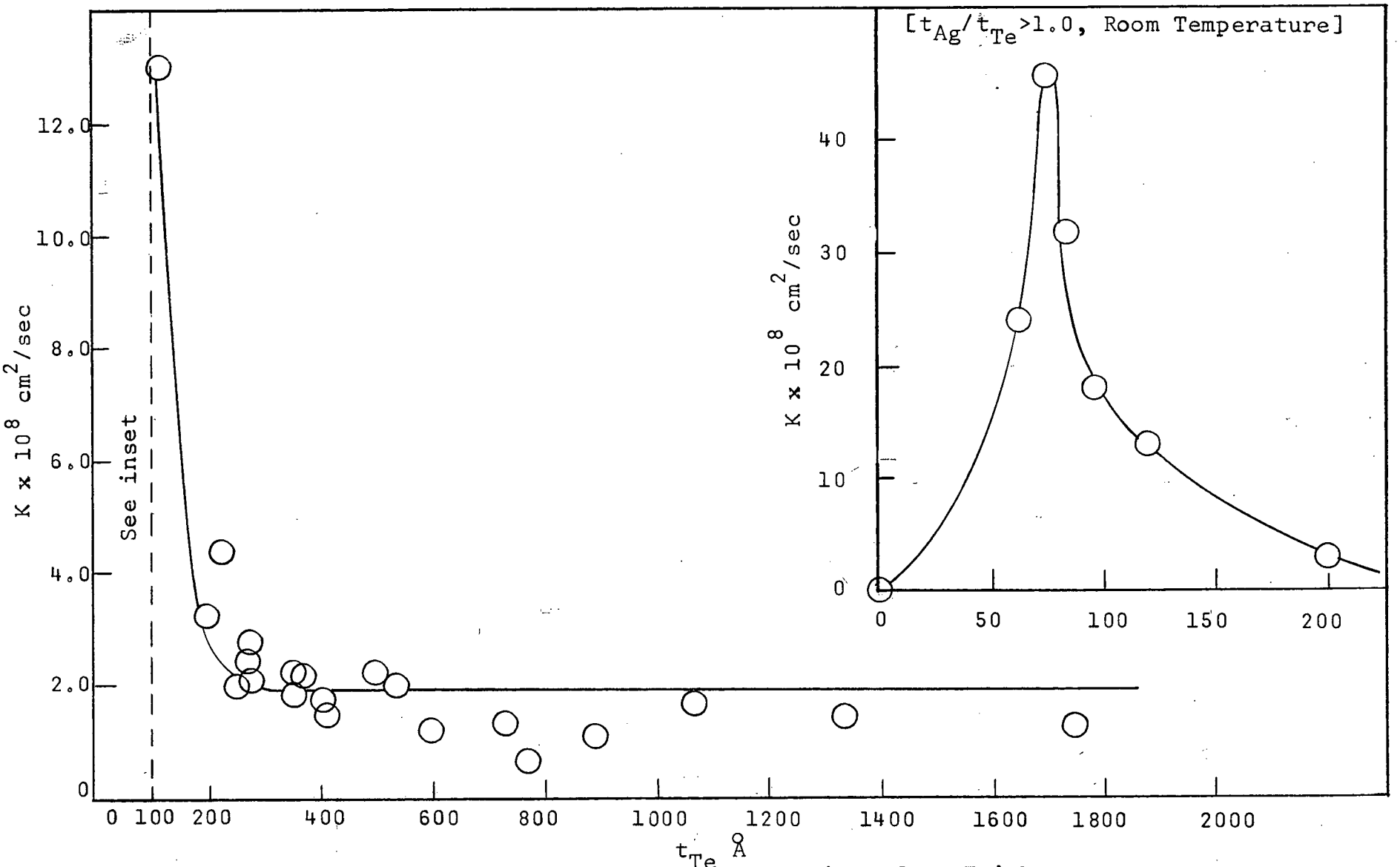

Figure 5.2 Rate Constant as a Function of Te Thickness

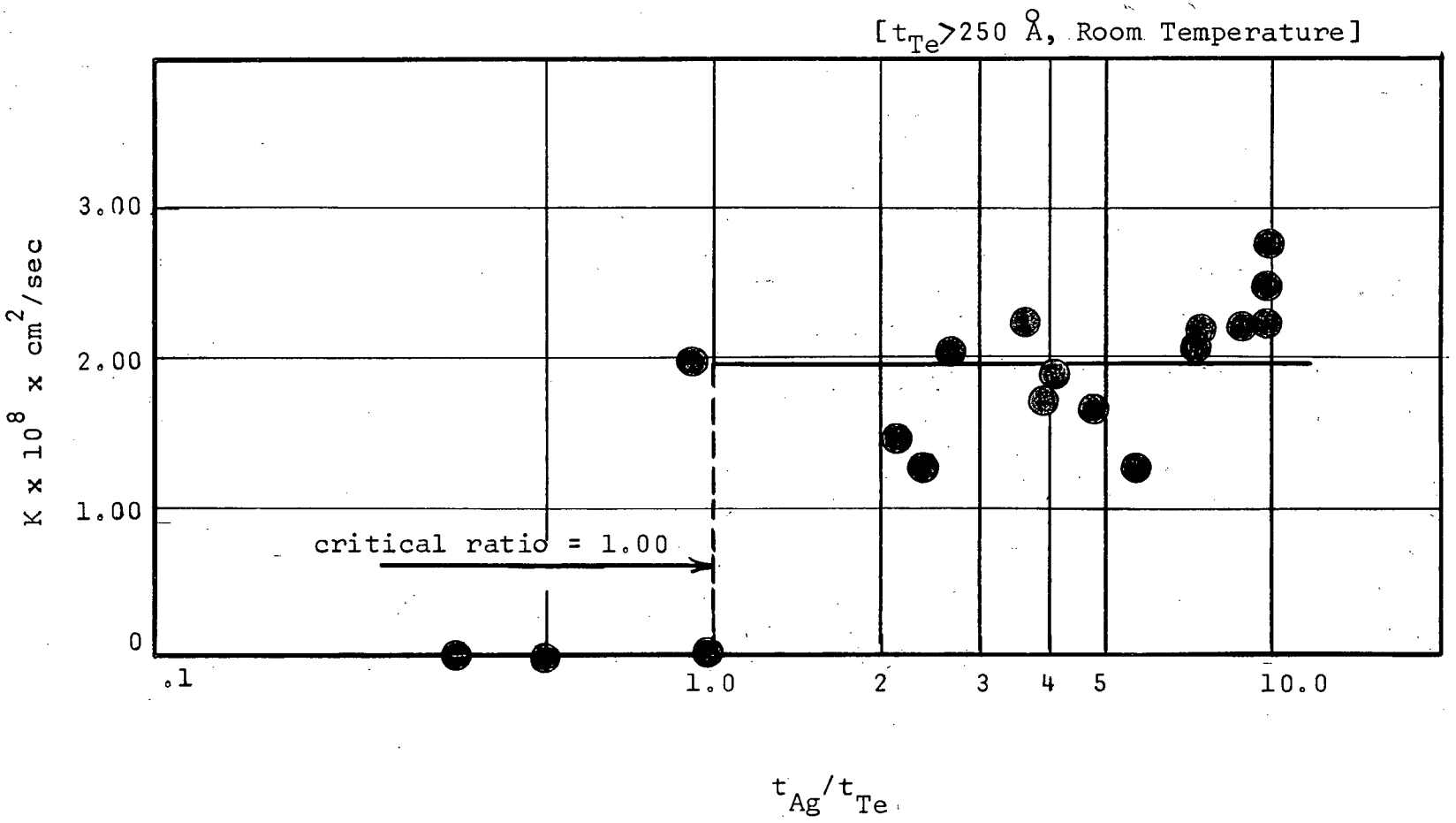

Figure 5.3 Growth Rate as a Function of Thickness Ratio

The temperature dependence of the rate constant was determined in the range 0-100°C. From the Arrhenius plot shown in Figure 5.4 the diffusion rate constant was found to be

$$K = 0.63 \exp\left[-\frac{10000}{RT}\right]$$

Also plotted in this figure is Mohr's[13] data which gives

$$K = 579 \exp\left[-\frac{13820}{RT}\right]$$

Although similar techniques were used in the two investigations, the agreement between the two sets of results is disappointing, especially at high temperatures where there is almost a one order of magnitude difference in the two measured rates. Mohr applied a correction to his growth rates to correct for volume expansion of the Te as Ag diffused in. No details of this correction are given in Mohr's paper but it would not be expected to alter the activation energy significantly.

It should be mentioned that in the two systems in which comparison was possible with the results of other workers, agreement at high temperatures was not good with the present work giving much slower rates than the other investigations. It is felt that there can be no experimental error in the present investigation which could explain anything like the observed differences in the growth rates. If there is a genuine difference in growth rates between

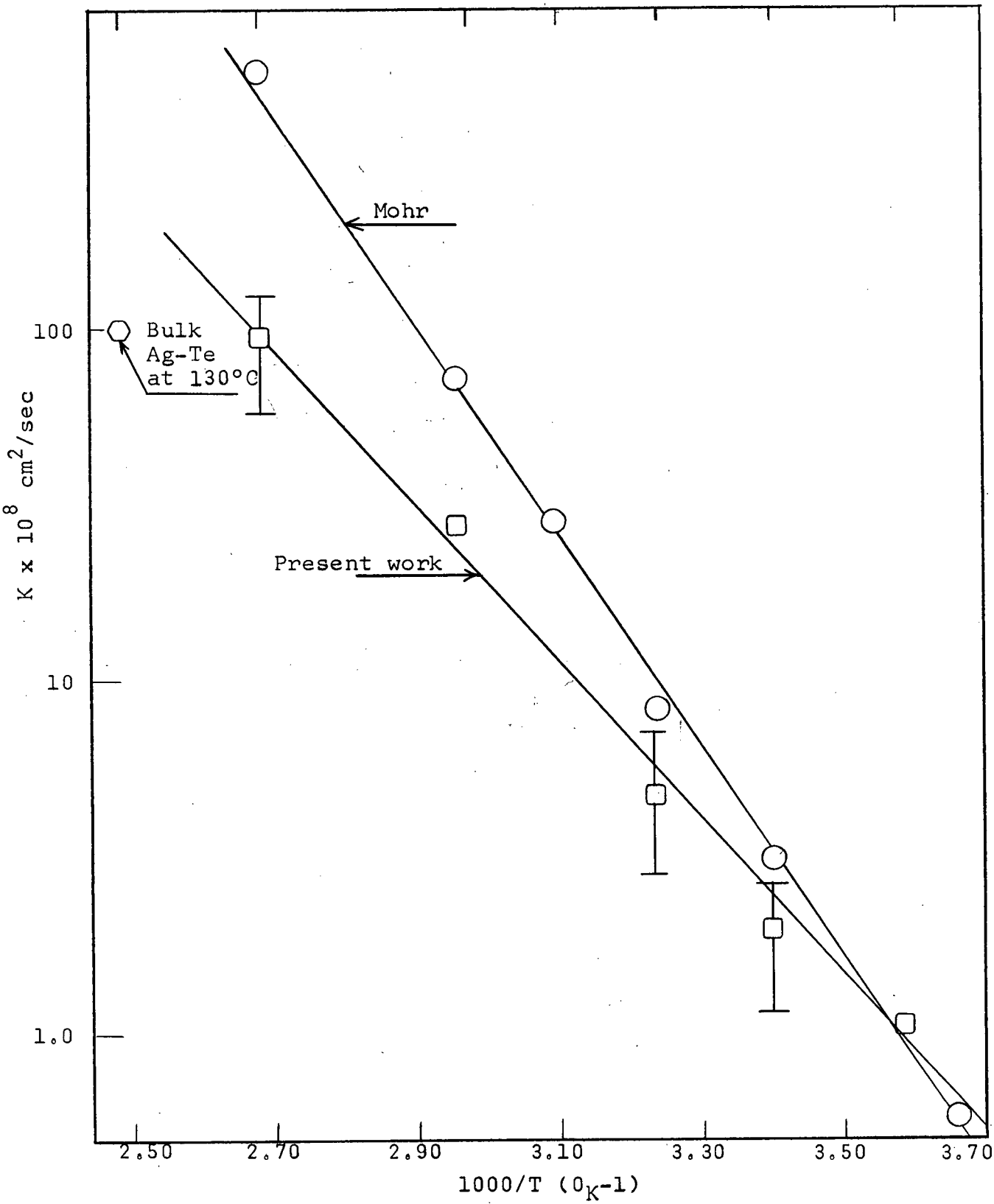

Figure 5.4 Arrhenius Plot for Ag-Te

between the two cases, this must presumably be due to some difference in structures which gives different contributions to grain boundary and volume diffusion. This might be due to different residual gas pressures, evaporation rates, or one of the many other variables which can affect film structure (see Introduction, section 1.4).

Behera[38] has shown that a study of diffusion in bulk Ag-Te couples is impossible because a proper diffusion zone is not formed. The bulk diffusion rate plotted in Figure 5.4 at 130°C is a very approximate value obtained from his work. A complete temperature study in bulk Ag-Te was not undertaken due to the irregular nature of the diffusion zones involved. However, the low value of activation energy obtained for the thin film couples does seem to indicate that some short circuit mechanism is important in the diffusion process.

5.3 Electron Microscopy

Transmission electron micrographs made of the Ag_2Te phase boundary showed that grain boundary diffusion plays a role in the diffusion process. The micrograph of the boundary interface in Figure 5.5 (a) shows many colonies of Ag_2Te lying ahead of the main diffusion zone but connected to it by "stringers" of Ag_2Te centered predominantly at the Te grain boundaries. Figure 5.5 (b) is the same interface after two hours showing essentially the same general features. The remaining two micrographs in Figure 5.5, made

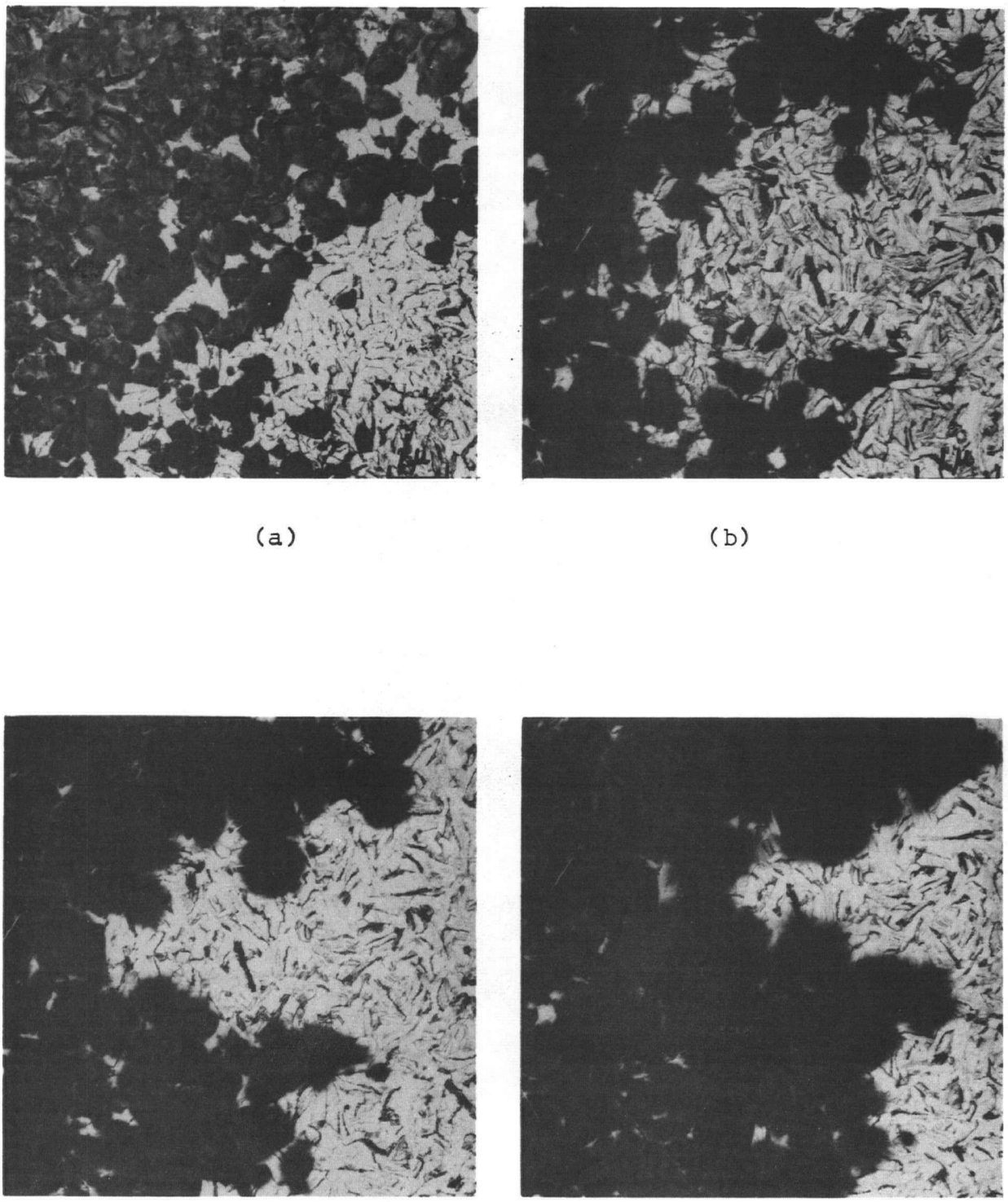

(a) (b)

(c) (d)

Figure 5.5 Phase Boundary Interface in a 210 Å Te Film

at 1 minute intervals after 5.5 (b), show how the effect of localized heating by the electron beam tends to obscure the grain boundary diffusion and makes the phase boundary interface very planar. The Te thickness in this series of pictures is about 200 Å. Figure 5.6 shows the phase boundary interface in a sample having a Te thickness of about 1000 Å. Once again, Ag_2Te has formed in Te grains ahead of the main body of the diffusion zone with stringers extending along the Te grain boundaries. In this micrograph it appears that some Ag_2Te colonies have begun their development at the grain boundary corners. This obvious tendency for grain boundary diffusion to occur is in full agreement with the large effect observed in 80-100 Å films in this system. It is probably due to a very large grain boundary diffusion coefficient in this system. The grain boundary effects in Ag-Te are much more pronounced than those in Cu-Te, which probably accounts for the higher growth rates observed in Ag-Te.

Selected area diffraction patterns were made of the diffusion zone of Ag-Te couples. The d-spacings calculated were in good agreement with the known d-spacings for β-Ag_2Te, the low temperature form of Ag_2Te. This substantiates the kinetic evidence in section 5.2 for growth of Ag_2Te rather than $Ag_{5-x}Te_3$ on the basis of agreement between experimental and theoretical values of the critical ratio. A typical set of diffraction results is

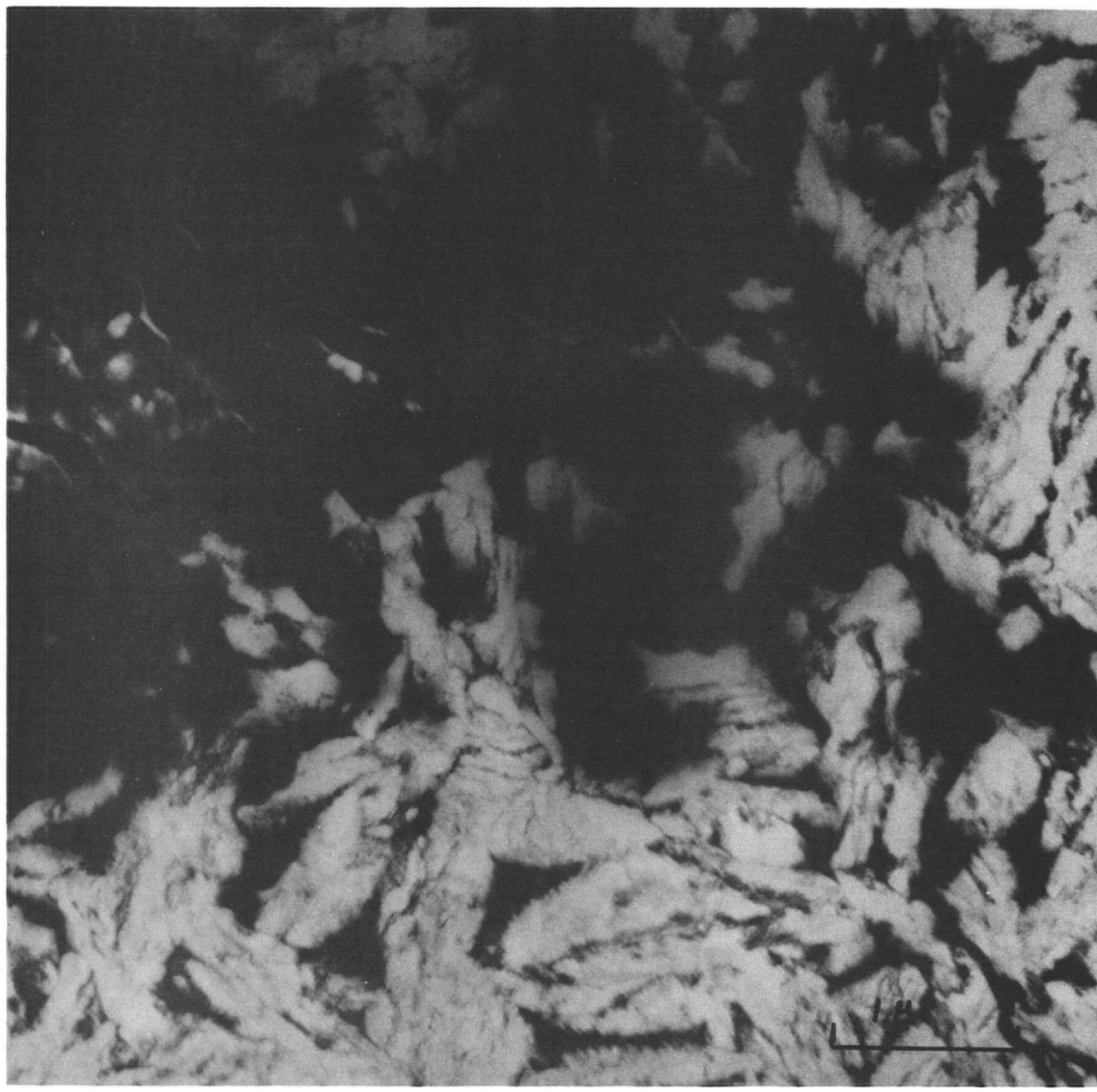

Figure 5.6 Evidence of Grain Boundary Diffusion in a 1000 Å Te film

shown in Figure 5.7.

Figure 5.8 (a) shows the result of an experiment in which high illumination levels were used in the electron microscope and the beam was focused on the Ag_2Te interface for a relatively long time; a thin band of the Te-rich phase $Ag_{5-x}Te_3$ ($x \sim 0.2$) appeared at the edge of the normal diffusion zone and began to grow into the Te at a rapid rate due to heating by the electron beam. This intermetallic phase was positively identified by a selected area diffraction pattern. The microstructure of the Ag_2Te phase in the main body of the diffusion zone is illustrated in Figure 5.8 (b). The Te thickness in this sample is about 200 Å. The exact temperature increase induced by the electron beam spot in such a small localized area is impossible to measure. It is to be expected, however, that if the appearance of this second phase during diffusion were due to thermal effects alone, a second phase would be observed in thin film couples annealed at high temperatures. Since this second phase was not present in the diffusion zones of samples heated up to 100°C, it is concluded that either the effective temperature rise produced by beam heating was greater than 100°C, or the growth of the phase was not entirely due to thermal effects.

The electron microscopy results suggest that grain boundary diffusion is an important factor in room temperature diffusion in Ag-Te. As the electron beam brings about a

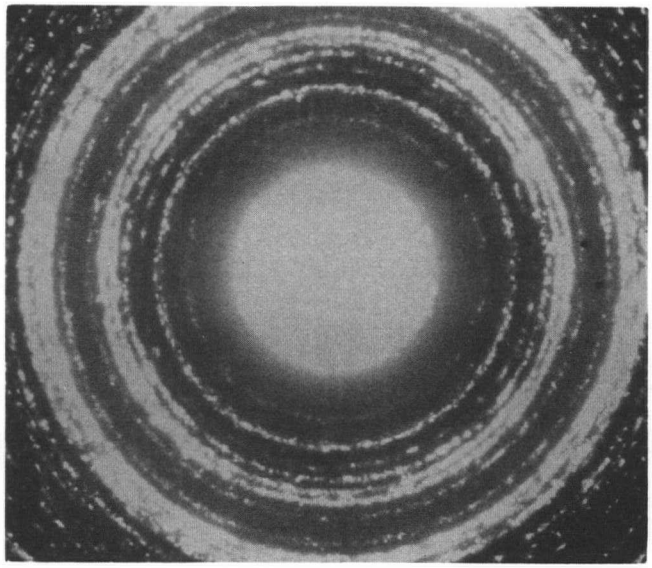

(a) S.A.D. of diffusion zone in Ag-Te

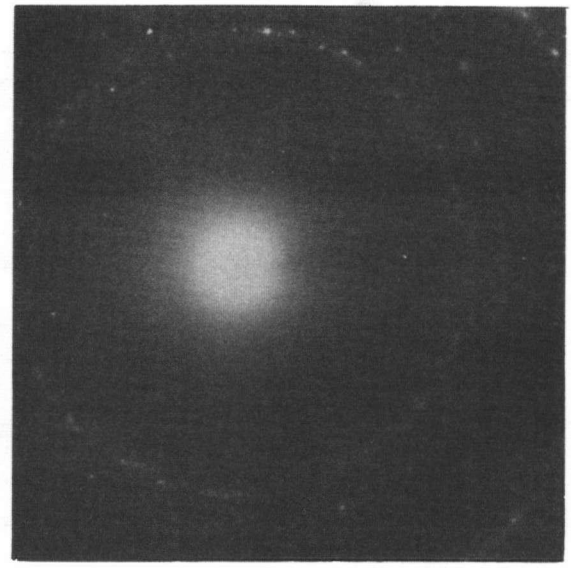

(b) Au Standard

Calculated d-spacings (Å)	d-spacings for β-Ag_2Te (Å)
7.14	7.14
6.85	
4.60	4.53
3.71	3.74
	3.40
3.19	3.19
3.01	3.01
2.88	2.87
2.73	2.80
	2.69
2.45	2.45

Figure 5.7 Selected Area Diffraction Pattern of the Diffusion Zone in Ag-Te

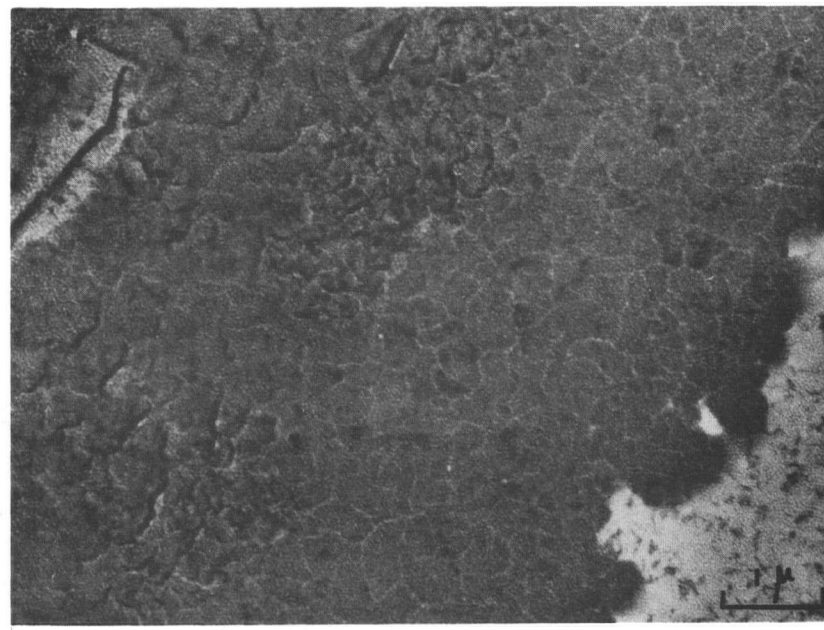

(a) Ag_{5-x} ($x \sim 0.2$) induced by electron beam heating

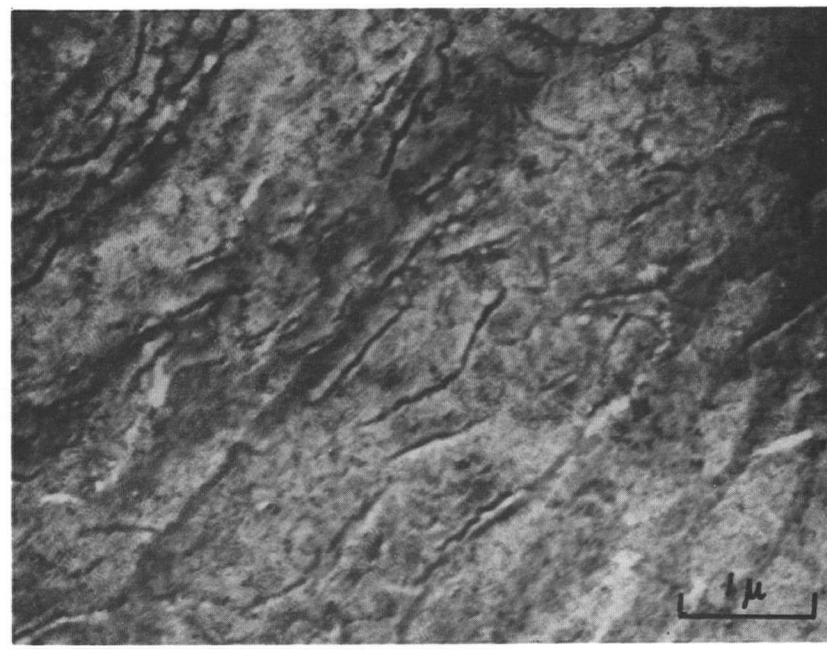

(b) Appearance of Ag_2Te phase in this sample

Figure 5.8 Electron Beam Heat-Induced Second Phase in Ag-Te

localized temperature increase at the phase boundary interface the grain boundary diffusion is obscured by rapid advance of an interface that has become increasingly planar as the temperature rose. This implies that grain boundary diffusion is not important at higher temperatures. Since the presence of a second phase was not detected during normal diffusion experiments at 100°C, it is conceivable that the electron beam heating produced by high illumination levels results in a temperature rise of greater than 100°C.

CHAPTER 6

LATERAL DIFFUSION IN Cu-Se

6.1 Introduction

A complete equilibrium phase diagram is not yet available for Cu-Se. The three intermediate phases that can be in thermal equilibrium at room temperature are $Cu_{2-x}Se$ ($0.0 < x < 0.2$), Cu_3Se_2, and CuSe[40]. $Cu_{2-x}Se$ is a copper deficient form of the stoichiometric intermetallic compound Cu_2Se (33.3 at % Se). The high temperature polymorph of this phase has an anti-isomorphous CaF_2 structure[41] in which Se atoms replace Ca atoms. As the deviation from stoichiometry in Cu_2Se increases, the transformation temperature decreases, so that the cubic structure becomes stable at room temperature. At the stoichiometric composition, however, the transformation temperature is around 100°C. Below this temperature, a number of metastable tetragonal or B.C.C. structures are encountered depending on the heating and cooling history[40,48,49]. The truly stable low temperature structure is not known. Cu_3Se_2 has a tetragonal structure. There is a strong possibility that this phase is a grossly defective $Cu_{4-x}Se_2$ compound

only approximating Cu_3Se_2 in composition. CuSe has a hexagonal structure.

6.2 Kinetics

6.2.1 Growth Rate

The graph of diffusion zone width (x) as a function of $\sqrt{t}$ for about 85% of all diffusion couples studied was of the form of curve I in Figure 6.1. Most of the remaining 15% exhibited the behaviour of curve II in this figure with only a small fraction being strictly parabolic in nature (curve III). The essential features of curves I and II are illustrated in Figure 6.2. The dependence of x on $\sqrt{t}$ in each "stage" of both curves was linear suggesting that growth was diffusion controlled. The basic difference between curves I and II is that stage 2 in the latter is much shorter, degenerating into stage 3, a region of more rapid growth. It should be emphasized that the physical implication of growth curves like I and II is that a very wide diffusion zone - 500 to 600 μ in some cases - develops in about one hour. A period of slower parabolic growth then follows. This may persist over a long time as curve I suggests or may be followed by a period of rapid growth (curve II). Such behaviour may, at first glance, appear to be due to the formation of a second phase during diffusion. However, no evidence of more than one phase was ever seen by optical microscopy. Therefore this explana-

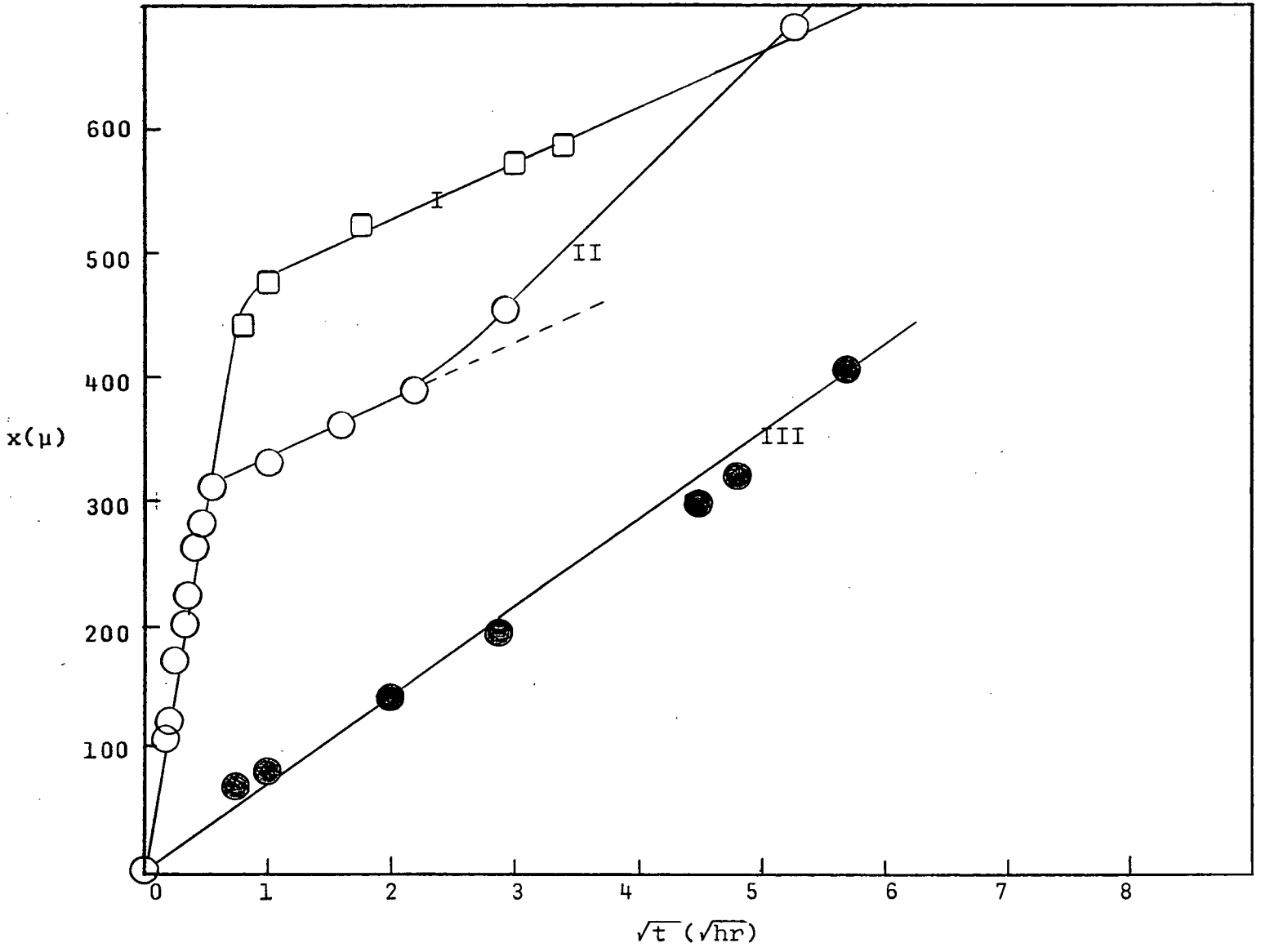

Figure 6.1 Typical Room Temperature Kinetics Plots

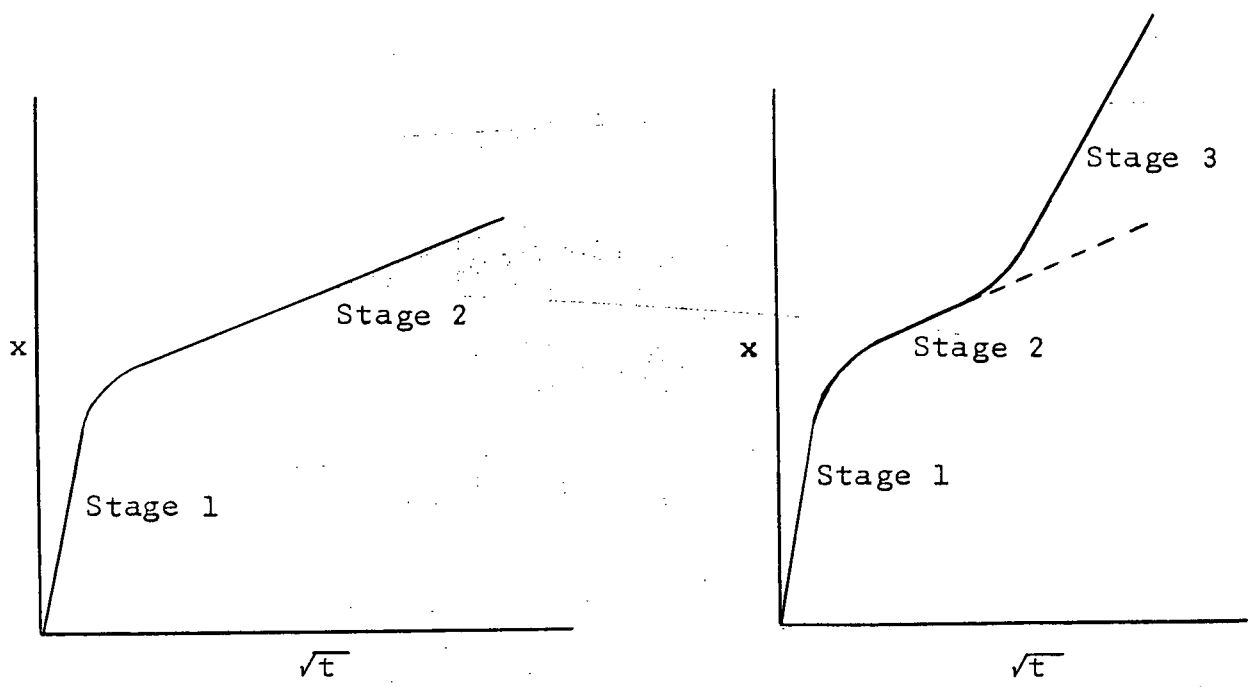

(a) Curve I (b) Curve II

Figure 6.2 General Form of Majority of Growth Plots.

tion does not account for the observed behaviour.

A diffusion rate constant was calculated from each of the linear regions of both types of curves I and II. It was found that in stage 1, the rate constants were widely variable bearing no apparent relationship to Se thickness or thickness ratio. Similarly, the rate constants determined in stage 3 showed a large degree of scatter, although the magnitudes of the slopes were of course much smaller than those in stage 1. Using the rate constants of stage 2, however, a set of results for the dependence of rate constant on Se thickness and on the ratio of Cu to Se thickness (t_{Cu}/t_{Se}) was obtained that was completely analogous to the other three systems. For this reason the rate constants calculated from stage 2 were taken as being representative of the lateral diffusion process in Cu-Se, although it may well be that the diffusion controlled region is in fact stage 1 with stage 2 being a region showing certain inhibitions to diffusion.

6.2.2 Dependence of Rate Constant on Se Thickness

Figure 6.3 shows the diffusion rate constant plotted as a function of Se thickness. At thicknesses greater than 180 Å the rate constant tends to a constant value of 0.80×10^{-8} cm^2/sec while at lower thicknesses it rises to a peak value of approximately 3.3×10^{-8} cm^2/sec at about 100 Å. This possible tendency for higher diffusion rates to occur in thin Se films appears to be consistent with the effect observed in Ag-Se where the maximum

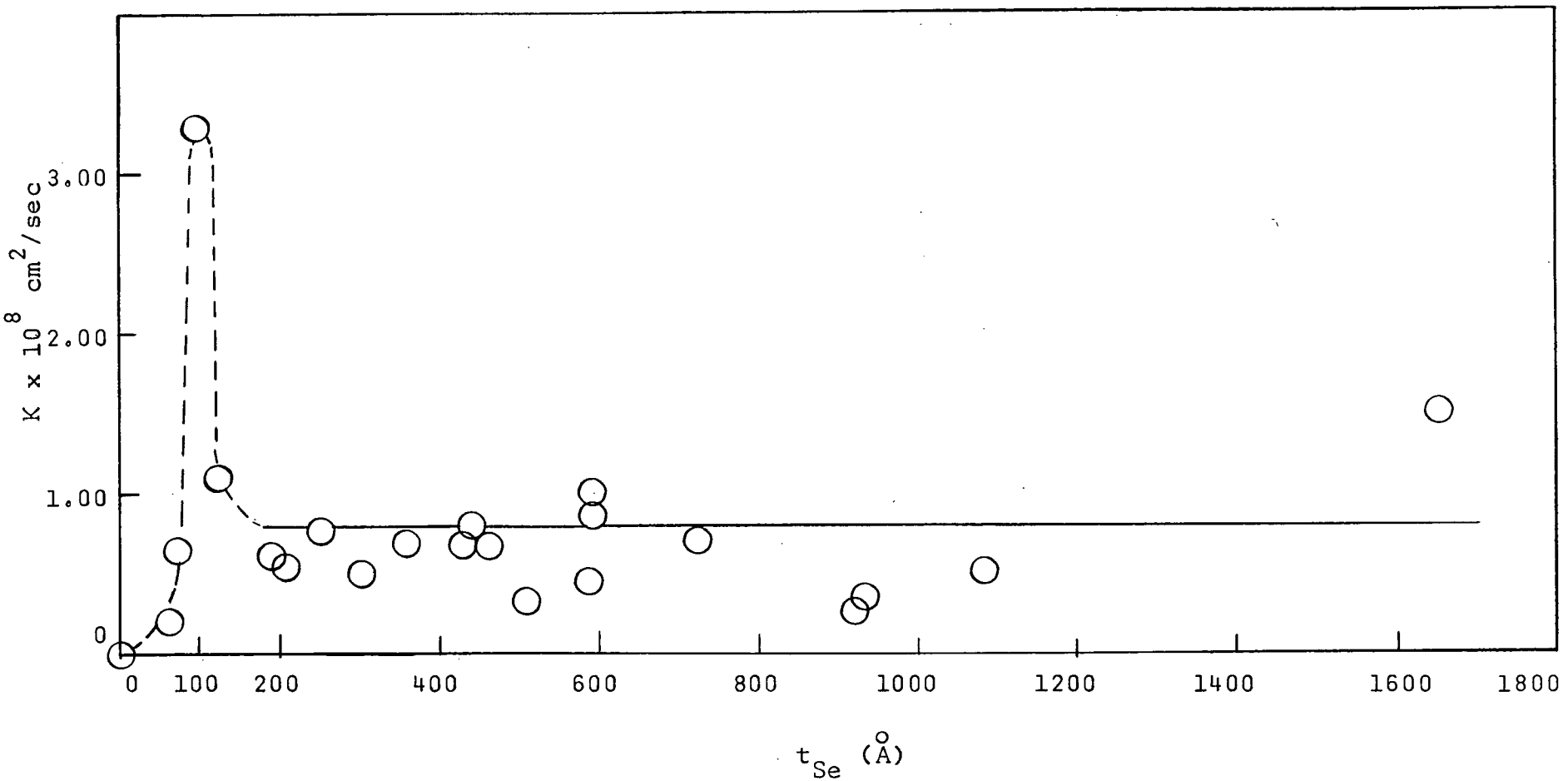

Figure 6.3 Rate Constant as a Function of Se Thickness

diffusion rate is also about four times the constant value obtained at Se thicknesses exceeding 180 Å. This is not unexpected since the structure of the Se films is the same in both cases. Therefore the same mechanism proposed for enhanced diffusion in Ag-Se (section 3.2.3) should be applicable to Cu-Se as well. The optical micrograph in Figure 6.4 illustrates the irregular nature of the phase boundary interface in a sample having a Se thickness of 125 Å. The wavelength of the minute projections on the interface is about 1 μ which is consistent with the inter-island spacing in the Se at this stage of growth.

6.2.3 Critical Ratio

The critical ratio in Cu-Se was found to be between 0.63 and 0.71. Below this range diffusion did not occur while above it, diffusion proceeded at a constant value of 0.80×10^{-8} cm^2/sec for couples in which the Se thickness was greater than 180 Å. The results of the thickness ratio (t_{Cu}/t_{Se}) study are shown in Figure 6.5. The theoretical values of R_c were calculated for each of the phases $Cu_{2-x}Se$, Cu_3Se_2, and CuSe and are listed in Table 6.1. Comparing these values with the experimental value for R_c, it was seen that the composition of the diffusion zone should be $Cu_{2-x}Se$. A determination of the critical ratio at Se thicknesses of 350 and 2380 Å gave values of 0.71 and 0.63 respectively. Thus the critical ratio was taken to be independent of the absolute Se thickness.

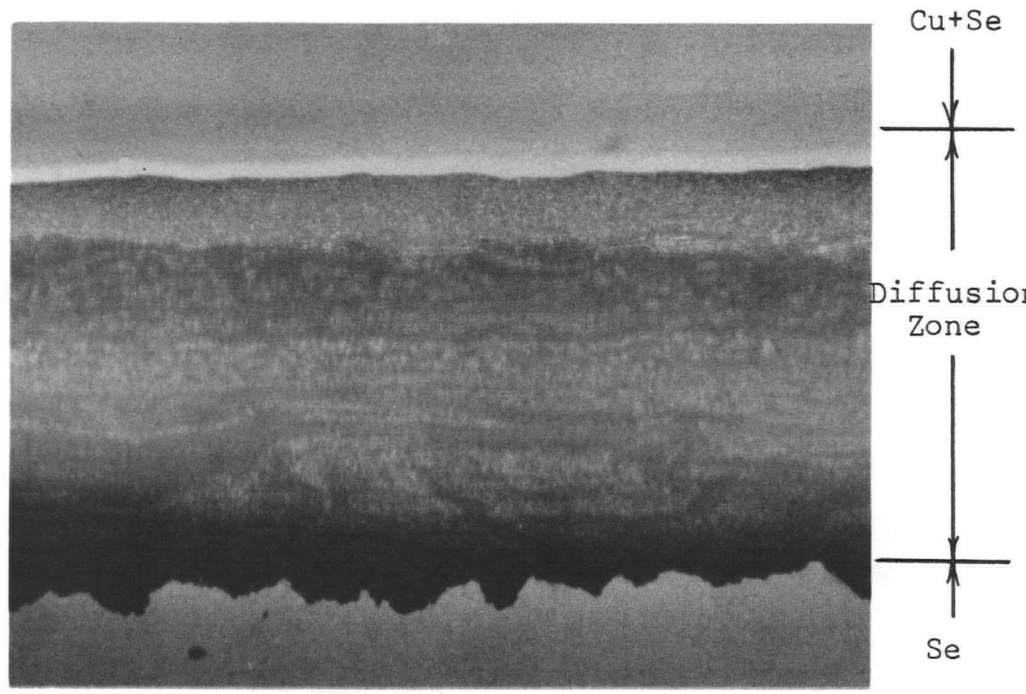

Figure 6.4 Phase Boundary Interface in a 125 Å Se Film (x71)

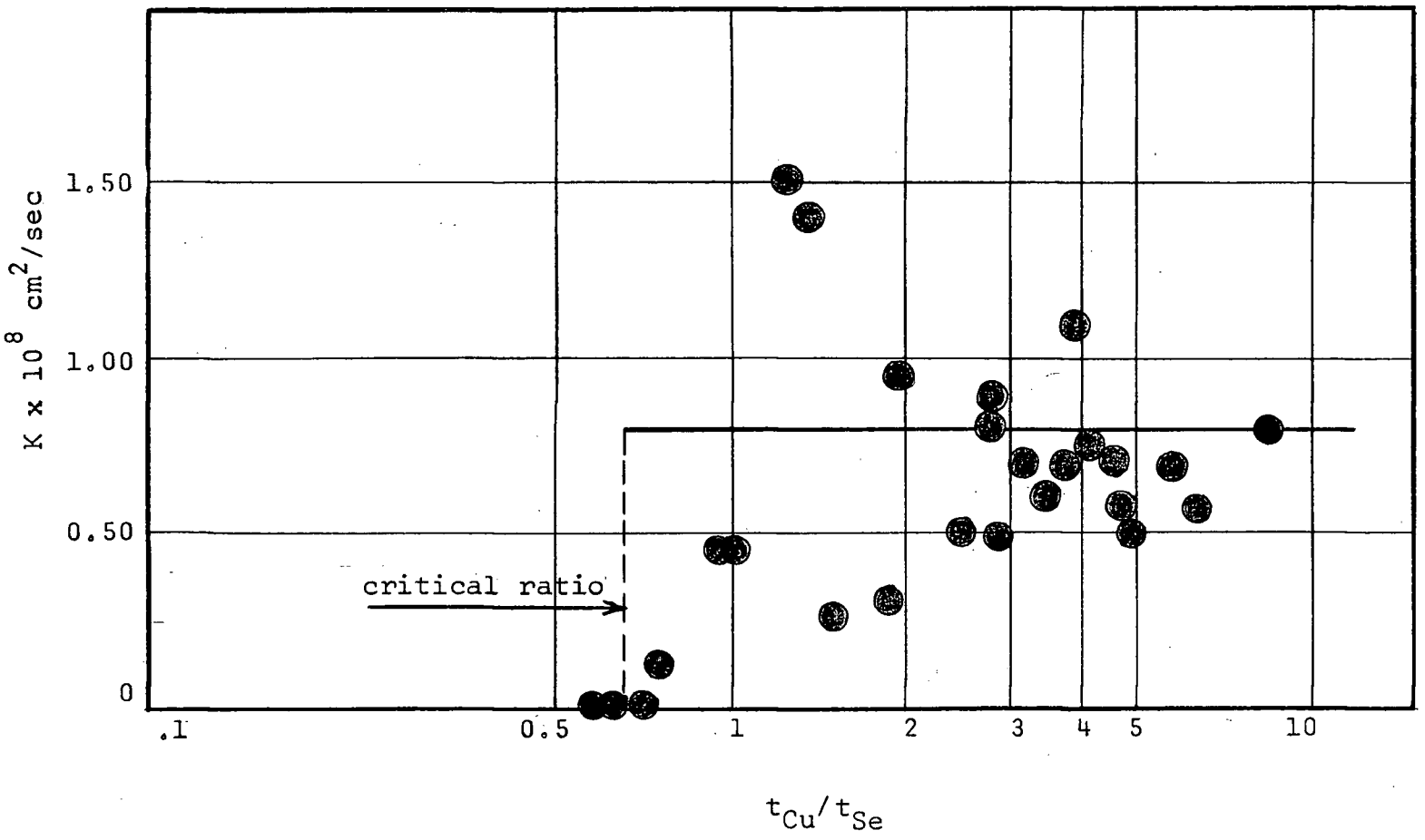

Figure 6.5 Rate Constant as a Function of Thickness Ratio

TABLE 6.1

Theoretical Critical Ratios in Cu-Se

Phase	Theoretical R_c
$Cu_{2-x}Se$, x=0.0	.720
$Cu_{2-x}Se$, x=0.2	.645
Cu_3Se_2	.513
CuSe	.375

6.2.4 Temperature Dependence

The temperature dependence of the rate constant was determined over the range 0-50°C. Higher temperatures were not used in order to avoid any aggregation of Se on the glass substrates. The shapes of the x versus $\sqrt{t}$ curves were not observed to change with temperature, most showing the two stages of parabolic growth discussed in section 6.2.1. Although growth rates in this system at room temperature are comparable with rates in other systems, the increase in growth rate with increasing temperature is much greater than that found in any other system. Taking the growth rate characterized by the second stage of the x versus $\sqrt{t}$ curves the temperature dependence of the rate constant determined from the Arrhenius plot in Figure 6.6 is given by

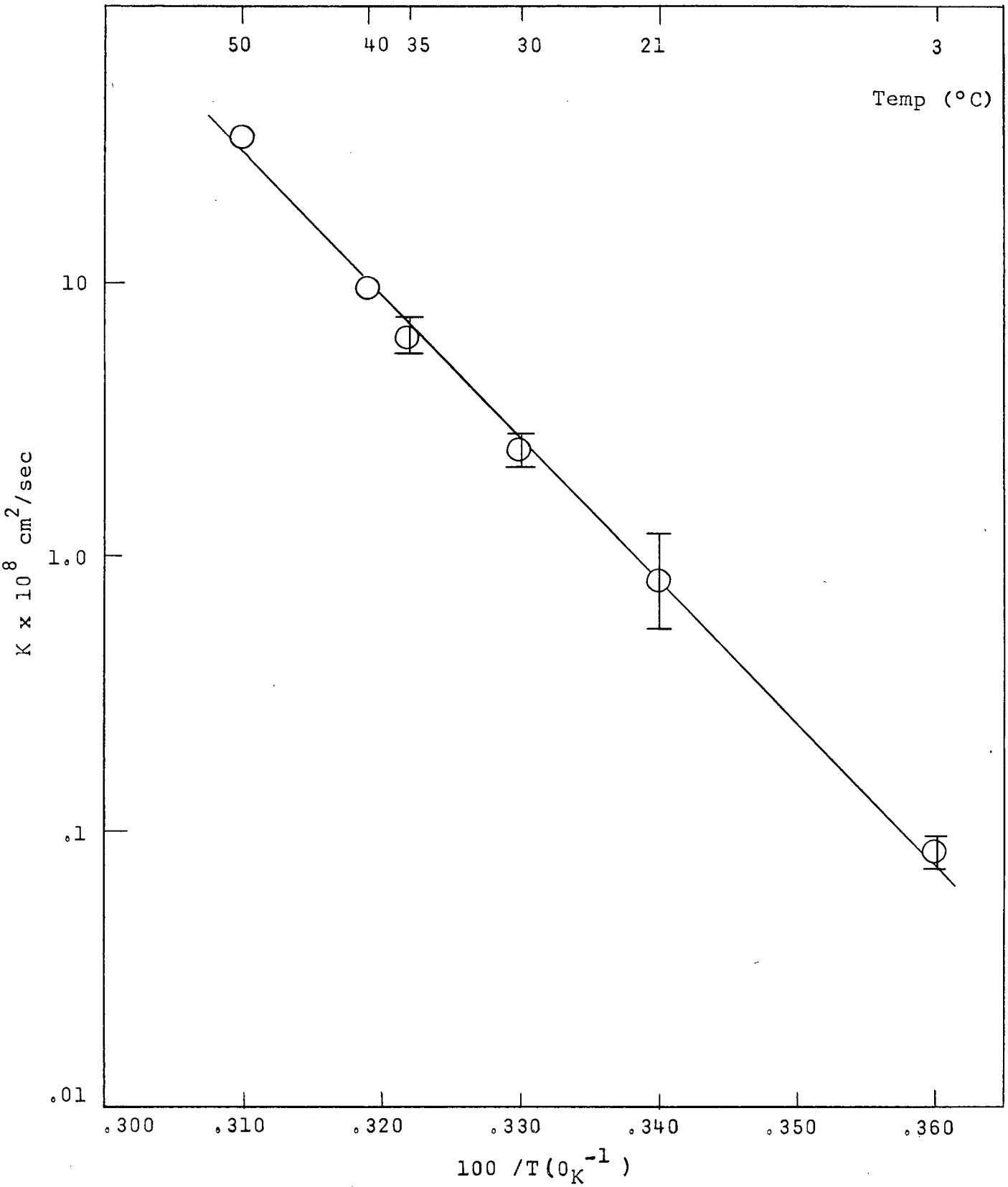

Figure 6.6 Arrhenius Plot for Cu-Se

$$K = 3.9 \times 10^{9} \exp\left[-\frac{23000}{RT}\right]$$

The very large activation energy reflects the large increase in growth rate with temperature in this system. The pre-exponential term is also extremely large and this is consistent with the fast growth rate observed at low temperatures relative to the high activation energy.

It is indeed difficult to give any convincing explanation for the very high activation energy and pre-exponential term in this system since the other Se-base system, Ag-Se, gave much more reasonable values. It seems possible that the large increase in growth rate with temperature is due not only to an increase in the diffusion coefficient D, but to some other effect which may be, for example, a progressive change in crystal structure of the intermetallic compound, with temperature[50] or crystallization of the amorphous Se film immediately ahead of the phase boundary. A combination of two such thermally activated processes would give a very high apparent activation energy for the system[28,29]. In any case it would appear that the diffusion mechanism in Cu-Se is very complicated and bears little resemblance to the mechanism for diffusion in the other three systems.

6.3 Electron Microscopy

6.3.1 Normal Growth

The dominant feature of the electron microscopy results in Cu-Se was the high sensitivity of the diffusion zone to heating by the electron beam. This was also observed to some extent in Ag-Te, in which, as discussed in Chapter 5, a second intermetallic phase formed at the diffusion zone front. In Cu-Se, however, the effect was much more pronounced. If extremely low illumination levels were used, the phase boundary motion appeared as shown in Figure 6.7. The interface appeared to be quite irregular and moved rapidly. The diffusion zone behind it consisted of columnar grains which increased in size the longer the beam was focused on the interface. The resulting difference in grain size is illustrated by micrographs 6.7 (1) and 6.7 (4). The elapsed time between these photographs was about two minutes. Figure 6.8 shows the directional nature of the elongated grains in the diffusion zone at higher magnification. The large arrow on this micrograph indicates the direction of the phase boundary advance. A selected area diffraction pattern made from the diffusion zone showed that its composition was $Cu_{2-x}Se$. This was in agreement with the composition predicted by the critical ratio study in Section 6.2.3. A selected area diffraction pattern and the d-spacing calculated from it are shown in Figure 6.9.

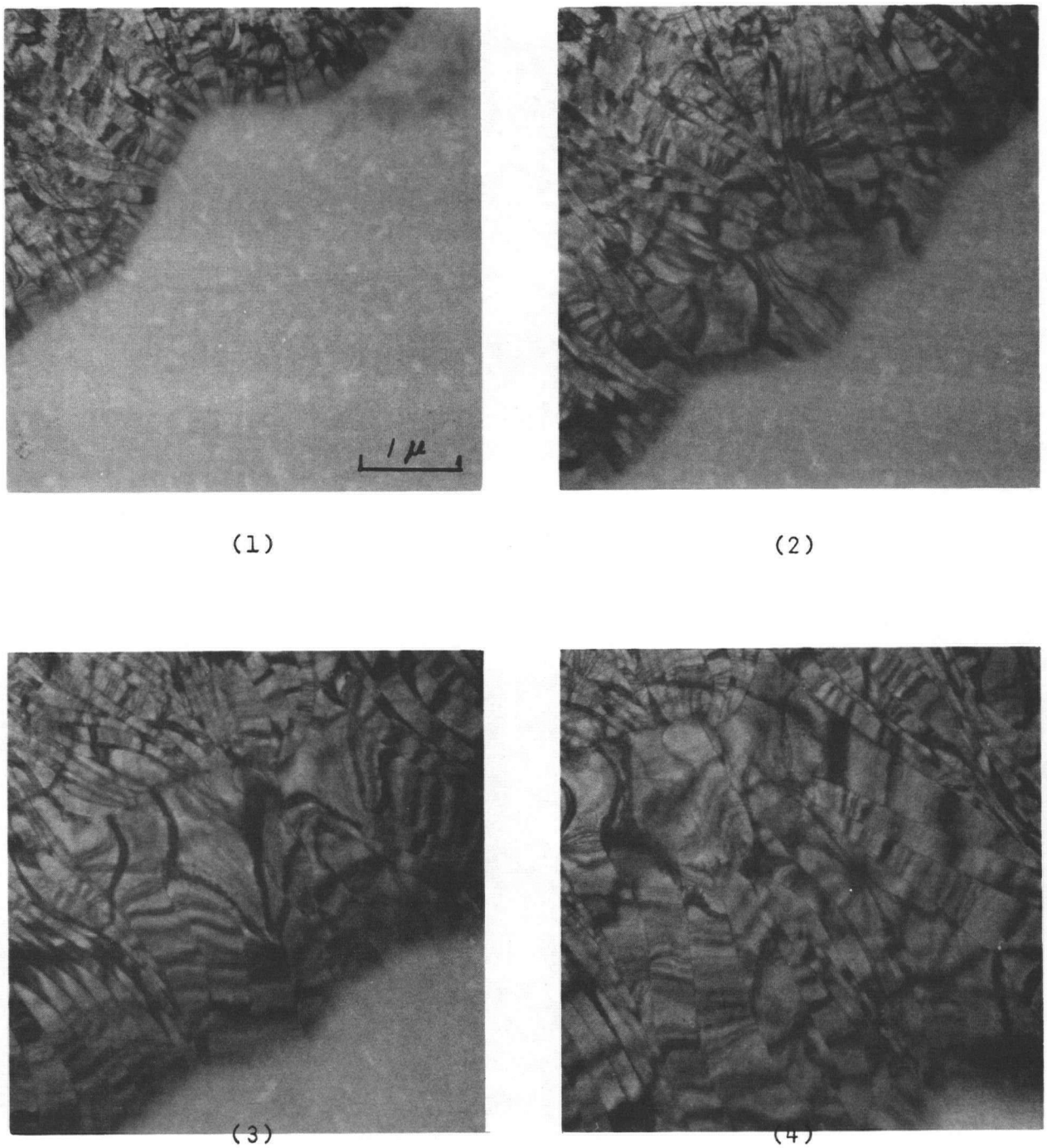

Figure 6.7 Motion of the Phase Boundary Interface in Cu-Se

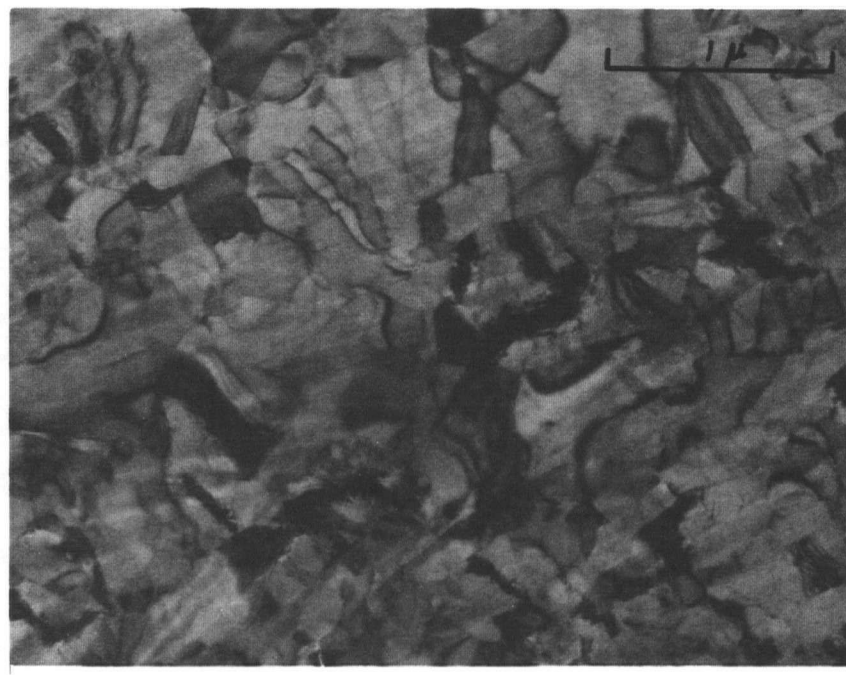

Direction of interface advance

Figure 6.8 Columnar Grains in Diffusion Zone

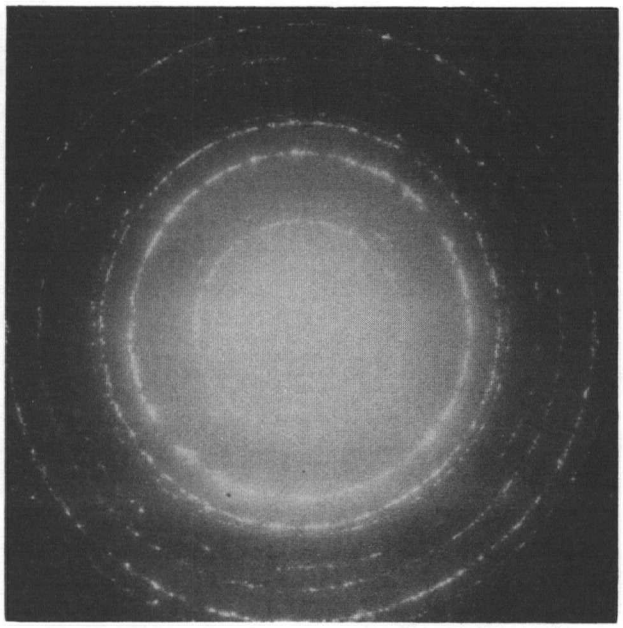

(a) S.A.D. of Diffusion Zone

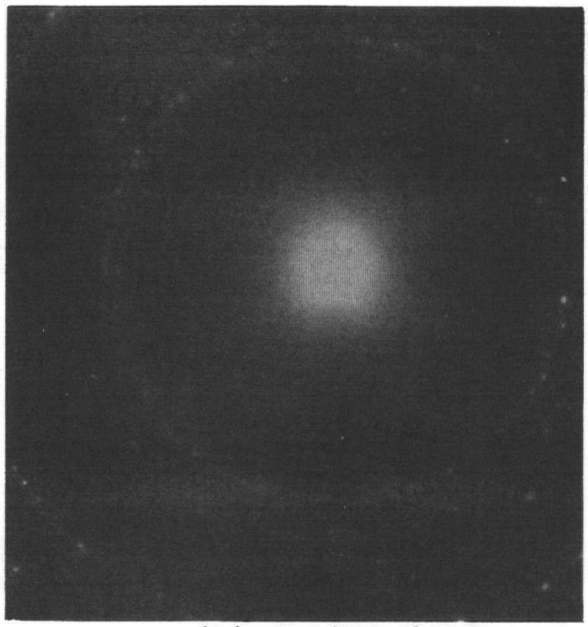

(b) Au Standard

Calculated d-spacings (Å)	d-spacings for $Cu_{2-x}Se$ (Å)
3.34	3.33
2.88	2.88
2.24	
2.03	2.02
1.73	1.73
1.65	1.65
1.42	1.43
1.31	1.32
1.28	
1.17	1.17
1.11	1.105
1.02	1.01
0.972	.969

Figure 6.9 Selected Area Diffraction Pattern of the Diffusion Zone

At high magnification the phase boundary interface appeared to consist of a series of parallel growth tips of varying size like that shown in Figure 6.10. The diffusion couple was cooled to -150°C in the microscope cold stage in order to prevent the interface from advancing. Selected area diffraction patterns were made on several of these tips. The patterns were single-crystalline in nature and exhibited pronounced streaking of the spots[50]. Two such diffraction patterns and their associated growth tips are shown in Figure 6.11. An interesting feature of these tips was that in each of them a series of fine striations running nearly parallel to the growth direction could be seen. These are clearly shown in Figures 6.10 and 6.11. In order to establish a growth direction on the diffraction patterns, a rotation calibration of the intermediate lens of the microscope was carried out with the same accelerating voltage and projector lens polepiece as was used to make the actual micrograph of the growth tips. Analysis[45,50] of the diffraction patterns of Figure 6.11 illustrated that the growth direction of the tips lay within 9° of the <111> direction and that the steaking direction of the spots was almost exactly perpendicular to this. Further analysis of other tips confirmed those relationships; in every case the growth direction of the tips was close to <111> and the striations were associated with {110} planes. These striations were the apparent cause of the streaking of the pattern spots.

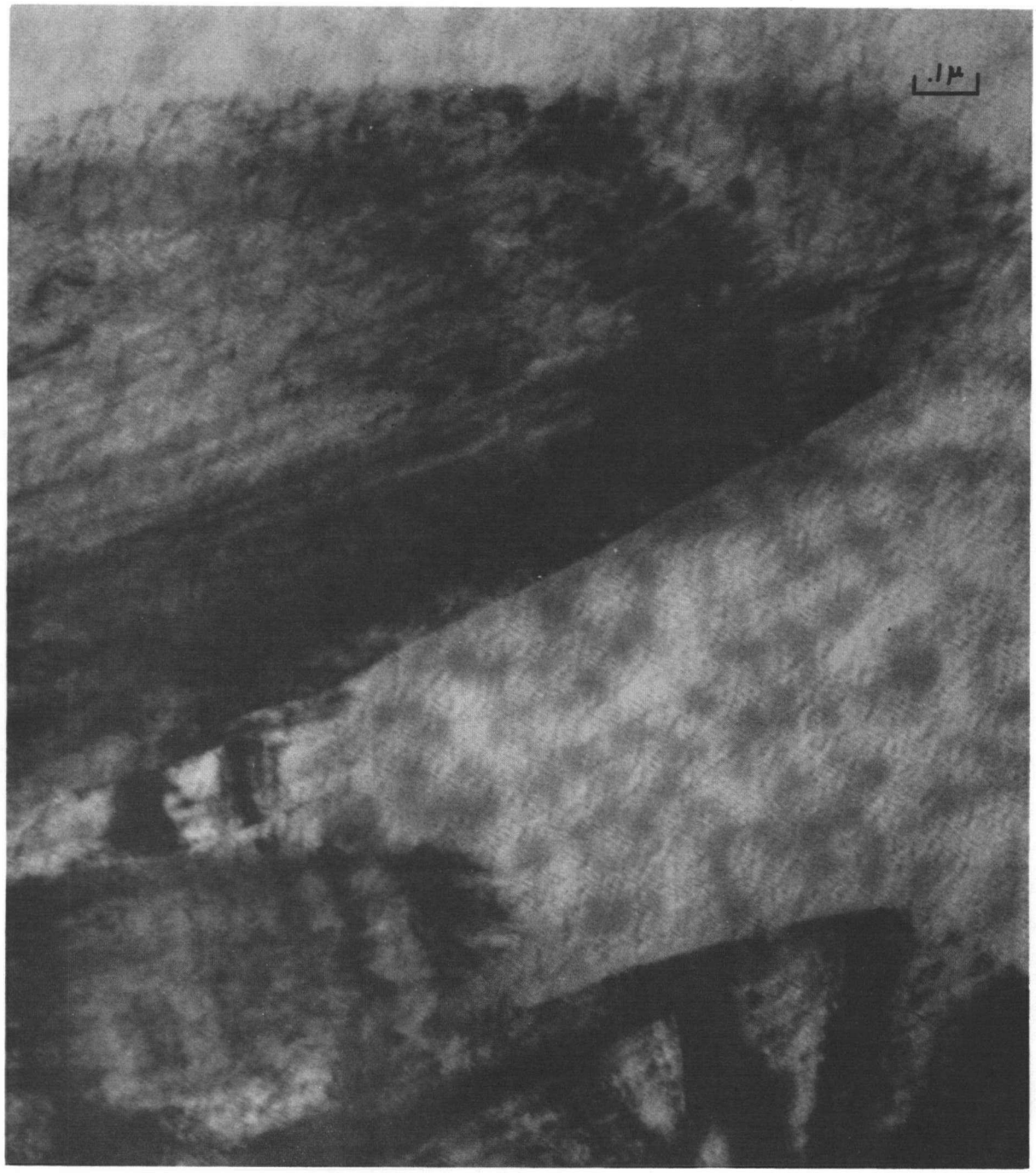

Figure 6.10 Growth Tip at High Magnification

Parallel fringes in this micrograph are believed to be due to astigmatism in the objective lens of the microscope.

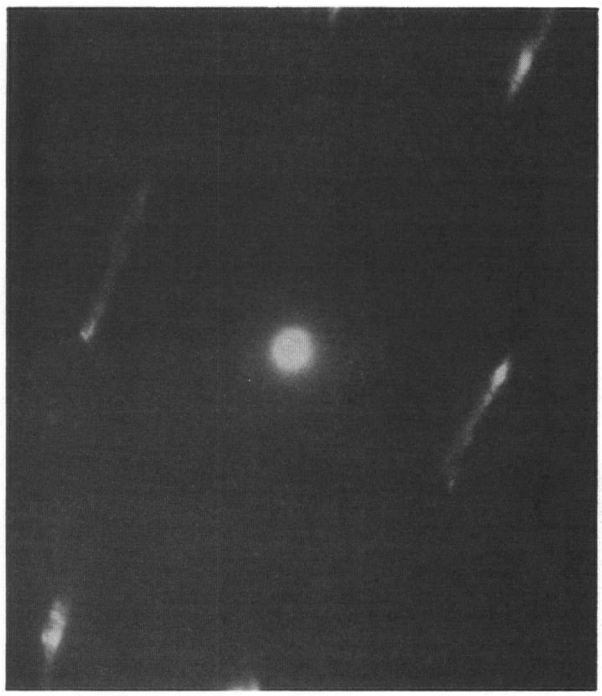

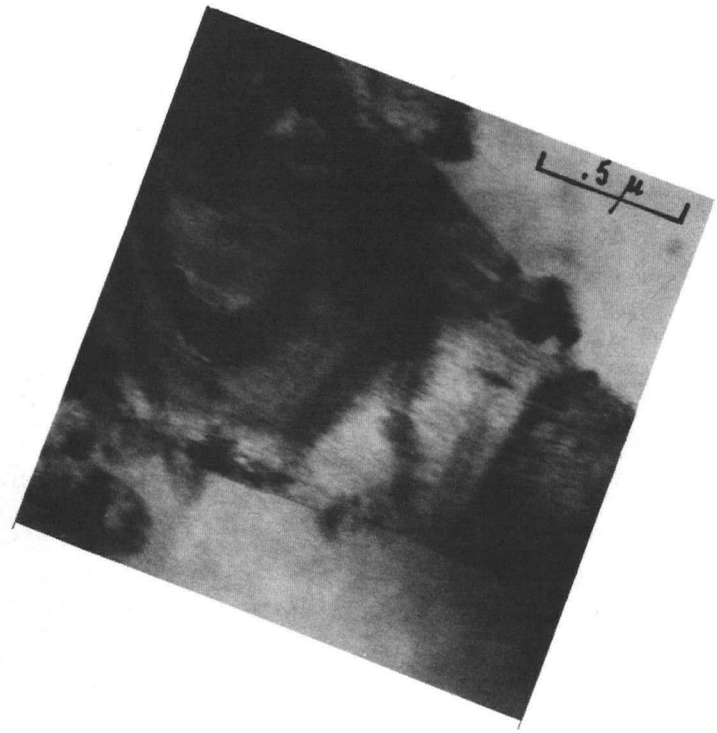

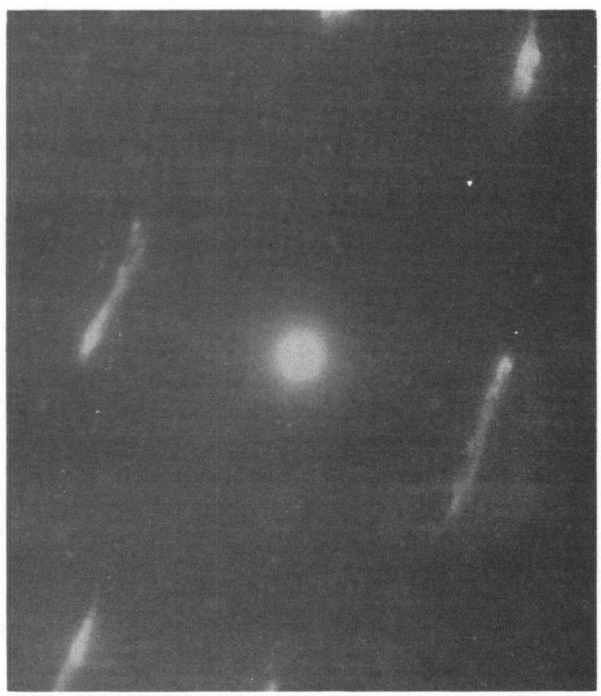

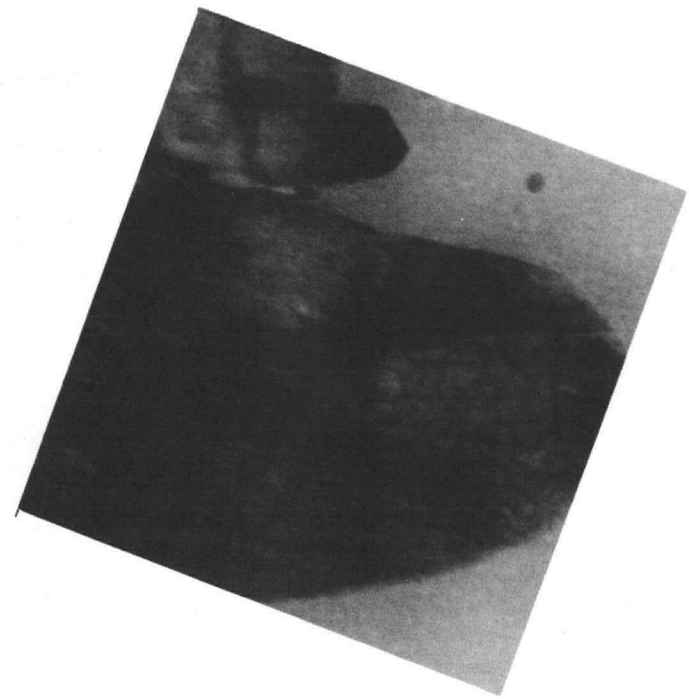

Figure 6.11 S.A.D. Patterns of Single Growth Tips

Figure 6.12 shows schematically the indexing of the single-crystal diffraction patterns of Figure 6.11.

In summary it was found that the grains of $Cu_{2-x}Se$ possessed a preferred growth direction, growing in a <111> direction. The fine striations appearing in the growth tips were related to {110} planes and were responsible for streaking of the diffraction patterns. The two main sources of streaking of diffraction spots are stacking faults and twins[51]. It is unlikely that the striations observed here are stacking faults. On the other hand {110} planes are not twinning planes in an anti-isomorphous CaF_2 structure like $Cu_{2-x}Se$[41]. Therefore these striations must be due to some other source. The growth direction is also difficult to account for by crystallographic considerations since the <111> direction is not a close-packed direction in the $Cu_{2-x}Se$ lattice. It should be noted, however, that the growth direction during formation of columnar crystals from the liquid (e.g. in steels) is not a close-packed direction. Apparently this is related to the ability of liquid atoms to "stick" more easily to planes other than the close-packed ones.

6.3.2 Dendritic Growth

When high illumination levels were used to observe the phase boundary interface in Cu-Se, a second phase appeared at the interface which grew rapidly in a dendritic manner. Once nucleated, this phase continued to grow even when illu-

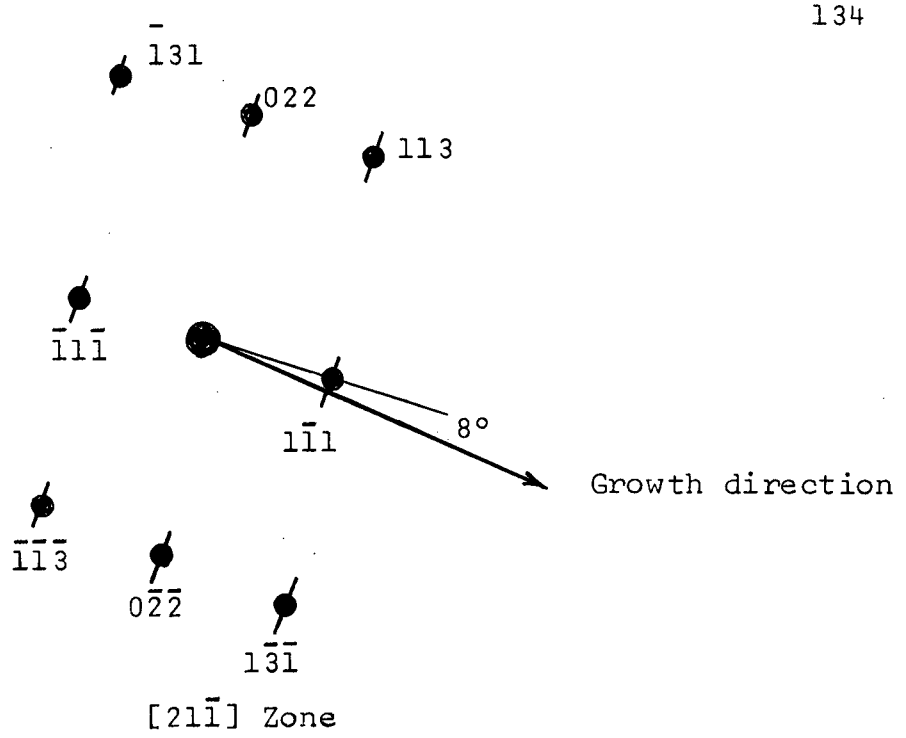

(a) Indexing of 6.11 (1)

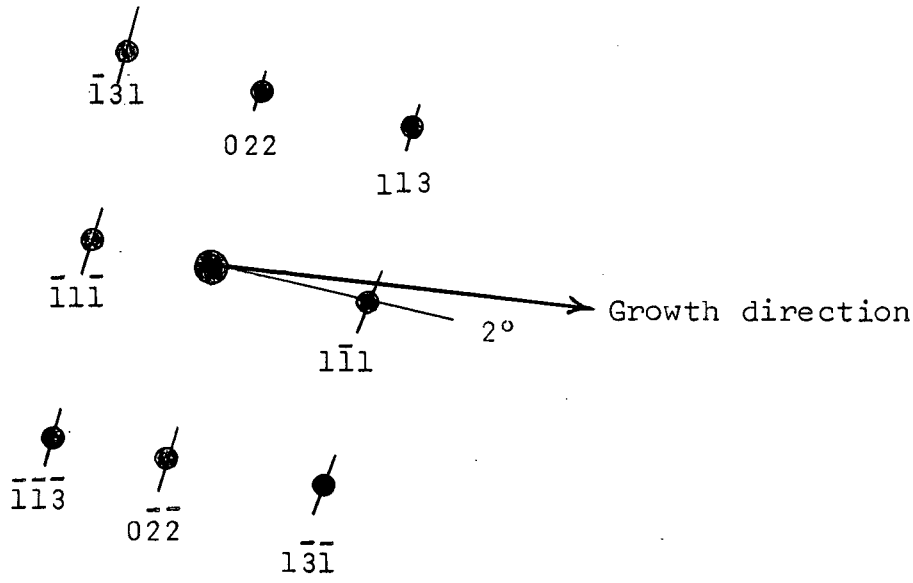

(b) Indexing of 6.11 (2)

Figure 6.12 Schematic Indexing of Diffraction Patterns

mination was greatly reduced. The structure was truly dendritic, exhibiting primary arms and numerous side-branches. Figure 6.13 shows the advance of the dendritic phase into the pure Se. The electron micrographs of Figure 6.14 clearly illustrate the appearance of a single primary dendrite at the phase boundary interface and the dendritic structure within the body of the phase. The boundary between the normal non-dendritic $Cu_{2-x}Se$ and the dendritic phase induced by electron beam heating is shown in Figure 6.15. This effect was found to be completely reproducible. A selected area diffraction pattern made from the dendritic phase showed that it was the tetragonal intermetallic compound Cu_3Se_2. A typical diffraction pattern and its associated d-spacings are given in Figure 6.16. These "d" values are in good agreement with the known d-spacings for Cu_3Se_2 listed in the same figure.

To determine the dendritic growth direction selected area diffraction patterns were made in the primary arms at -110°C using the cold stage. It was found that cooling of the sample to this temperature resulted in the dendritic structure being transformed into one consisting of only parallel primary arms with no side branches, similar in appearance to non-dendritic $Cu_{2-x}Se$. The composition and crystal structure was still that of Cu_3Se_2, however. Because the primary arms were quite narrow it was nearly impossible to obtain a pure single-crystal diffraction pattern. There-

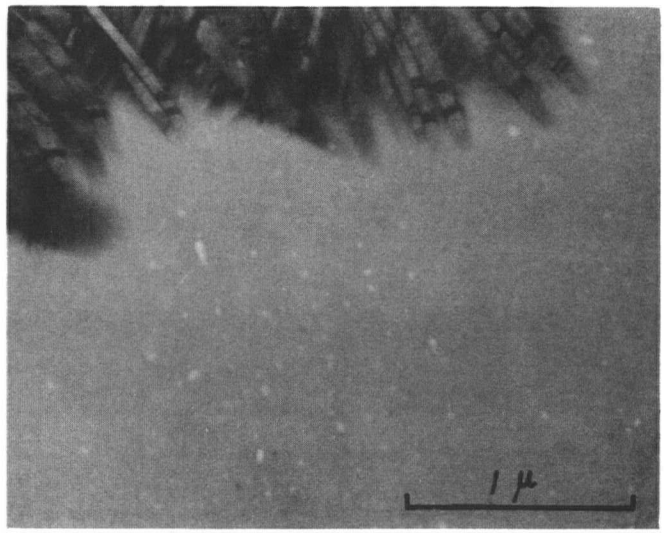

(1)

(2)

(3)

Figure 6.13 Motion of Dendritic Phase Interface

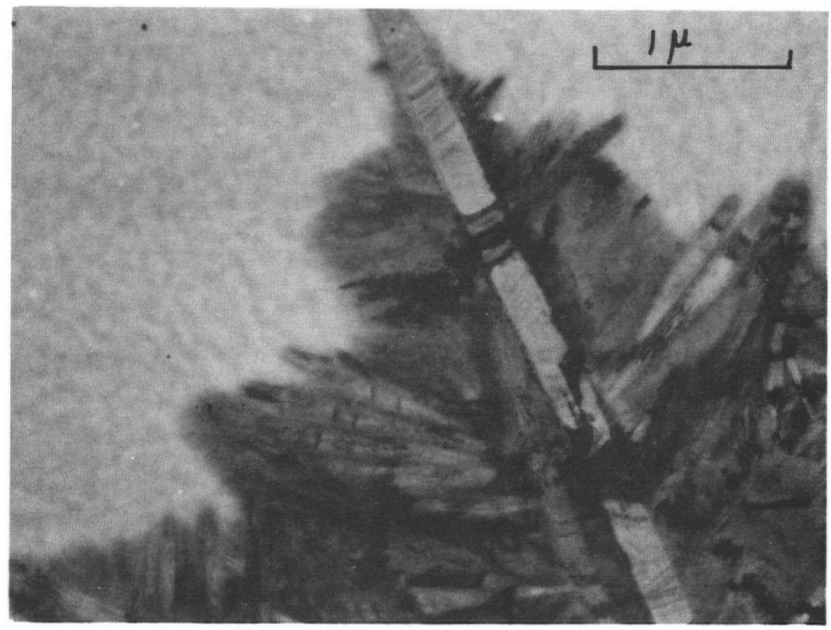

(1) Dendrite at the Phase Boundary Interface

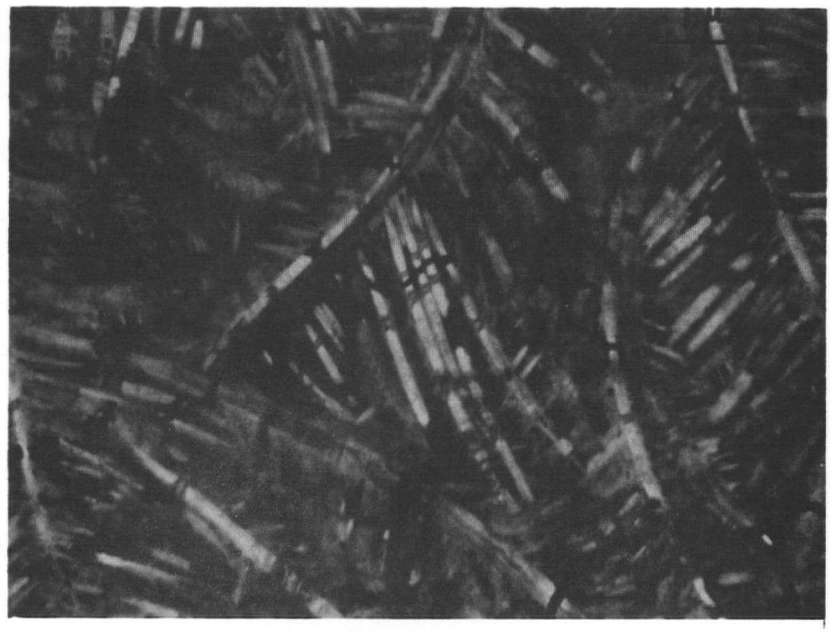

(2) Interior Microstructure of the Dendritic Phase

Figure 6.14 Nature of the Dendritic Phase

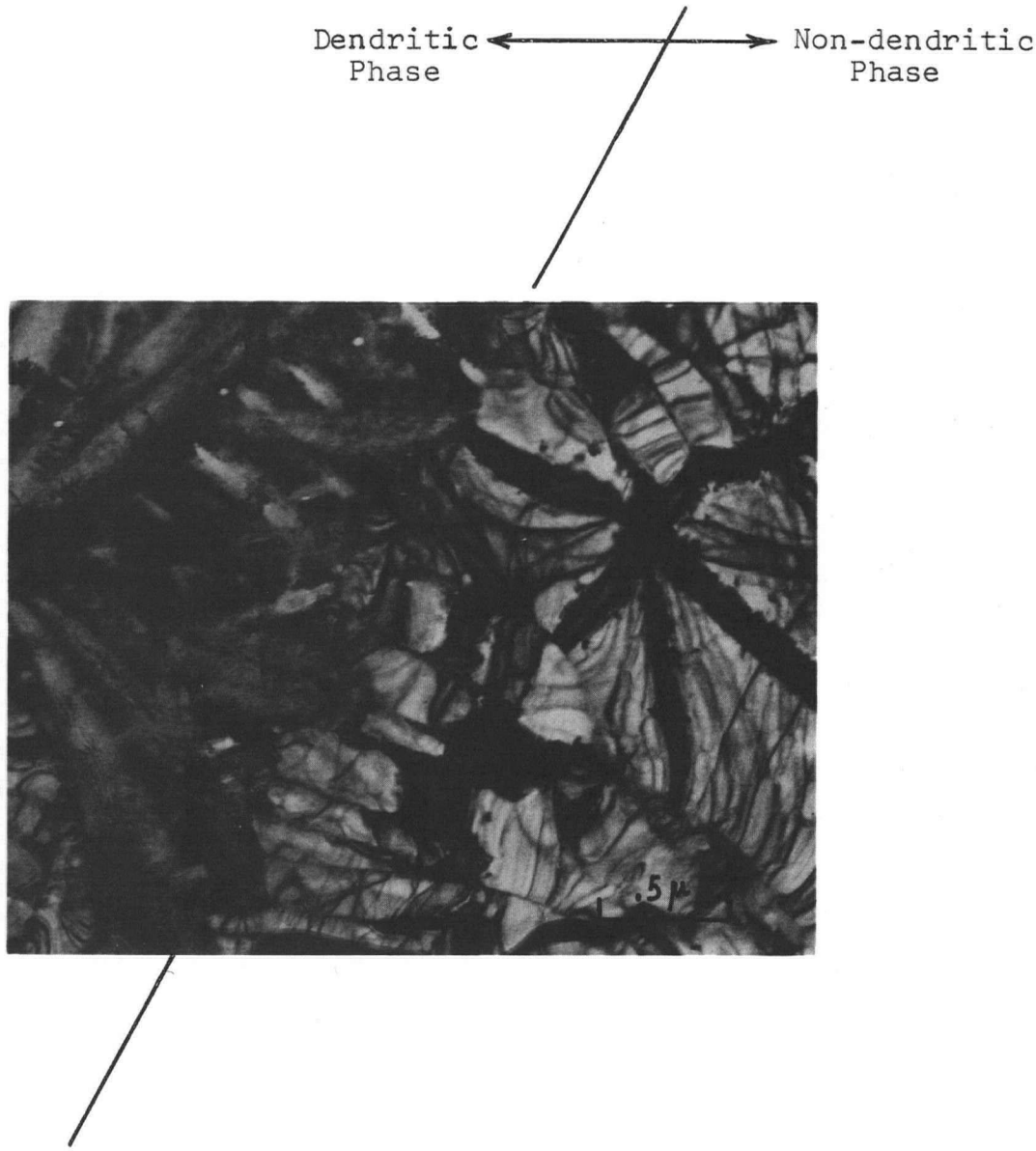

Figure 6.15 Boundary Between Dendritic and Non-dendritic Phase

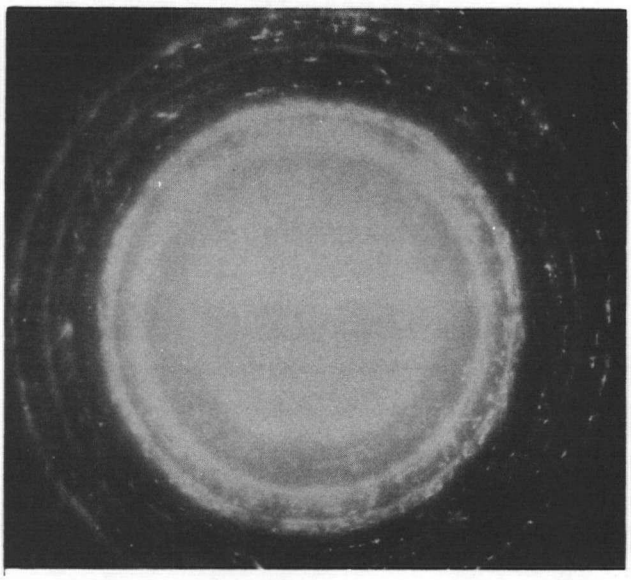

(a) S.A.D. of Diffusion Zone

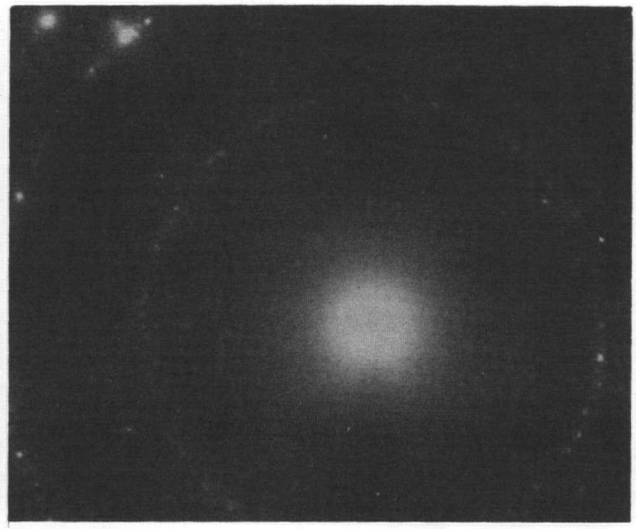

(b) Au Standard

Calculated d-spacings (Å)	d-spacings for Cu_3Se_2 (Å)
4.28	4.28
3.56	3.56
3.20	
	3.11
2.97	2.97
2.86	2.86
	2.62
2.56	2.56
2.49	2.49
2.38	2.38
2.26	2.26
2.14	2.14
	2.10
	2.08
	2.02
2.00	2.00
1.93	1.93
1.91	
1.83	1.83

Figure 6.16 S.A.D. Pattern of the Dendritic Phase in Cu-Se

fore, the diffraction patterns were invariably a superposition of at least two single-crystal patterns and their indexing was difficult. Pronounced streaking was in evidence on all the patterns. Figures 6.17 and 6.18 illustrate typical diffraction patterns obtained, their corresponding microstructures, and the schematic indexing of each[52]. Analyses of the diffraction patterns give the growth direction as being <101> and indicate that the streaks arise from fine striations (see Figure 6.18) associated with {111} planes. An investigation of possible twinning planes in the specific tetragonal structure of Cu_3Se_2 was not carried out. Therefore it is not possible to say whether the striations present in the micrographs are due to twins. It is unlikely, however, that they are stacking faults, since {111} is not a close-packed plane in this structure.

The occurrence of dendritic growth[19,53] in a solid state diffusion reaction is a very rare phenomenon. Malcolm and Purdy[54] observed the dendritic growth of γ brass from supersaturated β-brass in the solid state. In their work, however, a very favourable morphology existed between precipitate and parent grain. In the present investigation the observed growth of a dendritic phase appears to be due to thermal rather than crystallographic effects. Focusing of an intense beam of electrons on the normal diffusion zone interface results in rapid dendritic growth. Once the beam is removed from the interface, growth of the dendritic phase proceeds slowly (if at all).

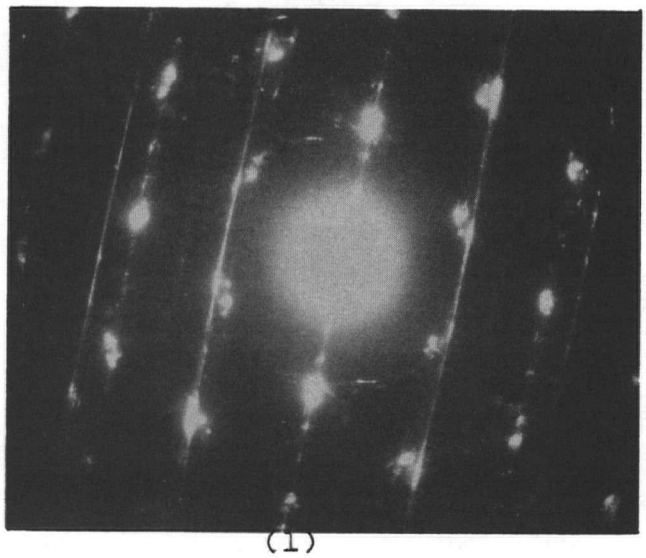

(1)

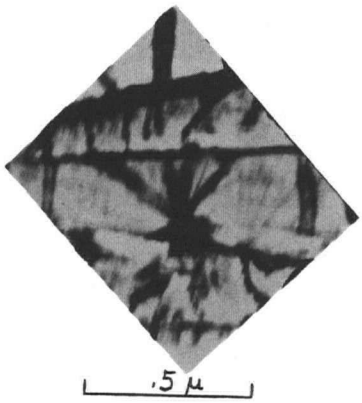

(2)

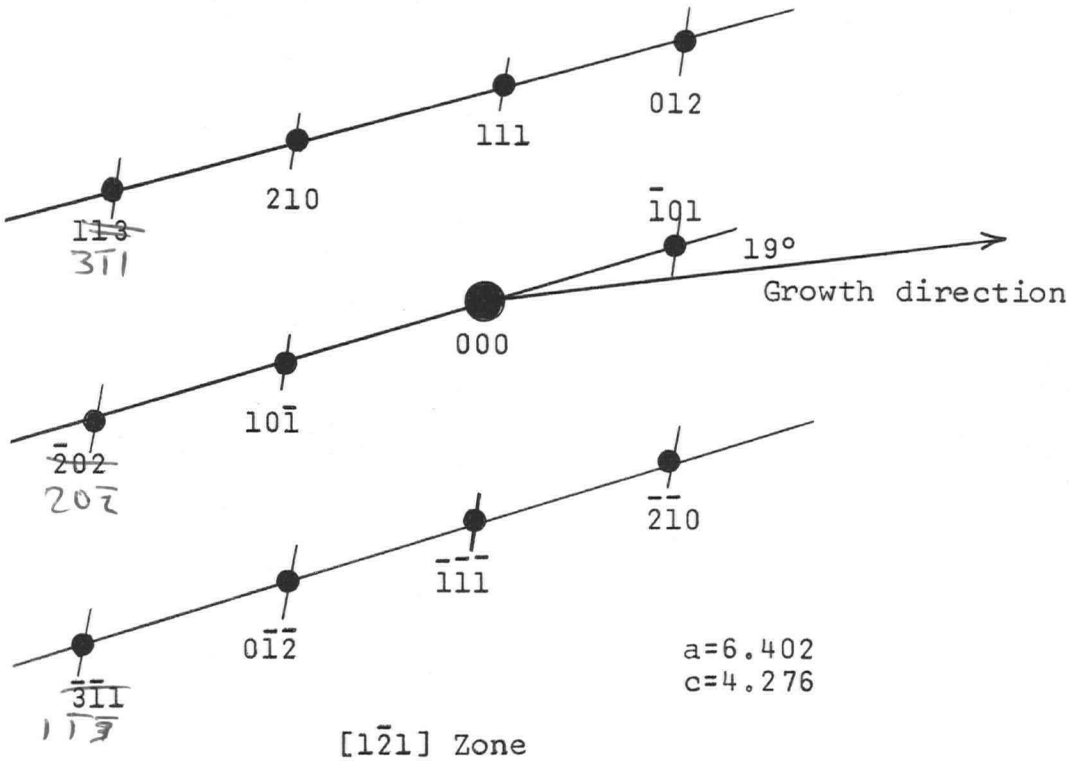

(3)

Figure 6.17 Dendrite Analysis

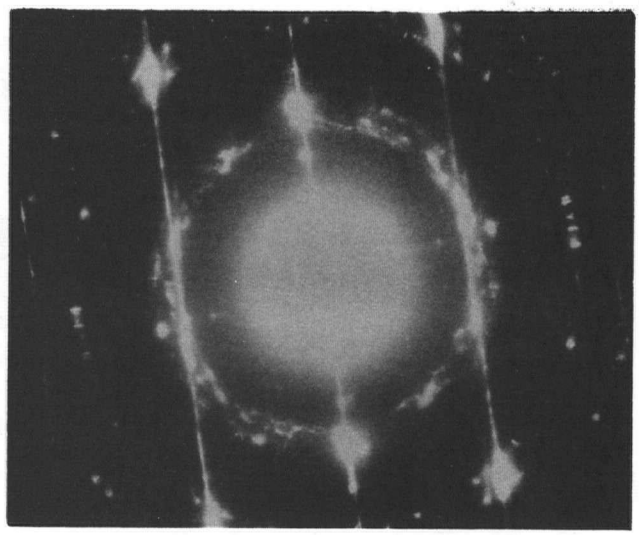

(1)

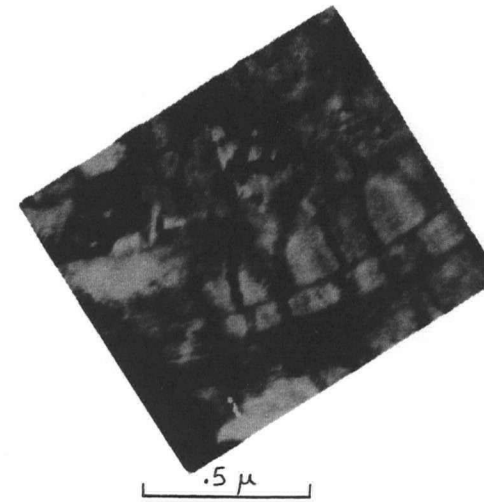

(2)

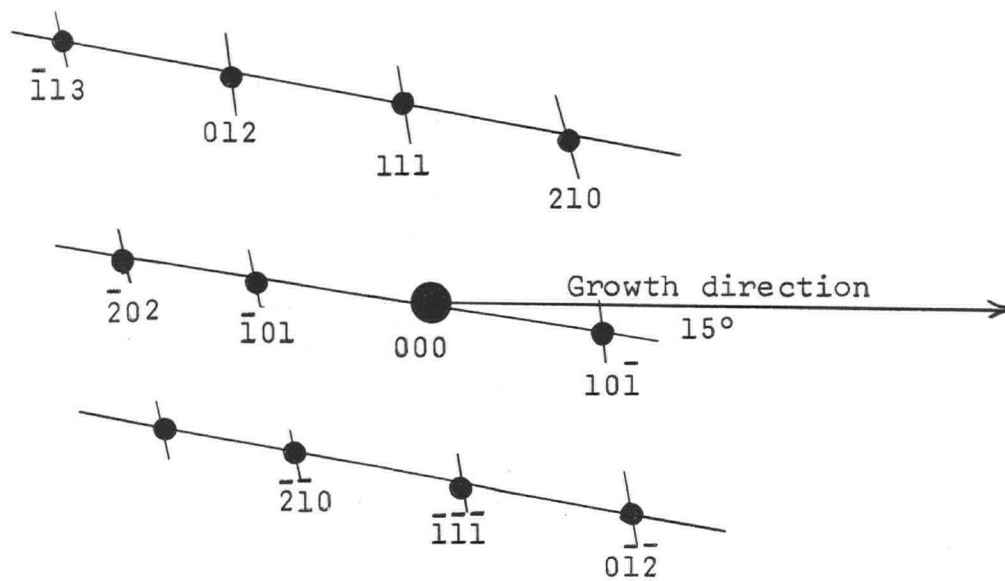

$[21\bar{1}]$ Zone

(3)

Figure 6.18 Dendrite Analysis

A possible explanation for the observed behaviour is that the localized heating produced by the beam at the interface excites Se atoms in the immediate vicinity making them quite mobile. The poor thermal conduction properties of Se prevents the beam heat from being conducted away readily from this region. Se is observed to aggregate at only 60°C suggesting that Se atoms are capable of surface migration even at this low temperature. This picture of high mobility is also consistent with the description of the amorphous state as being a highly viscous liquid[55]. The observed tendency of bulk amorphous Se to become plastic and flow at temperatures below 100°C (see page 30, Chapter 3) fits this description well. The net result of poor thermal conductivity in the Se and relatively good conduction in the intermetallic compound is that a layer of very mobile atoms is created ahead of the interface. The system then wants to transform as quickly as possible to form Cu_3Se_2. Plate-shaped or pointed precipitates can transform a greater volume per second than planar boundaries. Therefore a dendritic interface develops, provided the decrease in volume free energy more than counterbalances the increase in surface energy and the mobility of the diffusing species is sufficiently high.

Another conceivable explanation of the results is that Cu_3Se_2 is a high temperature derivative of $Cu_{2-x}Se$[40,48]. If this were so, the rapid lateral diffusion produced by

beam heating could be due to a polymorphic transformation[56]. At the present time, however, there is insufficient information available to say whether Cu_3Se_2 could be a high temperature form of $Cu_{2-x}Se$ resulting from an increased homogeneity range.

In summary it has been found that Cu-Se is a much more complicated system than the other three investigated. The growth kinetics are not strictly parabolic and the activation energy appears to be abnormally high for a system in which diffusion proceeds so rapidly. In addition the electron microscopy results indicate that the phase boundary interface is very sensitive to high illumination levels; if these become large enough, a second phase is initiated at the interface which moves very rapidly and grows dendritically. These results suggest that the actual diffusion mechanism in Cu-Se is quite complex.

CHAPTER 7

SUMMARY AND CONCLUSIONS

7.1 Discussion and Summary

7.1.1 Growth Kinetics

In each of the three systems Ag-Se, Cu-Te, and Ag-Te the graphs of diffusion zone width (x) as a function of $\sqrt{t}$ were linear implying that the growth of the diffusion zones was diffusion controlled. As discussed in section 6.2.1, most of the growth rate plots in Cu-Se were not strictly parabolic but instead appeared to consist of two or three stages of parabolic growth. The exact reason for this behaviour remains obscure, but it would seem that the diffusion zone growth in each stage is diffusion controlled. Lateral diffusion at room temperature was very rapid in all four systems investigated. The resulting diffusion zones tended to be very wrinkled or folded in nature and became partially detached from their underlying substrates. This effect was no doubt due to the volume expansion of the Se or Te lattice as Ag or Cu^{46} diffused in, since very large increases in a unit volume of Se and Te result when an intermetallic compound with Ag or Cu is formed. In Cu-Te, for

example, the volume expansion of the Te is about 40%.

7.1.2 Rate Constant Dependence[2] on Film Thickness

The original purpose of investigating the effect of Se and Te film thickness on the rate constant for couples in which the thickness ratio was greater than R_c was to see if the lateral diffusion process involved any surface diffusion along the Se or Te. It would be expected that the occurrence of surface diffusion should be reflected in a general decrease of the rate constant with increasing Se or Te thickness since the surface to volume ratio of a film is reduced as the thickness becomes greater. In each of the systems studied, however, it was found that beyond a certain Se or Te thickness, the rate constant was essentially independent of the thickness while below the thickness the rate constant tended to a peak value. This phenomenon was attributed to the structure of the thin films. An electron microscopy investigation of very thin Se and Te films showed that they consisted of coalesced islands with an inter-island network that undoubtedly contained many structural imperfections. This would be conducive to a short circuit diffusion process between the islands. The effect of low Se and Te thicknesses on the rate constant was seen to be much greater in the Te systems than in the Se ones. This was consistent with the definite evidence of grain boundary diffusion at all Te thicknesses observed in both Ag-Te and Cu-Te

using transmission electron microscopy.

7.1.3 Critical Ratio

The existence of a critical thickness ratio for the diffusion couple components was verified in all four systems. Above this thickness ratio diffusion proceeded at a rate independent of the Se or Te thickness, and below it, no diffusion took place. It was found that the experimentally observed critical ratio was independent of the absolute Se or Te thickness over the range of thickness in which growth rates were measured. Theoretical determinations of the critical ratios from stoichiometric considerations were in excellent agreement with the experimental values obtained except in the case of Cu-Te where a 30% difference was found. In Ag-Se, Cu-Se, and Ag-Te the compositions of the diffusion zones predicted by the kinetics were confirmed by electron diffraction studies.

7.1.4 Temperature Dependence

Table 7.1 summarizes the results obtained in each system for the temperature dependence of the rate constant. The three systems Ag-Se, Cu-Te, and Ag-Te all have relatively low activation energies. In Ag-Se and Cu-Te, comparison with activation energies for bulk diffusion couples was possible. The thin film activation energies were lower than the bulk activation energies. Thus the activation energies in the thin film results not only constitute very low values in them-

TABLE 7.1

Activation Energies for Thin Film Couples

System	Temperature Range Investigated (°C)	Thin Film Activation Energy (Kcal/mole)	Bulk Activation Energy (Kcal/mole)
Ag-Se	0-50	12,200	17,600
Cu-Te	0-100	7,800	15,000
Ag-Te	0-100	10,000	*
Cu-Se	0-50	23,000	*

* Not available

selves, but also tend to be much below the observed bulk activation energies. This suggests that a short circuit mechanism is responsible for diffusion. Examination of the phase boundary interfaces in Cu-Te and Ag-Te by electron microscopy provided definite evidence of grain boundary diffusion. The high activation energy for diffusion in Cu-Se is not consistent with the other results. The most probable explanation for this is that the diffusion in this system involves more than one process so that it is improper to ascribe an activation energy to it[28,29].

7.1.5 Electron Microscopy

The direct observation of the moving phase boundary interfaces in the electron microscope was in itself interesting since very little work of this type has been done before. In Cu-Te and Ag-Te there were definite indications that grain boundary diffusion was taking place. This was consistent with the low activation energy values obtained for diffusion in these systems. In the Se systems the microscopy results did not provide any definite information as to the nature of the diffusion mechanism. It was observed, however, that localized heating by the electron beam at the phase boundary interface resulted in some aggregation of the Se in the case of Ag-Se, and in Cu-Se to the nucleation of a second phase which grew dendritically. The formation of a second phase by beam heating was also seen to a less marked degree in Ag-Te. Such phenomena may suggest that the level of local-

ized heating produced in the electron beam is much greater than previously thought. Temperature increases of 100°C could well be involved.

Despite the evidence for grain boundary diffusion obtained in the Te systems, it was disappointing that a quantitative estimate of the relative rate of grain boundary to lateral diffusion could not be made. In Cu-Te, the grain boundary effect was not pronounced enough to assess the diffusion rate, while in Ag-Te, beam heating tended to obscure the grain boundary diffusion before any useful measurements could be made.

General Summary

The important features of the lateral diffusion process in each of Ag-Se, Cu-Te, Ag-Te and Cu-Se as outlined in the preceeding discussion are summarized in Table 7.2.

7.2 Estimation of Diffusion Coefficients

In the "Introduction" (page 15) it was shown that the rate constant found by measuring the width of the diffusion zone was related to the diffusion coefficient by the formula

$$K = D \frac{2(C_2-C_1)(C_3-C_2)}{(C_1-C_o)(C_3-C_2+C_1-C_o)} \qquad (7.1)$$

if the composition range of the intermediate phase involved is small. This is a valid approximation in the case of each

TABLE 7.2

Summary of Lateral Diffusion in the Four Systems Investigated

System	Diffusion Zone Composition	Room Temperature Growth Rate (cm^2/sec)	Kinetics	Critical Ratio for Diffusion	Proposed Diffusion Mechanism	Special Characteristics
Ag-Se	Ag_2Se	1.1×10^{-8}	parabolic	$1.1 \pm .1$	Short circuit (e.g. grain boundary)	Se is amorphous Growth rate higher in thin Se films.
Cu-Te	$Cu_{2-x}Te$ ($x \sim 0.6$)	2.1×10^{-9}	parabolic	$0.63 \pm .1$	Grain boundary	Growth rate higher in thin Te films; effect is much more pronounced than in Se systems.
Ag-Te	Ag_2Te	1.9×10^{-8}	parabolic	$1.0 \pm .1$	Grain boundary	Effect of very thin Te films on growth is extremely marked.
Cu-Se	$Cu_{2-x}Se$ ($0 \leq x \leq 0.2$)	0.80×10^{-8}	separate stages of parabolic growth	0.63-0.71	--	Very large diffusion zone widths observed. Electron beam heating induces second phase at phase boundary interface which grows dendritically.

of the systems studied so that it is possible to use equation 7.1 to estimate the diffusion coefficients in each system. This has been done using the room temperature value of the rate constant; that is, the value obtained for couples in which the thickness ratio is greater than the critical ratio and the Se or Te thickness is beyond the region where the structure of the film results in higher growth rates. The calculated values of D are given in Table 7.3. From this it can be seen that the diffusion coefficients are about two orders of magnitude greater than the rate constants except for the system Ag-Se in which the difference involves a factor of 500 due to the very small composition range of Ag_2Se. It is obvious, therefore, that the diffusion coefficients in all these systems are very large indeed. Although very little is known about the variation with temperature of the composition ranges of the intermetallic compounds formed during diffusion in each of the four systems, present evidence[40,48] suggests that the phase boundary compositions do not change significantly up to temperatures of 500-600°C. Therefore the activation energies observed represent those of the diffusion process alone.

TABLE 7.3

Calculation of Diffusion Coefficients

System	Steady State Rate Constant K (cm^2/sec)	Intermetallic Phase Present	Composition Range of Phase (C_2-C_1) (at %)	Calculated Diffusion Coefficient D (cm^2/sec)
Ag-Se	1.1×10^{-8}	Ag_2Se	0.2	5.5×10^{-6}
Cu-Te	2.1×10^{-9}	$Cu_{2-x}Te$ ($x \sim 0.6$)	0.9	1.6×10^{-7}
Ag-Te	1.9×10^{-8}	Ag_2Te	0.9	2.1×10^{-6}
Cu-Se	0.80×10^{-8}	$Cu_{2-x}Se$ ($0 \leq x \leq 0.2$)	2.4	2.9×10^{-7}

7.3 The Mechanism of Rapid Diffusion

Rapid diffusion at room temperature is a rarely-occurring phenomenon. In the present work it was observed in only four systems out of the 22 investigated. Therefore it is natural to raise the question as to why very rapid diffusion is observed in these systems and not in others.

Present results in thin film diffusion couples suggest that grain boundary diffusion and possibly "pipe" diffusion are the predominant mechanisms in Ag-Se, Cu-Te, and Ag-Te. The bulk data available in these systems, however, shows that high growth rates are also encountered at relatively low temperatures (100-200°C) in bulk diffusion couples. In Cu-Se the diffusion mechanism does not appear to be consistent with that of the other three systems and its exact nature remains obscure. Nevertheless, very large growth rates are observed in this system as well.

All of the intermetallic phases formed during diffusion have several interesting features in common. They are known to be small band gap semiconducting compounds in which cation vacancies act as acceptors[42,48,57]. Each of the compounds exists in at least two stable polymorphs in different temperature ranges[26]. In every case both the high temperature and low temperature modifications are regarded as being defect intermetallic compounds with cation vacancies constituting the main inperfection. Finally, the bonding in all four compounds is essentially covalent rather

than metallic. This is not surprising, however, in compounds involving Se and Te which have been referred to by various authors as "metalloids" or semiconductors.

The high temperature modifications of Ag_2Se, Ag_2Te, $Cu_{2-x}Se$, and $Cu_{1.8}S$ are similar to α-Ag_2S (see Introduction, page 10) in that they are substances in which only the anions occupy a regular lattice while the cations are practically "molten" and are not bound to definite lattice positions[26]. Measurements of electrical conductivities and transference numbers in α-Ag_2S, for example, have shown that the cations possess abnormally high mobility equal to that of ions in aqueous solution while the anions are essentially immobile. This behaviour is probably due to:

(1) The large size difference between cation and anion which enables the smaller cation to readily occupy an interstitial lattice site.

(2) The inherent defect structure of these compounds which tend to be deficient in the cation species. This creates extra sites to which cations in the lattice can migrate.

(3) The nature of the covalent bonding is such as to facilitate the breaking of cation-anion bonds. In this regard it should be pointed out that the order of increasing metallic character (decreasing electronegativity[58,59]) of the anions is S, Se, Te, and all of these are much less electronegative than any of the halides. The room temperature

structures of these compounds have not been studied as extensively as the high temperature modifications, but it would be expected that there is a strong possibility that the cation partial lattices contain a large number of lattice defects. In these low temperature modifications, however, the cations are now restricted to definite lattice sites. Nevertheless, the cation mobility, although much less than in the high temperature structure, will still be comparatively high.

The present work indicates that diffusion in Ag-Se, Cu-Se, and Cu-Te is controlled by the migration of Ag or Cu through the diffusion zone which in each case involves an intermetallic compound analogous in composition and structure to Ag_2S. It is doubtful that the rapid growth rates encountered are related to the free energy of formation of the various intermetallic phases[60]. Sulphide formation studies in Cu and Ag allcys involving various impurity additions[61,62] have shown that the rate of sulphide attack is comparable in both cases despite the large difference in the standard free energy of formation of Ag_2S and Cu_2S (-17.8 kcal/mole versus -28.2 kcal/mole). From this it is concluded that only the diffusivity of Ag and Cu in the sulphide layers is significant in the sulphidation process. By analogy with this it is expected that the rate-controlling process in the systems Ag-Se, Cu-Te, Ag-Te, and possibly Cu-Se is the diffusivity of Cu and Ag in the diffusion zone compound.

Scaling experiments in the Ag-S system[26,63] have revealed that the sulphide phase forms as a result of diffusion of Ag ions through the Ag_2S layer. This is accompanied by a motion of electrons in the same direction as the ion flux. The electrons move rapidly in large numbers, causing an additional electrical potential gradient in addition to the chemical potential gradients due to the Ag ions which are already present; this in turn causes an increase in the transport rate of the silver ions through the tarnishing layer. Similar experiments on Ag and Cu with Se and Te[64,65] have not led to any consistent data on the diffusion process. The possibility that the diffusion of Ag and Cu in the Se and Te systems is increased by the existence of an additional electrical potential cannot be ruled out. However the effect of this potential is merely to double or triple the diffusion rate[63].

It is proposed, therefore, that the mechanism for rapid diffusion in the four systems investigated in this work is a combination of high Ag and Cu diffusivity in the intermetallic compounds that are formed during diffusion and the short circuit diffusion processes which occur readily at low temperatures in thin films. The high atomic diffusivities in each of the intermetallic compounds are the result of the unique chemical properties of the compounds and specifically, their defect structures, in which cations tend to be abnormally mobile.

7.4 Conclusions

The observations and interpretations of lateral diffusion in the four systems Ag-Se, Cu-Te, Ag-Te, and Cu-Se lead to the following conclusions:

(1) The growth rate in Ag-Se, Cu-Te, and Ag-Te is diffusion controlled. In Cu-Se two or three stages of diffusion controlled growth occur with the initial growth rate being much faster than succeeding ones.

(2) In all four systems the diffusion rates of Cu and Ag are much greater than those of Se and Te. This would lead to the development of extensive Kirkendall porosity on the Se or Te side of a diffusion couple and would impede the diffusion of these atoms across the interface. For this reason, a study of the lateral diffusion of Se or Te along Cu or Ag was not possible.

(3) The lateral diffusion process in each system is controlled by the motion of Cu or Ag ions through the diffusion zone which is crystalline in nature. Thus, in the Se systems, diffusion is not affected by the amorphous microstructure of the Se.

(4) The diffusion rate constant is independent of the Se or Te film thicknesses for any thickness at which the film is continuous. This implies that surface diffusion is not involved in the lateral diffusion along the Se or Te since the surface to volume

ratio decreases as the film thickness increases.

(5) Se and Te films become continuous at about 180 to 200 Å. Below this thickness the structure of the films is such that the diffusion rate constant tends to a peak value due to short-circuit diffusion in the inter-island channels. The effect of structure is much more pronounced in Cu-Te and Ag-Te due to the fact that grain boundary diffusion takes place quite readily in these systems.

(6) In order for lateral diffusion to occur, a definite ratio of Cu or Ag thickness to that of Se or Te must be exceeded. This critical thickness ratio is determined only by the stoichiometry of the intermetallic phase formed during diffusion and is independent of the structure of the Se or Te film.

(7) A grain boundary diffusion mechanism accounts for the rapid room temperature growth rates in Cu-Te and Ag-Te. Short circuit diffusion such as grain boundary or "pipe" diffusion is also responsible for rapid growth in Ag-Se. Therefore, in these systems, the growth rates observed in the thin film couples are considerably greater than those observed in bulk couples at room temperature.

(8) The occurrence of rapid room temperature diffusion along a film is restricted to the four Se and Te systems investigated. There are no obvious extensions

of the present work on lateral diffusion to other systems.

(9) The rapid diffusion processes taking place in Ag, Cu-Se and Ag, Cu-Te are due to their unique chemical properties and to the defect structures of the compounds formed during diffusion. In thin film diffusion couples involving these systems short circuit diffusion processes result in an acceleration of normal growth rates and enable diffusion to proceed rapidly at room temperature.

APPENDIX

WHITE ZONE

The "white zone" described in section 3.2.1 was observed in all of the systems studied and its width was observed to decrease as the relative thicknesses of the diffusion couple components (e.g. Ag and Se) became comparable. In any given sample the white zone width remained constant at all times and was not included in the diffusion zone width in the kinetics graphs. Figure A.1, a growth plot in Ag-Te, shows the true diffusion zone width and the total diffusion zone plus white zone width plotted against $\sqrt{t}$. It can be seen that the diffusion zone graph is parabolic passing through t=0 while the total width plot, although still parabolic, is displaced from the other curve by about 18 μ and does not pass through the origin. It was thus concluded that the white zone was associated with the downward diffusion process rather than with lateral diffusion.

The origin of the white zone is probably due to the masking of the substrate in order to produce a Ag step. Consider Figure A.2 which represents the Ag vapour incident on the mask and substrate configuration (A.2(a)), and the

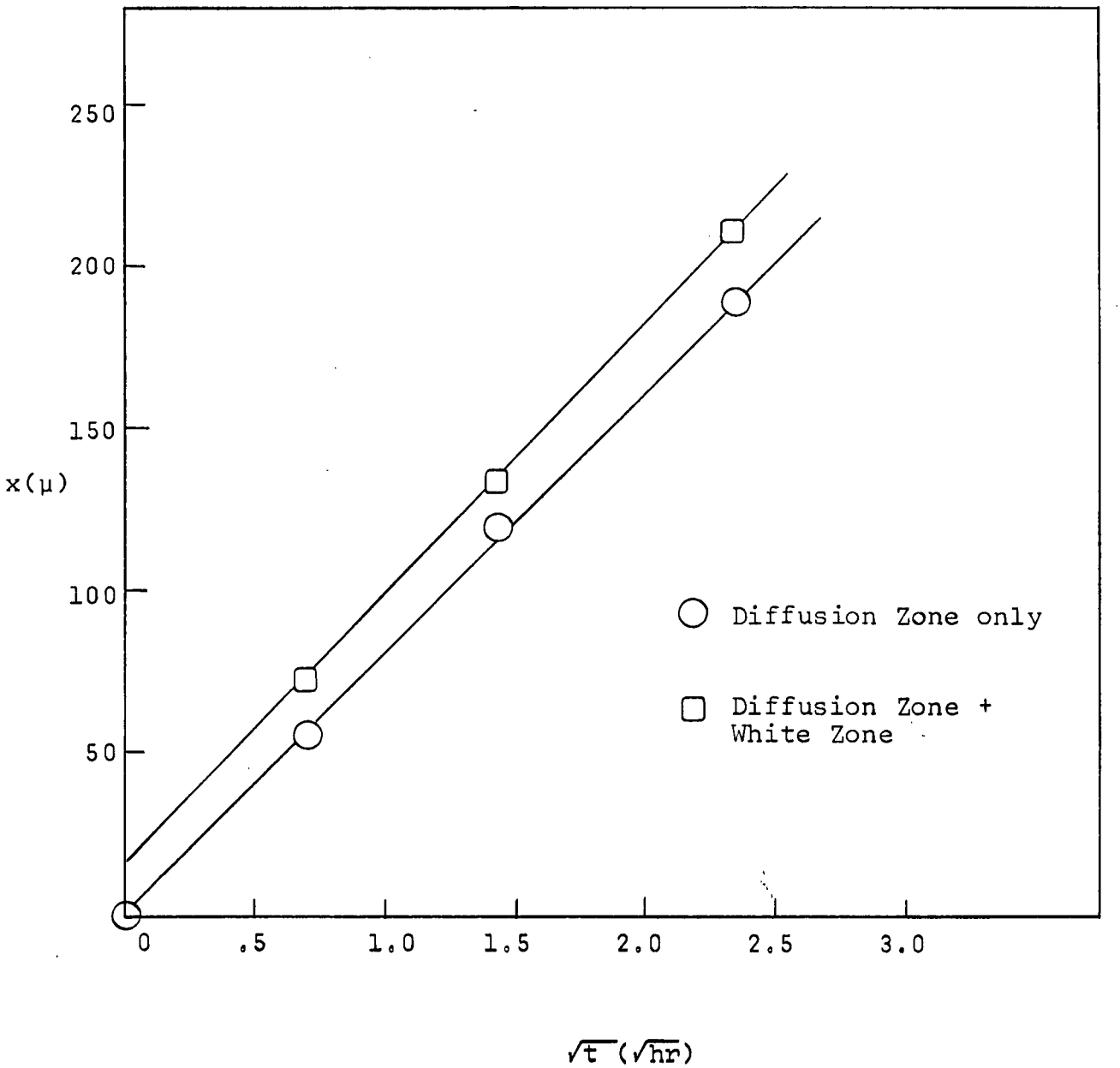

Figure A.1 x versus $\sqrt{t}$ in Ag-Te

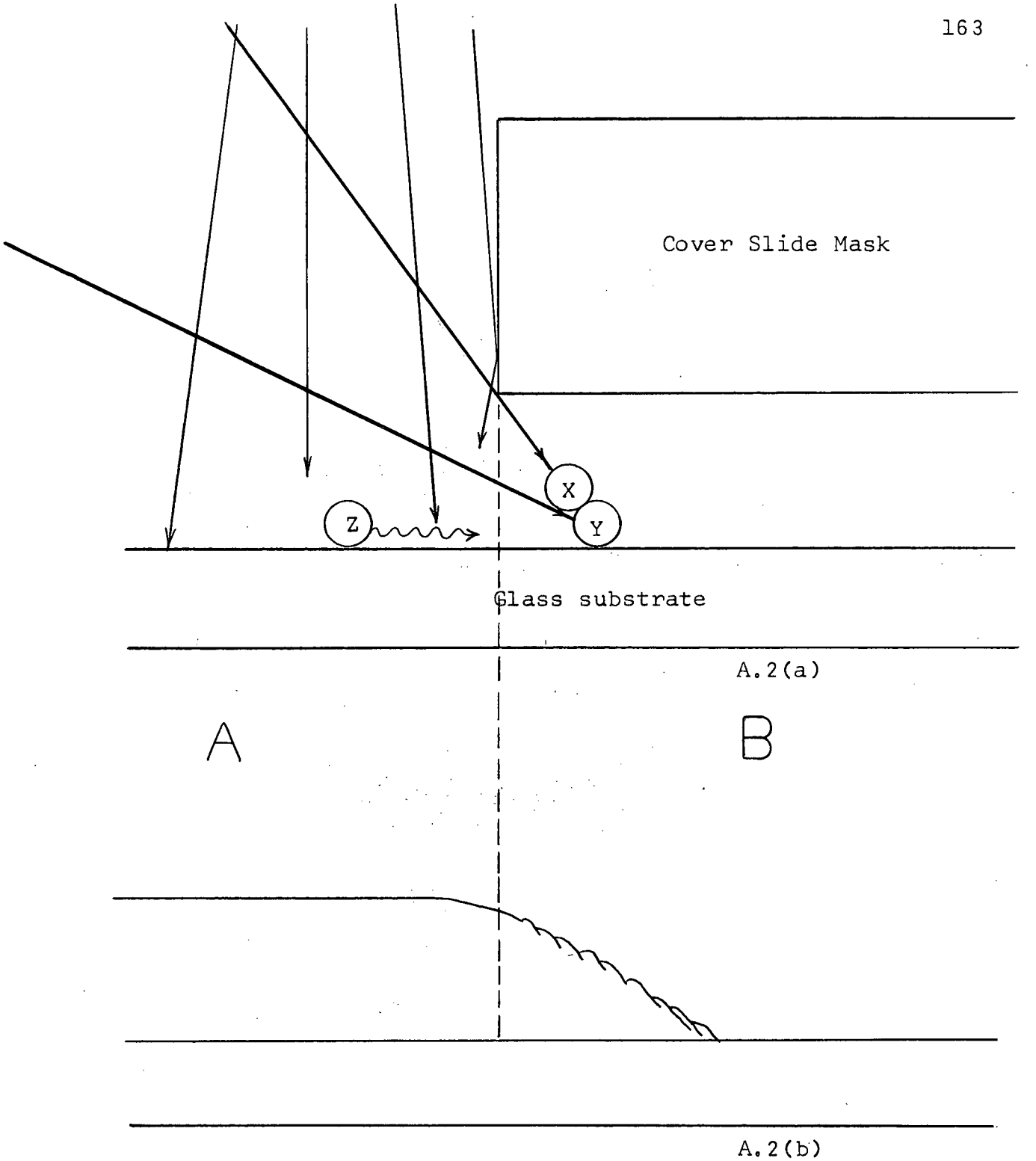

Figure A.2 Effect of Non-Ideal Masking on Resulting Film Step

resulting Ag step produced (A.2(b)). In practice it is not possible to achieve perfect contact between mask and substrate so that there is always a narrow gap between them. This permits a small fraction of Ag atoms to occupy sites in region B of the substrate. This may occur when atoms such as X and Y in A.2(a) strike the substrate at a high angle of incidence due to rebounding of the chimney walls or collision with other atoms in the beam. Some Ag atoms (e.g. Z in A.2(a)) may migrate from region A to region B by surface diffusion especially if their kinetic energy on collision with the substrate is sufficiently high to enable them to move out of bound surface sites, but insufficient to cause them to re-evaporate. The result of these two processes is a film structure which becomes increasingly aggregated and porous towards the edge of the Ag[2,66]. Figure A.3 illustrates what happens when Se is evaporated over such a step to produce a diffusion couple. The Se in the aggregated portion of the step essentially "fills in" the pores in the Ag resulting in an effective reduction of the Se thickness in this region. Diffusion still takes place between the Ag and Se to form Ag_2Se but because the net Se thickness is less in this region the optical contrast is different and this area is observed as the white zone. Evaporation of thicker and thicker Se films reduces the white zone by building up a thick layer of Se at either end of the step distribution and so decreasing the area of effective Se thickness reduction. This argument was con-

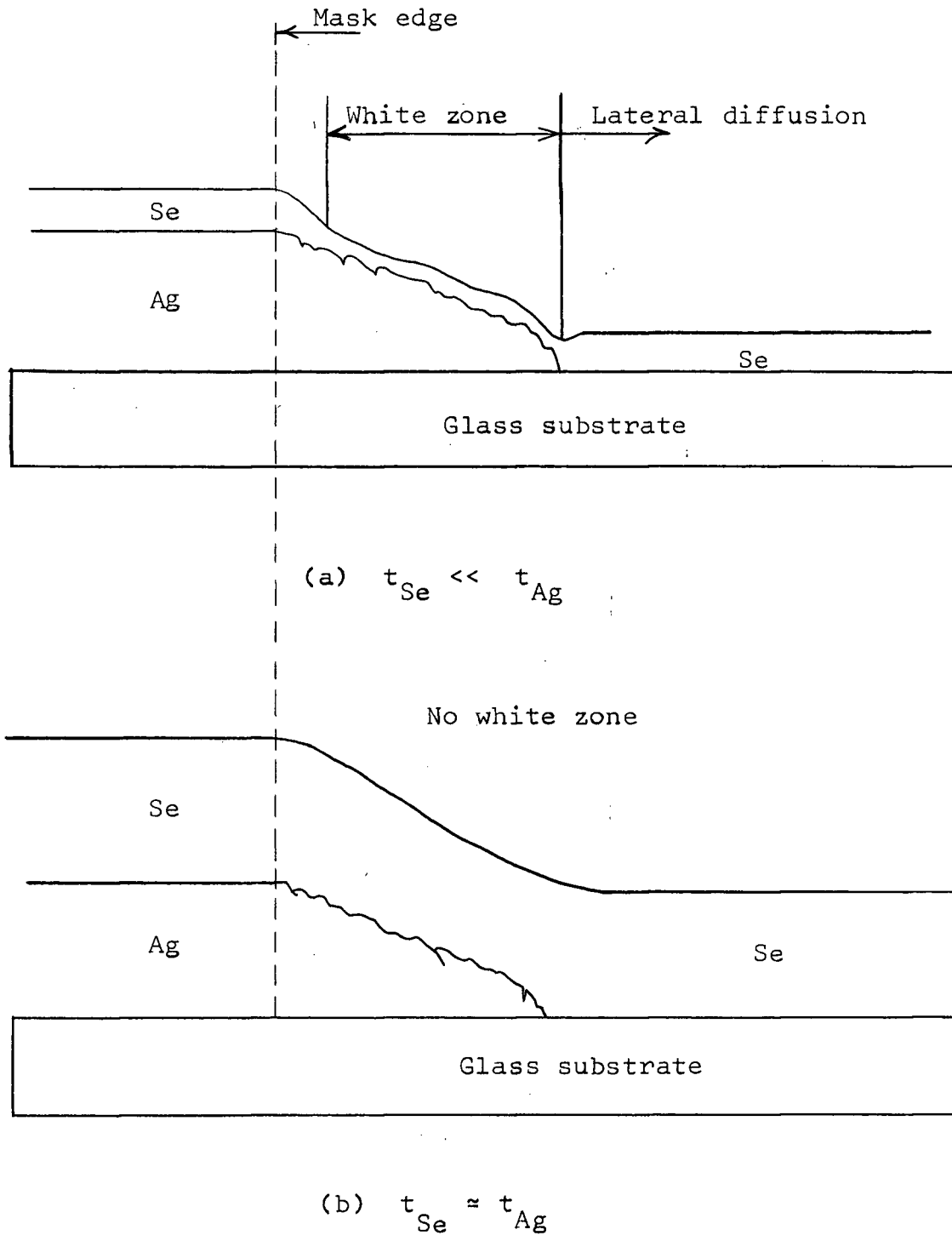

Figure A.3 Evaporation of Se across an Actual Ag Step

firmed by evaporating a Ag-Te couple with the mask raised 2 mm above the substrate at one end and in contact with the substrate at the opposite end. The width of the white zone at the "poor mask" end was about 150 μ while at the "good" end it was 18 μ. The diffusion zone at the "poor mask" end appeared very porous or diffuse in the early stages of growth making the exact position of $x = 0$ very difficult to establish. The beginning of the lateral diffusion zone, however, appeared to coincide with the very edge of the ill-defined Ag step on the glass immediately adjacent to the Se film. No difference in the diffusion rate was detected at the "good" and "poor" mask ends, confirming that the white zone is of no significance in the lateral diffusion process.

BIBLIOGRAPHY

1. "Physics of Thin Films", Vol. 2, Ed. by G. Hass and R.E. Thun, Academic Press, New York & London (1964).

2. J.C. Anderson, "The Use of Thin Films in Physical Investigations", Academic Press, New York & London (1966).

3. R.W. Hoffman, "Physics of Thin Films", Vol. 3, Ed. by G. Hass and R. E. Thun, Academic Press, New York & London, p. 211 (1966).

4. R.E. Thun, "Physics of Thin Films", Vol. 1, Ed. by G. Hass, Academic Press, New York & London, p. 187 (1963).

5. "Thin Films", A.S.M. Seminar, Ed. by H. Wilsdorf (1963).

6. O.S. Heavens, "Optical Properties of Thin Solid Films", Butterworths Publications, London, (1955).

7. "Structure and Properties of Thin Films", Ed. by C.A. Neugebauer, J.B. Newkirk, D.A. Vermilyea, Wiley and Sons, New York, (1959).

8. C. Weaver and R.M. Hill, Phil. Mag. Supplement, 8, No. 32, p. 375 (1959).

9. C. Weaver and L.C. Brown, Phil. Mag., 8, p. 1379 (1963).

10. H. Schopper. Z. Physik, 143, p. 93 (1955).

11. G.C. Monch, Ibid., 14, p. 363 (1954).

12. T. Mohr, Wiss. Z., Martin-Luther Univ., Halle-Wittenberg, 2, p. 601 (1952).

13. T. Mohr, Ibid., 14, p. 377 (1954).

14. G. Kienel, Ann. Phys., Lpz., 6, p. 1 (1955).

15. V. Zorll, Ibid., 16, p. 7 (1955).

Bibliography (Cont'd)

16. D.T. Parkinson, University of Strathclyde, unpublished work (1963).

17. A.D. LeClaire, "Progress in Metal Physics", Vol. 4, Ed. by B. Chalmers, Pergamon Press, London (1953).

18. P.G. Shewmon, "Diffusion in Solids", McGraw-Hill, p. 116 (1963).

19. R.E. Reed-Hill, "Physical Metallurgy Principles", Van Nostrand Company, New Jersey, p. 378 (1964).

20. D. Turnbull, "Atom Movements", A.S.M., Cleveland, p. 129 (1951).

21. N.A. Gjostein, "Metal Surfaces", A.S.M. Seminar, Ed. by W.D. Robertson and N.A. Gjostein, p. 114 (1962).

22. R.A. Nickerson and E.R. Parker, Trans. A.S.M., 42, p. 376 (1950).

23. W.W. Mullins, J. Appl. Physics, 28, p. 333 (1957).

24. J. Choi and P. Shewmon, Trans. AIME, 224, p. 589 (1962).

25. D. Lazarus, "Energetics in Metallurgical Phenomena", Vol. 1, Ed. by W.M. Mueller, Gordon and Breach, p. 1 (1965).

26. W. Jost, "Diffusion in Solids, Liquids, Gases", Academic Press, New York, p. 87 (1952).

27. A.H. Cottrell, "Theoretical Structural Metallurgy", Edward Arnold Publishers, London, p. 154 (1954).

28. H. Bückle, Colloquium on Solid State Diffusion: Saclay, France, North Holland Publ. Co., Amsterdam, p. 170 (1958).

29. G.V. Kidson, J. Nuc. Mat., 3, No. 1, p. 21 (1960).

30. J.P. Hirth and G.U. Pound, "Condensation and Evaporation", Pergamon Press, New York, (1963).

31. L. Holland, "Vacuum Deposition of Thin Films", Chapman and Hall Ltd., London (1958).

32. D.W. Pashley, Advances in Phys., 14, p. 330 (1965).

Bibliography (Cont'd)

33. R.S. Sennett and G.D. Scott, J. Opt. Soc. Amer., 40, p. 203 (1950).

34. L.E. Murc and M.C. Inman, Phil. Mag., 13, p. 135 (1966.

35. J.S. Halliday, T.B. Rymer, and K.H.R. Wright, Proc. Royal Soc., A 224, p. 548 (1954).

36. R.B. Belser, J. Appl. Phys., 31, p. 562 (1960).

37. S. Tolansky, "Multiple-Beam Interferometry", Clarendon Press, Oxoford, p. 147 (1948).

38. S.K. Behera, Private Communication.

39. S.D. Gertsriken, I. Ya. Dekhtyar, "Solid State Diffusion in Metals and Alloys", United States Atomic Energy Commission, translation of a publication of the State Publishing House for Physical-Mathematical Literature, Moscow, p. 478 (1960).

40. M. Hansen, Constitution of Binary Alloys, McGraw-Hill, New York (1958).

41. C.S. Barrett, "Structure of Metals", McGraw-Hill, New York, p. 230 (1952).

42. N.B. Hannay, "Semiconductors", Reinhold Publishing Co., New York, (1960).

43. C.A. Hampel, "Rare Metals Handbook", Reinhold Publishing Corp., pp. 447 and 519 (1961).

44. G. Thomas, "Transmission Electron Microscopy of Metals", John Wiley and Sons, New York (1962).

45. M. Wayman and R. Bennett, University of British Columbia, unpublished work (1964).

46. L.C. Brown, C.S. Sanderson, and C. St. John, Trans. AIME, 236, p. 1539 (1966).

47. R. Dalven, J. Appl. Phys., 37, No. 6, p. 2271 (1966).

48. R.P. Elliot, "Constitution of Binary Alloys, First Supplement", McGraw-Hill, p. 384 (1965).

Bibliography (Cont'd)

49. W.B. Pearson, "Handbook of Lattice Spacings and Structures of Metals", 2, Pergamon Press, p. 885 (1967).

50. R.W. Hill, "Reactivity of Solids", Ed. by J.H. De Boer, Proceedings of the 4th International Symposium on the Reactivity of Solids, Elsevier Pub. Co., New York, p. 294 (1961).

51. P.B. Hirsch, A. Howie, R.B. Nicholsen, P.W. Paschley, N.J. Whelan, "Electron Microscopy of Thin Crystals", Butterworths, London, pp. 133 ff and 320 ff (1965).

52. A. Taylor, "x-Ray Metallography", John Wiley and Sons, New York (1964).

53. R.W. Cahn, "Physical Metallurgy", North-Holland Publishing Co., Amsterdam (1965).

54. J.A. Malcolm and G.R. Purdy, Trans. AIME, 239, No. 9, p. 1391 (1967).

55. L.H. Van Vlack, "Elements of Materials Science", Addison-Wesley Publishing Co., Reading, Massachusetts, p. 67 (1960).

56. J.W. Christian, "The Theory of Transformations in Metals and Alloys", Permagon Press, p. 594 (1965).

57. S.G. Ellis, J. Appl. Phys., 38, No. 7, p. 2906 (1967).

58. C. Kittel, "Introduction to Solid State Physics", John Wiley and Sons, New York, p. 63 (1962).

59. E.S. Gould, "Inorganic Reactions and Structure", Henry Holt and Company, New York, p. 134 (1958).

60. O. Kubaschewski, E.H. Evans and C.B. Alcock, "Metallurgical Thermochemistry", Pergamon Press, p. 304 (1967).

61. R.T. Foley, M.J. Bolton, and W. Morill, J. Electrochem. Soc., 100, p. 538 (1953).

62. B.D. Lichter and C. Wagner, J. Electrochem. Soc., 107, p. 168 (1960).

63. K. Hauffe, "Oxidation of Metals", Plenum Press, New York, p. 365 ff (1965).

Bibliography (Cont'd)

64. H. Reinhold and H. Seidel, Z. Physik. Che., B (38), p. 245 (1937).

65. V.I. Arkharov and S. Mardeshev, Dokl. Akad. Nauk. SSSR, SS, 517 (1954).

66. J.M. Niewenhuizen and H.B. Haanstra, Philips Research Laboratories Scientific and Analytical Equipment Bulletin, 79.177/EM9, (1967).